SUMAR - SOMMAIRE - CONTENTS - INHALT

EPR INVESTIGATION OF THE Fe_2O_3-Bi_2O_3-PbO-As_2O_3 GLASS SYSTEM

M.PETEANU, C.BORŞA, I.ARDELEAN

Faculty of Physics, Babeş-Bolyai University,
3400 Cluj-Napoca, Romania

ABSTRACT. Glasses of the system $xFe_2O_3 \cdot (100-x)[Bi_2O_3 \cdot PbO \cdot As_2O_3]$ where prepared for $0 \leq x \leq 30$ mol %. Structural changes of the vitreous matrix and the concentration dependence of the paramagnetic ions distribution were revealed by means of EPR of Fe^{3+} ions. Valence states distribution of the iron impurities was also evidenced as depending on Fe_2O_3 content of the glass.

1. Introduction

Fe^{3+} ions revealed as suitable probes in exploring the structure of vitreous systems by means of their EPR absorption spectra [1-14]. Glasses containing iron and synthesized under oxidizing conditions exhibit EPR absorption lines at $g \approx 4.3$ and $g \approx 2.0$ both involving the Fe^{3+} ions. There are several site symmetries of the Fe^{3+} ion appropriate to split the $^6S_{5/2}$ state ground level into three doublets. The resonance line at $g \approx 4.3$ arises from an isotropic transition inside one of the Kramers doublets [1-4]. For high spin d^5 systems general conditions for the occurrence of one isotropic g-tensor with a 4.3 value were obtained in terms of the spin-Hamiltonian parameters [5-9]. The $g \approx 2.0$ resonance is commonly attributed either to isolated paramagnetic centers in sites of octahedral symmetry or to exchange coupled pairs [10]. Usually iron enters the glass as Fe^{3+} and Fe^{2+} ions, its redox equilibrium being dependent on series of factors as the base composition, melt temperature, oxygen fugacity, concentration and presence of other redox species [11-13]. Though Fe^{2+} ions do not exhibit any EPR absorption at room temperature, they interact with Fe^{3+} ions altering thus their spectra [14-16].

2. Experimental technique and results

Due to their capacity of accepting transition metal ions in both network-former and network-modifier sites, glasses based on heavy metal oxides can be obtained as homogeneous systems for high concentrations of such ions [17]. We succeeded, therefore, in obtaining glasses of the system $xFe_2O_3 \cdot (100-x)[Bi_2O_3 \cdot PbO \cdot As_2O_3]$ within $0 \le x \le 30$ mol %.

Pure reagent grade oxides were used as starting materials. The melting was performed in air, in a preheated electric furnace at 1000^oC, using sintered corundum crucibles. The time of melting (10 minutes) was chosen to avoid the substance losses due to evaporation. The molten material was quenched to room temperature by pouring onto a stainless-steel plate.

The sample structure was tested by X-ray diffraction analysis. Patterns typical of vitreous samples were obtained up to 30 mol % Fe_2O_3 for both series of glasses.

EPR spectra were recorded at room temperature using a JEOL equipment, operating in the X frequency band, and 100 kHz field modulation. Powdered samples encapsulated in quartz tubes to avoid moisture effects, were studied. The obtained absorption spectra presented in Fig. 1 are typical for paramagnetic Fe^{3+} ions. One remarks the dependence
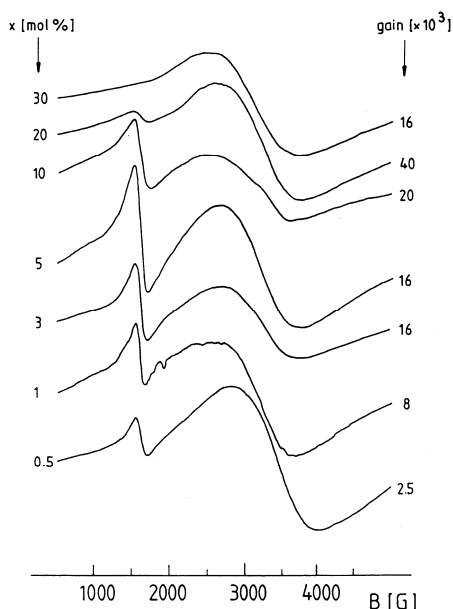
Fig. 1. EPR absorption spectra of Fe^{3+} ions in glasses of the system $xFe_2O_3 \cdot (100-x)[Bi_2O_3 \cdot PbO \cdot As_2O_3]$.

of the spectral features on the Fe_2O_3 content of the sample which reflects structural changes when iron accumulates in the vitreous matrix. This evolution was followed by plotting the concentration dependence of the resonance line parameters, namely the peak-to-peak width, ΔB, and the intensity approximated as $J = I(\Delta B)^2$, where I denotes the line-amplitude. The corresponding graphs are presented in Fig. 2 for the $g \approx 4.3$ absorption line, and Fig. 3 for the $g \approx 2.0$ one.
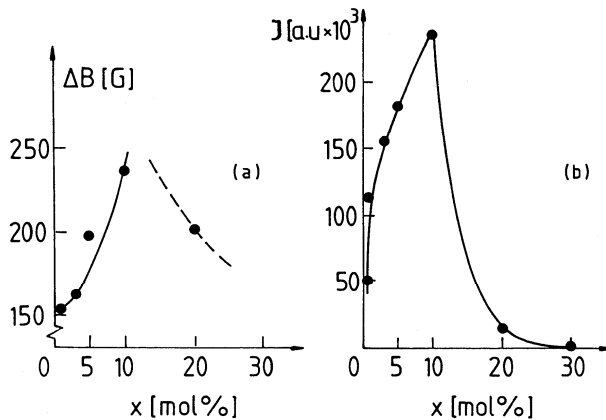
Fig. 2. Concentration dependence of the line-width (a) and intensity (b) for $g \approx 4.3$ absorption line in spectra of $xFe_2O_3 \cdot (100-x)[Bi_2O_3 \cdot PbO \cdot As_2O_3]$ glasses.
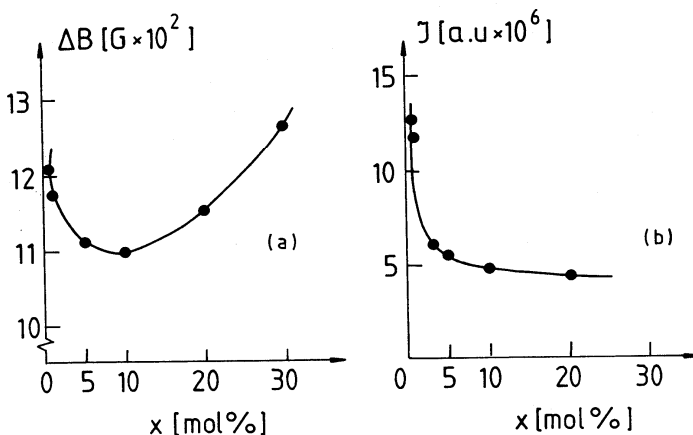
Fig. 3. Concentration dependence of the line-width (a) and intensity (b) for $g \approx 2.0$ absorptions in spectra of $xFe_2O_3 \cdot (100-x)[Bi_2O_3 \cdot PbO \cdot As_2O_3]$ glasse.

3. Discussion

The obtained EPR absorption spectra attest the presence of Fe^{3+} ($3d^5$; $^6S_{5/2}$) ions in the studied glasses within the investigated concentration range. For samples of our system the spectra consist in resonance lines centered at $g \approx 4.3$ and $g \approx 2.0$ their prevalence depending on the Fe_2O_3 content (Fig. 1).

The $g \approx 4.3$ absorption line is due to isolated paramagnetic $3d^5$ ions in distorted octahedral symmetric sites subjected to strong crystal field effects. This resonance line may result due to transitions between the lines of the median Kramers doublet when the site symmetry is rhombic [1-4] or the transition may be induced between the lines of the lowest doublet in the case of tetragonal sites or cubic tetragonally distorted sites [8, 9]. The line-width increasing (Fig. 2) is due to dipolar broadening characteristic for isolated ions. The apparently lower values of ΔB when x > 10 mol % Fe_2O_3 are rather due to the partial overlapping of $g \approx 4.3$ signal by the broaden $g \approx 2.0$ one, than to real narrowing effects. The intensity of the line increases up to 10 mol % Fe_2O_3 and abruptly decreases for higher concentrations. This behaviour confirms structural effects reflected by the $g \approx 4.3$ resonance line, due to ions involved in structural units of different configuration. The gradual increasing of iron destroys the neighbours configuration in the Fe^{3+} ion vicinity, so the structural units as characteristic entities involving Fe^{3+} become less represented. The local ordering is compromised and structureless formations of cluster type are favored.

For samples of our system absorption lines at $g \approx 2.0$ characteristic to clusters are also present (Fig. 1). The line-width shows a complex evolution due to the balance of narrowing and broadening mechanisms (Fig. 3a). Within $0.5 \leq x < 10$ mol % Fe_2O_3 the line-width decreases that denotes exchange coupling of cluster involved ions. The line broadening for x > 10 mol % cannot be attributed to dipolar interactions at this concentration level and is rather due to interactions between ions in multivalent states [18]. The presence of Fe^{2+} ions in increased amount for samples with x > 10 mol % Fe_2O_3 would explain the line broadening and also the line-intensity gradual decreasing (Fig. 3b). Even when present in clusters Fe^{3+} ions are less able to resonate. Their electronic state is changed due to the Fe^{2+} ions surrounding. Further magnetic investigation is obviously necessary to clarify these aspects.

4. Conclusions

Glasses of the system $xFe_2O_3 \cdot (100-x)[Bi_2O_3 \cdot PbO \cdot As_2O_3]$ were obtained within a large concentration range, up to 30 mol % Fe_2O_3.

EPR absorption spectra evidence the presence of Fe^{3+} paramagnetic ions within the whole investigated concentration range, namely $0.5 \leq x \leq 30$ mol %. Resonance lines at $g \approx 4.3$ due to isolated ions in distorted sites of octahedral symmetry are detected within a relatively large concentration range. Therefore, one may conclude that iron enters the investigated matrix in network-former sites of well defined configuration and symmetry, up to 10 mol % Fe_2O_3. For higher concentration the local ordering in glass is compromised.

Cluster of Fe^{3+} ions giving rise to resonances at $g \approx 2.0$ are detected. The line-intensity decreasing despite the increasing of the Fe_2O_3 concentration in the melt, when samples were prepared, suggests an increased amount of Fe^{2+} ions simultaneously present in the vitreous matrix.

REFERENCES

1. T. Castner, G.S. Newell, W.C. Holton, C.P. Slichter, J. Chem. Phys. 32, 668 (1960).
2. H.H. Wickman, M.P. Klein, D.A. Shirley, J. Chem. Phys. 42, 213 (1965).
3. R.W. Kedzie, D.H. Lyons, M. Kestigian, Phys. Rev. 138A, 918 (1965).
4. D. Loveridge, S. Parke, Phys. Chem. Glasses 12, 19 (1971).
5. D.L. Griscom, R.E. Griscom, J. Chem. Phys. 47, 2771 (1967).
6. R.D. Dowsing, J.F. Gibson, J. Chem. Phys. 50, 294 (1969).
7. M.Ya. Shcherbakova, V.E. Istomin, Phys. Status Solidi (b) 67, 461 (1975).
8. V. Cerny, B. Petrova, M. Frumar, J. Non-Cryst. Solids 125, 17 (1990).
9. V. Cerny, B. Frumarova, J. Rosa, I.L. Licholit, M. Frumar, J.Non-Cryst. Solids 192&193, 165 (1995).
10. D.L. Griscom, J. Non-Cryst. Solids 40, 211 (1980).
11. H.D. Schreiber, H.V.Lauer, T.Tanyasiri, Geochim. Cosmochim. Acta 44, 1599 (1980).
12. B. Kumar, S.Liu, J. Amer. Ceram. Soc. 74 (1), 226 (1991).
13. B. Kumar, C.Chen, Phys. Chem. Glasses 33 (5), 204 (1992).
14. M. Peteanu, L.. Cociu, I. Ardelean, J. Mater. Sci. Technol. 10, 97 (1994).
15. I.Ardelean, M.Peteanu, S.Filip, V.Simon, G.Györffy, Solid State Commun. 102, 341 (1997).
16. I. Ardelean, M. Peteanu, V. Simon, S. Filip, F. Ciorcas, I. Todor, J.Magn.Magn.Mat. 196-197, 257 (1999).
17. D.L. Griscom, Glass. Sci. Technol. 48, 151 (1990).
18. C. Kittel, E. Abrahams, Phys. Rev. 90, 238 (1963).

ESR STUDY OF GAMMA-IRRADIATED TETRABUTYLAMMONIUMIODID

I. BARBUR[a)*],V. CHIŞ[a)]

a) Babeş-Bolyai University, Faculty of PhysicsRO-3400 Cluj-Napoca, Romania[*]) Corresponding author

ABSTRACT. The effect of gamma-irradiation on tetrabutil-ammoniumiodid (TBAI) is reported. The ESR spectrum of freee radicals produced consistes of seven lines arrising from hyperfine interaction of the unpaired electron with six protons of three CH_2 groups. The simulated spectrum was obtained based on the following parameters: $A_H = 13.4$ G, $g = 2.0043$ and $\Delta H_{pp} = 6.5$ G.

Introduction

Among ABX_3 or A_2BX_4 compounds, those obtained with A as ammonium, tetramethylammonium or tetraethylammonium group are known as compounds with ferroelectric or ferroelastic activity [1-3]. Moreover, such compounds exhibit high ionic conductivity [4]. Therefore we decided to investigate whether tetrabutylammoniumiodide $(CH_3CH_2CH_2CH_2)_4NI$ -TBAI belongs to above mentioned class of compounds.

In this paper we will present the results of an ESR study of gamma-irradiated TBAI at room temperature.

Experimental

The powdered sample of TBAI was of high purity grade (Fluka) and used without further purification. The sample was irradiated in air at room temperature using a ^{60}Co gamma source with a debit dose of 35Gy/hour. ESR spectra were recorded using a JEOL-JES-3B modified X-band spectrometer. The instrument setting were: microwave frequency 9500 MHz, modulation frequency 100 KHz, field scan 200 G, time constant 1 s, cavity TE_{102}, sensitivity $3 \cdot 10^{11}$ spins/gauss and microwave power 10 mW. The calibration of magnetic field for g factor and hyperfine splitting values was performed by using NMR signal of protons (NMR magnetometer of MJ110R type). The ESR spectrum was simulated using a spin Hamiltonian that

contains a g-tensor and up to ten hyperfine tensors for a radical. The program generates the powder pattern by means of Gauss-Legendre numerical quadrature. ESR spectrum is then obtained by convoluting the powder pattern with Lorentzian or Gaussian lineshape functions of convenient widths. More spectra of different radicals can be added together in various ratios.

Results and discussions

The ESR spectrum of gamma-irradiated TBAI is shown in Fig.1. No change was observed in the shape of the spectrum as the irradiation dose was increased, suggesting that only one type of radical is formed. The spectrum consists of seven line arrising from hyperfine interaction of the unpaired electron with six equivalent protons. The only possible way of producing the free radicals is by methyl abstraction, resulting one unpaired electron highly delocalized over the chain formed by the three CH_2 groups. The best agreement between the experimental spectrum and the simulated one was obtained based on the following parameters: A_H=13.4G, g=2.0043, ΔH_{pp}=6.5G.
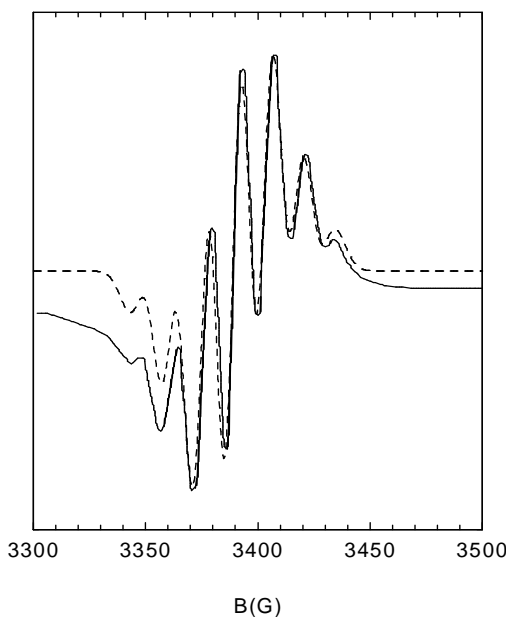
Fig.1. Experimental (continous line) and simulated (dashed line) ESR spectra of gamma-irradiated TBAI at room temperature

The gamma induced free radicals in TBAI are not stable at room temperature. The relative decreasing of the concentration of the free radicals was estimated by the ESR signal amplitude attenuation with time, after gamma-irradiation (Fig.2).
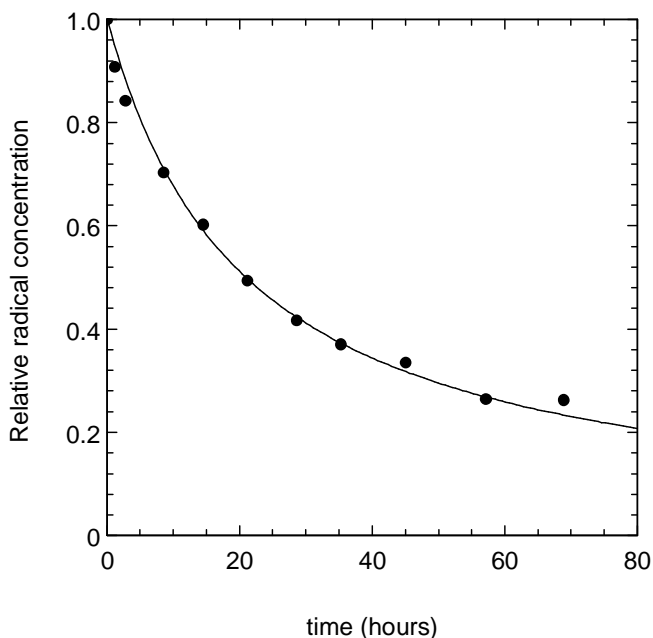
Fig.2. The relative decreasing of the concentration of the free radicals with time, after gamma-irradiation

Experimental data shown in Fig.2 were fitted by a function given by Pchjetckii et al. [12]:

$$\frac{1}{R} - \frac{1}{R_0} = kt \qquad (1)$$

where R_0 is the initial concentration of the free radicals, R is the concentration at a time t and k is the rate constant. A value of $1.325 \cdot 10^{-5}$ was obtained for k, in good agreement with other values corresponding to free radicals in solid state [12].

Conclusions

The gamma irradiation of TBAI induced free radicals, unstable at room temperature. The free radicals are formed by methyl abstraction and interaction of unpaired electron with six equivalent protons arrising from three CH_2 groups.

The rate constant of the free radicals recombination process is in good agreement with other values corresponding to the free radicals in solid state.

REFERENCES

1. T.Oka, T.Mitsui, Y.Shiroishi, S.Sawada, J.Phys.Soc.Japan., 40,913(1976).
2. T.Yamaguchi, H.Suzuki, F.Shimizu, S.Sawada, Jpn.J.Appl.Phys., 24, Suplement 24-2,359(1985).
3. J.M.Perez-Mato, I.Etxbarria, G.Madariaga, Physica Scripta, 38,91(1990).
4. R.Blinc, G.Lahajnar, I.Zupancic, Solid State Communications, 51,751(1984).

CARBON- 13 CONCENTRATIONS IN HUMAN BREATH MEASURED BY MASS SPECTROMETRY

STELA CUNA[1], ONUC COZAR[2], GABRIELA BALAS[1]

ABSTRACT. We have developed a specific and sensitiv test for detection of Helicobacter pylori that has been associated with gastrits, ulcers and some forms of gastric cancer. The test uses the ability of the urease (an enzyme produced by Helicobacter pylori) to break urea labeled with ^{13}C to carbon dioxide and ammonia. The carbon dioxide ($^{13}CO_2$) is release first into the blood and very rapidly into the breath. $^{13}CO_2$ is collected, purified and analysed by isotope ratio mass spectrometry. An increase in $^{13}CO_2$ in the breath confirms that the patient is infected with Helicobacter pylori.

This test has performed to a patient suspected to be infected with Helicobacter pylori. We used 75 mg ^{13}C-urea and we have collected and analysed CO_2 respiratory before the administration of ^{13}C-urea and after the administration of ^{13}C-urea at 20, 40 and 60 min. The results showed an increase up to 60 % of $^{13}CO_2$ in the breath, it means an intensive activity of the urease, namely the patient has been infected with Helicobacter pylori. The validity of the results has been performed by endoscopy.

Introduction

The use of stable isotopes in metabolic research on human is expanding rapidly due to the increasing variety of labeled compounds, greater availibility of analytical facilities and absence of health risk from radiation.

In vivo studies of human metabolism using ^{13}C-labeled substrates can provide several types of information including:
1. presence and activity of specific enzymes
2. absorbtion, malabsorbtion and oxidization of dietary nutriens
3. synthesis and degradation (turnover rates) of biochemicals

---

[1] National Institute of Research and Development for Isotopic and Molecular Technology, Cluj-Napoca
[2] Babes- Bolyai University, Dept. of Physics, Cluj-Napoca

4. presence or absence of disease or metabolic disorders

These applications have been reviewed extensively [1], [2], [3], [4].

This paper will focus on methodology required for in vivo studies to detect infection of the gastric mucosa by Helicobacter pylori which can result in ulcers and some forms of gastric cancer [5]. The method uses as a metabolic substrat ^{13}C-labeled urea that is given orally to the patient. Helicobacter pylori produces large amounts of an enzyme (urease) which hydrolyses urea resulting $^{13}CO_2$ and ammonia. Urea otherwise cannot be digested by humans. $^{13}CO_2$ circulates to the lungs and is expelled in the breath where it can be detected.

The increase in $^{13}CO_2$ in the breath confirms that the patient is infected with Helicobacter pylori and that eradication therapy is indicated.

$$O = {}^{13}C \Big\langle \begin{array}{c} NH_2 \\ NH_2 \end{array} \xrightarrow{\text{enzyme activity}} \text{Breath } {}^{13}CO_2 + NH_3$$
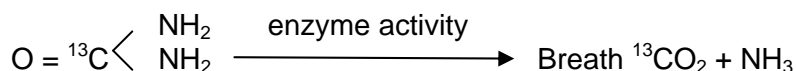
The method is named ^{13}C – Urea Breath Test (^{13}C-UBT). In priciple, the ^{13}C – UBT protocol require the patient to drink a nutrient meal following a fasting period, typically of more than 4 hours. A sample of the patient's breath is then taken and retained in a collection tube to provide a "baseline" measurements of $^{13}CO_2$. The patient drinks a solution of ^{13}C labeled urea (typically 75-125 mg) and another breath sample is taken (typically after 30 minutes) and retained in a collection tube to provide a "test" measurement of $^{13}CO_2$ by isotope ratio mass spectrometry [6].

The other breath tests available are:
- ^{13}C-Octanoic acid breath test used to diagnose delayed gastric, emptying of solid food a condition often associated with diabetes [7]
- ^{13}C-Mixed Triglyceride breath test used to identify pancreatic insuficiently leading to a problem in digesting and assimilating dietary fat [8]
- ^{13}C-Starch breath test to detect pancreatic disease [9]

Material and methods

The ^{13}C – Urea Breath Test involves:

(i)   – instrumentation for measurement of carbon isotope ratios
(ii)   – ^{13}C – labeled substrates
(iii)   – sample collection equipment
(iv)   – sample preparation equipment

i) Instrumentation for measuring of carbon isotope ratios

Stable carbon isotope ratios ($^{13}C/^{12}C$) from respiratory CO_2 are measured with high precision (<0.1 $^0/_{00}$) by a dual inlet isotope ratio mass spectrometer (IRMS) equiped with two ion beam collectors. The high precision afforded by this mass spectrometer is due to simultaneous collection of the two ion beam (masses) of interest (44 and 45) and to repeated measurements of sample and standard gases during a single isotope ratio determination. A 100 μmol of CO_2 at STP is required for a carbon isotope ratio measurement.

The quantity measured is not the absolute isotope ratio of the sample, but the relative difference between the isotope ratios of the sample and standard gases. As a result, a differential notation known as the delta (δ) notation has been adopted for expressing relative differences in stable carbon isotope ratios between samples and standards. The $\delta^{13}C$ value is calculated from the measured carbon isotope ratios of the sample and standard gases as:

$$\delta^{13}C\left(^0/_{00}\right) = \left[\frac{R_{sp} - R_{st}}{R_{st}}\right] x 10^3$$

where R is the $^{13}C/^{12}C$ ratio of the sample (R_{sp}) or standard (R_{st}) gas.

By international convention, $\delta^{13}C$ values are always expressed relative to a calcium carbonate standard known as PDB. This standard was a limestone fossil of Belemnitella americana from Cretaceous Pee Dee formation in South Carolina. Isotope ratios that have been measured against another standard can be related to PDB by equations:

$$\delta_{(X-PDB)} = \delta_{(X-B)} + \delta_{(B-PDB)} + 10^{-3}\delta_{(X-B)}\,\delta_{(B-PDB)}$$

where all δ values have units of $^0/_{00}$, $\delta_{(X-PDB)}$ is the isotope ratio of the sample relative to PDB, $\delta_{(X-B)}$ is the isotope ratio of the sample relative to some standard B and the isotope variation of the standard B relative to PDB is $\delta_{(B-PDB)}$. We have utilised as standard B Carrara marble with $\delta^{13}C$ = + 1.990 $^0/_{00}$ vs. PDB.

(ii) ^{13}C – labeled substrate

Urea highly enriched with ^{13}C (99 atom %) are available commercially (the price for urea 99 atom % is 120 DM/g).

The dose utilised in our study was 75 mg $^{13}CO(NH_2)_2$ for one test.

(iii)Sample collection equipment

The most important consideration for samples is preservation of isotopic integrity during collection, storage and sample preparation. The simplest method for collecting respiratory CO_2 is with a 1 liter colection bag (Fig.1). The collection bag is equipped with a sample port to which a one-way stopcock (1) and a syringe needle are attached and a tube to which a one-way stopcock (2) is attached. The patient blowes breath air through the tube into the collection bag. When the collection bag is full, the stopcock (2) is closed, the syringe needle pushes through the rubber septum on a 20-ml Vacutainer[R] (Becton Dickinson Co.) and the stopcock (1) is opened. Because the Vacutainer is under vacuum, a 20 ml aliquot of the breath sample is pulled into the tube. To avoid isotopic memory effects, the breath collection bag should be throughly emptied between samples. The large volume of respiratory gas (1 l) collected in the bag during each sample ensures that memory is not a problem if this precaution is taken.

Samples collected and stored in Vacutainers retain their isotopic composition for at least 3 months.
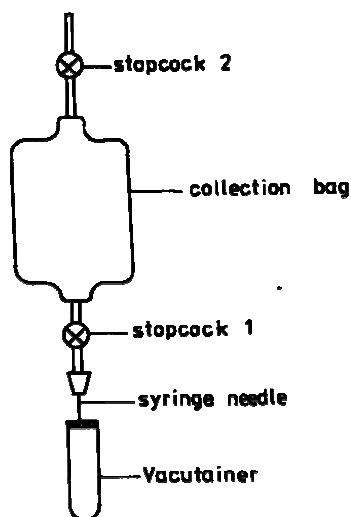
Fig.1. The collection bag

(iv) Sample preparation equipment and purification of respiratory CO_2

Carbon dioxide must be isolated from other respiratory gases by cryogenic distillation prior to mass spectrometric analysis. This can be accomplished using the vacuum system shown in Fig. 2.

If the respiratory gases are collected and stored in Vacutainers, the vacuum system must be equipped with a needle for puncturing the septum of the Vacutainer to admit the respiratory gases into system. The system has two cold traps, three valves and a mechanical vacuum pump.

First, a sample bulb is attached to the vacuum system and valves 2, 3 and 4 are all opend to evacuate the system to $< 10^{-2}$ torr. When a suitable vacuum has been achieved, a Vacutainer should be pushed only far enough onto the needle to completely cover the opening of the needle. Then valve 1 can be opened and the dead space between valve 1 and Vacutainer evacuated.
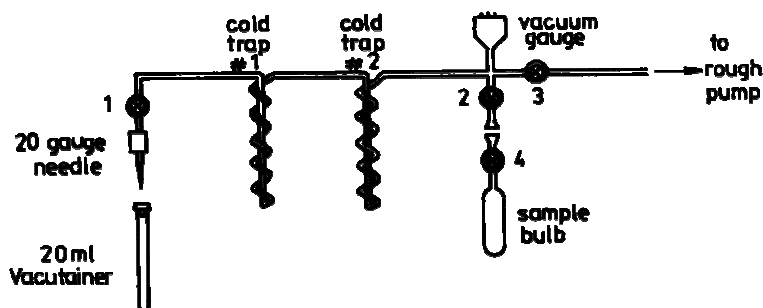
Fig. 2. Vacuum system for isolation and purification of respiratory CO_2 from breath samples

When a vacuum of $< 10^{-2}$ torr has been achieved, liquid nitrogen Dewars are placed around cold traps 1 and 2 and valves 2 and 3 are closed. The Vacutainer is pushed upwards until the needle fully penetrates the septum and the CO_2 and water are allowed to freeze into the traps for 4 min. Then, valve 3 is opened to ensure that all respiratory gases are pulled out of the Vacutainer and through the traps. All CO_2 and water is frozen in cold trap 1, but cold trap 2 ensures that no CO_2 is pumped away. Nitrogen, oxygen and other respiratory gases not frozen at lquid nitrogen temperature are pumped away. When a vacuum of $< 10^{-2}$ torr has been reached, valves 1 and 3 are closed, 2 and 4 opened, the liquid nitrogen Dewars on cold traps 1 and 2 replaced with ethanol-dry ice Dewars and the sample bulb immersed in liquid nitrogen. This allows the frozen CO_2 in cold traps 1 and 2 to sublime and diffuse into the sample bulb. The transfer of CO_2 can be monitored with the vacuum gauge and can be considered complete when a

vacuum of $< 10^{-2}$ torr has been restored. At least 3 min should be allowed for the transfer. At this time valves 4 and 2 are closed and the sample bulb is detached from the vacuum system and taken to the mass spectrometer for isotopic analysis.

Results and discussion

We made a ^{13}C-urea breath test for a patient suspected to have the Helicobacter pylori infection in the upper gastrointestinal tract.

The protocol of the method was:
1. a base sample of breath was taken before administrating ^{13}C-marked urea and was analysed for ^{13}C
2. a 75 mg ^{13}C- marked urea was administrated to the patient together with 0.1 N citric acid to inhibit gastric emptiyng
3. breath samples were collected at 20, 40 and 60 min from the patient
4. the samples were purified
5. the isotopic composition of CO_2 breath was analysed

The results are shown in Table 1.

Table 1.

Relative variation of ^{13}C in CO_2 respiratory before and following administration of ^{13}CO(NH$_2$)$_2$

Collection time (min)	δ^{13}C vs. PDB ($^o/_{oo}$)	Δ^{13}C ($^o/_{oo}$)
0	- 23.41	0
20	- 16.02	7.39
40	- 14.56	8.85
60	- 18.81	4.60

Δ^{13}C is the difference between the isotopic composition of the CO_2 respiratory collected at t = 20, 40, 60 min after the administration of ^{13}CO(NH$_2$)$_2$ and the isotopic composition of CO_2 before the administration of ^{13}CO(NH$_2$)$_2$. The isotopic composition before the administration of ^{13}CO(NH$_2$)$_2$ was δ^{13}C= - 23.41 $^o/_{oo}$

$$\Delta^{13}C = (\delta^{13}C)_t - (\delta^{13}C)_{t=0}$$

Δ^{13}C shows the change in isotopic composition of CO_2 respiratory and if it rises after the administration of ^{13}CO(NH$_2$)$_2$ it will mean a positiv test, namely the presence of Helicobacter pylori infection.

From Tabel 1 results that at t=20 min after the administration of ^{13}CO(NH$_2$)$_2$, Δ^{13}C was 7.39 $^o/_{oo}$ and at t=40 min Δ^{13}C was 8.85 $^o/_{oo}$. This means that our subject is certainly infected with Helicobacter pylori.

The natural background of ^{13}C in CO_2 respiratory (-23.41 $^o/_{oo}$ in this case study) depends on:
- the usual diet of the subject
- the physiological state of the subject (fasted or fed, rested or stressed) at the time of sampling

The ^{13}C background in respiratory CO_2 can be minimized by requiring subjects to fast during and for 12 hours before the test and to remain at rest (preferably lying down) during the test.

If the subject was fed and didn't rest during the test, resulting in up to 5 $^o/_{oo}$ excursions of the background ^{13}C in breath.

We have compared our results with the results obtained by another laboratory [10] for a non-infected patient and an infected patient with Helicobacter pylori. In Fig. 3 we show the variations of $\Delta^{13}C$ both the literature and the our study.
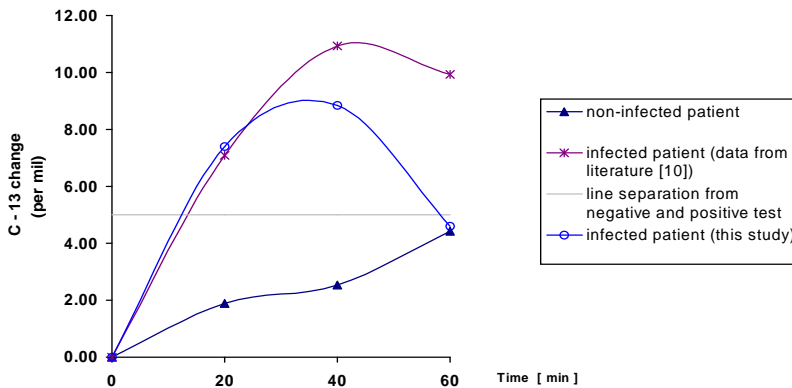
Fig.3. The evolution of the enrichment of CO_2 following the administration of ^{13}C-labeled urea

Because 5 $^o/_{oo}$ is the maximum excursion due to the background of ^{13}C in the breath, all the values $\Delta^{13}C$ greater than 5 $^o/_{oo}$ show a positive test and all the values $\Delta^{13}C$ resulting in up to 5 $^o/_{oo}$ show a negative test. In our test there is a slower rise in the ^{13}C content of the breath than in the reference. We have supposed that it is due of the less presence of the urease in the stomach.

We have concluded that the test is good to detect infection of the upper gastrointestinal tract. The diagnosis was confirmed by endoscopy.

Conclusion

Breath testing is a new technique wich offers real benefits for both patient and doctor. Breath tests use metabolic substances labelled with a non- radioactive isotope of carbon. We have developped a breath test in wich a disease causing stomach bacterium (Helicobacter pylori) is detected because it breaks ^{13}C-urea to ammonia and carbon dioxide. In this test an increase in $^{13}CO_2$ in the breath confirms that the patient is infected with Helicobacter pylori and that eradication terapy is indicated. The level of $^{13}CO_2$ in the breath was measured by isotope ratio mass spectrometry.

The ^{13}C – UBT is easy to use, non-invasive and non-radioactive method. No contraindication of the test are known. The efficacy of the test in detecting active Helicobacter pylori identifies it as the new gold standard.

REFERENCES

1. Hachey D. L., Wong W. W., Boutton T. W. And Klein P. D., *Isotope ratio measurements in nutritions and biomedical research,* Mass Spectrometry Reviews, 6 , 1987, pp. 289-328.
2. Bier D. M. and Matthews D. E., *Stable isotope tracer methods for in vivo investigations*, Fed. Proc., 41, 1982, pp. 2679-2685.
3. Halliday D. and Rennie M. J., *The use of stable isotopes for diagnosis and clinical research*, Clin. Sci., 63, 1982, pp. 485-496.
4. Lojen S., Ogrinc N., Osredkar J. and Usaj A., *Carbon stable isotopes in medical diagnostics and in physiological studies*, Materials and Geoenvironment, 45, 1998, pp. 110-114.
5. *Curent European concepts in the management of Helicobacter pylori infection*, The Maastrich Consensus Report, 41, pp. 8-13, 1997.
6. Platzner I. T., Habfast K., Walder A. J. and Goetz A., *Modern Isotope Ratio Mass Spectrometry*, Ed. Winefordner J. D., John Willey & Sons, New York, 1997, pp. 11-83, 424-427.
7. Watkins J. B., Klein P. D., Scholler D. A., Kirschner B. S., Tark R. And Perman J. A., *Diagnosis and differentiation of fat malabsorbtion in children using ^{13}C-labelled lipids: Trioctanoin, Triolein and Palmitic Acid Btreat Tests*, Gastroenterol., 82, 1982, pp. 911-917.
8. Klein P. D., Hachey O. L., Opekun A. R., Tacquard P. E. and Kyle D., *Hiolein for fat malabsorbtion*, Presented at American Gastroenteterlogical Association meeting, May 19-22, 1991, New Orleans, LA, USA.
9. Hiele M., Ghoos Y., Rutgeerts P. & Vantrappen G., *Starch digestion in normal subjects and patients with pancreatic disease, using $^{13}CO_2$ breath test*, Gastroenterolog., 96, 1989, pp. 503-509.
10. *Automated Breath $^{13}Carbon$ Analyser*, Innovation No. 9, 1995, Ed. Steve Brooks, Europa Scientific Ltd., England.

CORRELATION TIME AND MAGNETIC INTERACTIONS BETWEEN TEMPYO SPIN LABEL AND BLOOD PROTEINS

S. CAVALU[1*], S. SIMON[2], G. DAMIAN[2], M. DÂNŞOREANU[3], C.M. LUCACIU[3]

[1]University of Oradea, Faculty of Medicine and Pharmacy, Dept. of Biophysics, P-ta 1 Decembrie No.10, 3700 Oradea, ROMANIA, e-mail: meda@medanet.ro
[2]Babes-Bolyai University, Faculty of Physics,Kogălniceanu No.1, 3400 Cluj-Napoca, ROMANIA, e-mail: simons@phys.ubbcluj.ro
[3]University of Medicine and Pharmacy, E.Isac No.13, 3400 Cluj-Napoca, ROMANIA, e-mail: clucaciu@umfcluj.ro

ABSTRACT. Nitroxyl radicals exihibit a number of chemical and physical properties that make them extremely useful molecules for studyng biochemical systems, especially the metaloporphyrins. The EPR spectrum can be affected by the motional constrains and orientationof the label in the sistem, by the polarity of the sistem and by the presence of other species in the system such as reducing agent and paramagnetic ions.Conversely, a spin label can affect the properties of system. The aim of this work was to investigate the tempyo spin label as a report group for the interactions and the conformational changes of hemoglobin and bovine serum albumin, as function of pH.

X band EPR spectra of Tempyo spin label were recorded at room temperature for lyophylized samples containing bovin serum albumin and hemoglobin at various pH values, in order to follow the different type of interactions between the nitroxide radical and functional groups of proteins as well as the pH influence on molecular motion.

The rotational correlation time, in the framework of the "moderate jump diffusion" model for rotational difussion, is strongly influenced by pH variation. In both cases, the mobility of tempyo has a reduced value in acidic environment, and encreased in basic environment as a consequence of electrostatic interactions and hydrogen bonding formation.

Keywords: EPR, spin label, serum albumin, hemoglobin.

[1*] Corresponding author

Introduction

Interactions of spin label with hemic or nonhemic proteins might affect the spin label spectra and in the same time it is well known that the pH strongly influences the conformation of proteins leading to significant changes in the type and degree of these interactions. In the pH range from 2.5 to 11 we followed the effect of protein conformational changes on the interactions between the nitroxide and the active site of proteins and also the pH influence on molecular motion emphasized by the EPR spectra of the spin label.

The successful application of spin labeling to protein structure investigations is limited by the possibility to chemically change specific side chains in proteins. However, useful information on protein properties can be obtained by noncovalent spin labeling if the affinity of the protein for the label molecules is great enough to affect their motional freedom [1-4].

In the same time, EPR has been an invaluable tool for probing microscopic molecular motions in a variety of systems, including izotropic solvents [5,6], liquid crystals [7,8], model membranes and biomolecules [9,10]. The EPR spectrum of a nitroxide radical depends not only on the magnetic interactions of the unpaired electron spin but also on the reorientational motion of the probe molecule. The dependence is relatively simple when the reorientation is sufficiently fast, or more specifically, when $\tau\Delta\omega \ll 1$, where τ is the correlation time characterizing the motion and $\Delta\omega$ is a measure of magnitude of the orientation dependent part of the spin Hamiltonian. In this case the EPR spectrum is a simple superposition of Lorentzian lines.

For slower rotations, i.e., when $\tau\Delta\omega \geq 1$, the EPR spectrum depends in a much more complicated fashion on the combined influences of molecular motion and magnetic interactions and the line shape can be analyzed only by using a theoretical approach [11]. These "slow-motional" line shapes are most often calculated using the stochastic Liouville equation, which can be solved numerically [12] to obtain the EPR spectra for fast or slow motions and for various Markovian models for reorientation.

In the present work, noncovalent spin labelled bovin serum albumin (BSA) and bovine hemoglobin (BH) with Tempyo spin label (3-carbamoyl-2,2,5,5-tetramethyl-3-pyrrolin-1-yloxy) were investigated both in liquid and lyophylized samples, in the pH range $2,5 \div 11$, in order to obtain useful information related to the interaction between the nitroxide group and the active site of the proteins.

Materials and Methods

Powder bovin serum albumin and hemoglobin (>95% methemoglobin) from SIGMA Chemicals, were used without further purification. Proteins were hydrated in phosphate buffer physiological saline at a final concentration of 10^{-3} M. Tempyo spin-label (3-carbamoyl-2,2,5,5-tetramethyl-3-pyrrolin-1-yloxy), from SIGMA Chemicals (fig.1), was added to the liquid samples of each protein in a final concentration of 10^{-3} M (protein/spin label molar ratio 1:1) and the pH values were adjusted to the desired value in the range 2,5÷11. The amount of 5 ml from each sample was lyophylized for 30 hours at –5°C and used for the EPR measurement, at room temperature.

EPR spectra for lyophylized samples, were recorded at room temperature with a JEOL-JES-3B spectrometer, operating in X-band (9.5 GHz), equipped with a computer acquisition system. Samples were placed in quartz capillary tubes. The spectrometer settings were: modulation frequency 100 kHz, field modulation 1 G, microwave power 20mW. The computer simulation analysis of spectra, for obtaining the magnetic characteristic parameters, was made by using a program that is available to the public through the Internet (http://alfred.niehs.nih/LMB).

Results and Discussion

Figure 2 and figure 3 show a structural model for the conformations of these proteins, as well as a detailed view of the functional group of these proteins: the heme group of hemoglobin and the helix linked by disulphidric bonds in BSA. The characteristic powder EPR spectrum of a nitroxyl radical at X band is due primarily to anisotropy in the nitrogen hiperfine coupling. Fig.4 display the experimental and simulated spectra for tempyo labelled BSA, lyophilised. When the external magnetic field is along this axis, the nitrogen hyperfine splitting, A_{ZZ} , is about 35 G, while in the perpendicular plane, A_{XX} and A_{YY} are around 6.5 G. Computer simulation analysis of tempyo labelled BSA emphasize a Gaussian lineshape and a single paramagnetic species for the best fit of experimental spectra. Acording with [12,14], when rotational motion is slow enough that the spectra approach the powder spectrum limit, the rotational correlation time (τ) can be evalueated using the relation: $\tau = \alpha\ (1\text{-}\ A_{ZZ'}/A_{ZZ})^{\ \beta}$, where $\alpha = 2.25\ 10^{-9}$, $\beta = -0.615$ and $A_{ZZ'}/A_{ZZ}$ is the ratio of the observed splitting between the derivative extrema $2A_{ZZ'}$ and the principal value of A_{ZZ} determined from the powder spectrum. The results are consistent with the "moderate jump diffusion" model for rotational diffusion [11,14] in which the molecule has a fixed orientation for some average residence time τ and then "jumps" through an average angle of $(6D\tau)^{1/2}$ radians, where D is the diffusion coefficient.

As showed in fig. 6, the pH strogly influence the rotational correlation time with respect to BSA. In acid pH range, the NH_2 groups of the label molecule as well as those of the aminoacids residues are protonated. The fact that τ shows greater values in this range followed by a significant decrease in bazic pH range, indicate a low mobility of tempyo label in acid environment while a significant increase of mobility can be noticed in bazic pH range. A minimum mobility can be observed around the izoelectric point ($pH_i = 4,8$) of this protein. The pH dependence of correlation time (involving the mobility of the label as well) results on the one hand from the electrostatic interactions which are stronger in acid environment, and on the other hand, the mobility is reduced by forming hydrogen bonding with the exposed aminoacids residues of the protein [15]. One can correlate this observation with the fact that serum albumin undergoes reversible izomerization in the pH range $2,7 \div 7$ from expanded form caracterised by 35% α-helix content to normal form caracterised by 55% α-helix content , accompanied by a decrease in β- sheet [16,17]. It is wellknown that β- sheet conformation favourises the formation of hydrogen bonding.

Fig. 5 show the spectra of tempyo labelled hemoglobin. In perpendicular plane, the nitrogen hyperfine splittings are A_{xx} = 6.8 G and A_{yy} = 7.5 G, on the average. Along the z axis, A_{zz} = 35 G on the average, the values being similar to those calculated for covalently labelled methemoglobin and other porphyrins in frozen samples under 50 K [18,19]

In the present study of noncovalent labelled hemoglobin, the best fit of the experimental spectra can be obtained by assuming the presence of two sites in hemoglobin, associated with two nonequivalent paramagnetic species [10]. Computer simulations indicate weighted sum of Gaussian lineshapes (static case) and Lorentzian lineshapes (dinamic case). The first species, with Gaussian lineshape and well resolved hyperfine splitting, is not influenced by the presence of the hemic iron.The correlation time versus pH (fig.6) reveals that in acid pH range the mobility of tempyo decreased and has a mimimum value near the izoelectric pH of hemoglobin (pH_i =6.8). By comparing with BSA case, we can notice that the mobility of tempyo is greater with respect to hemoglobin, which is not surprising if we take into account that hydrogen bonding opportunities depends on the β-sheet content: in hemoglobin the β-sheets represent around 50% while in BSA the percentage varies from 70% to 45%, depending on pH.

The second species in hemoglobin, with Lorentzian lineshape, is obviously influenced by the presence of the hemic iron. The lack of hyperfine structure of this specia is due the dipolar and spin-spin interaction between the nitroxide radical and the paramagnetic iron of the hem group. As shown in fig.6 the mobility of this species increases in acid environment, reaching a maximum value corresponding to pH_i =6.8 followed by a slow

decrease. We suggest that in bazic pH range, where the label is not subject to strong electrostatic interactions, dipolar and spin-spin interactions are preferential manifested. However, the latter are less intense than the former, as results from fig.6. By comparing these results with other results obtained for cytochrome c (another hemic protein) and ovalbumin (nonhemic, globular protein) we can notice that, on the averrage, the correlation time respect the following order:

$$\tau_{Hb} < \tau_{CIT} < \tau_{OVALB} < \tau_{BSA}$$

Hence, we can conclude that in hemoglobin, the mobility of tempyo label is less affected by the pH variation. This conclusion is supported by the comparison presented in fig.7.

Conclusion

Noncovalent labeling of proteins can give valuable informations on the magnetic interactions between the label molecule and the paramagnetic center of the proteins. The relevance of this interaction can be obtained from lineshape analysis: computer simulation for nonhemic protein assume a Gaussian lineshape, while for hemic protein is assumed a weighted sum of Lorentzian and Gaussian components. In the framework of the "moderate jump diffusion" model for rotational difussion, the rotational correlation time is strongly influenced by pH, due to the electrostatic intrreactions and hydrogen bonding.

REFERENCES

1. Morrisett, J.D., Wien, R.W., McConnell, H.M. (1973), *Ann. N.Y. Acad. Sci.* (1973), 222, 149-162.
2. Jost, P., Griffith, O.H. (1972) in *Methods in Pharmacology*, Chignell C. Ed., Appleton, New York (1972), p.223-276.
3. Morrisett, J.D., Pownall, H.J., Gotto, A.M., *J.Biol.Chem.* (1975), 250, 2487-2494.
4. Morrisett, J.D. in *Spin Labelling – Theory and application*, Berliner J. Ed., Acad.Press, (1975) pp. 273-331.
5. Hwang, J.S., Mason, R.P., Hwang, L-P., Freed, J.H., *J.Phys.Chem.* (1975), 79, 489.
6. Zager, S.A., Freed, J.H., *J.Chem.Phys.* (1982), 77, 3344-3360.
7. Polnaszek, C.F., Freed, J.H., *J.Phys.Chem.* (1975), 79, 2283.
8. Meirovitch, E., Igner, D., Moro, G., Freed, J.H., *J.Chem.Phys.* (1982), 77, 3915.
9. Tanaka, H., Freed, J.H., *J.Phys.Chem.* (1985), 89, 350.

10. Marsh, D., Horvath, L. I., in *Advance EPR – Application in Biology and Biochemistry* Hoff, A.J. Ed., Elsevier, Amsterdam (1989), p.707-752.
11. Earle, K.A., Budil, D.E., Freed, J.H., *J.Phys.Chem.* (1993), 97, 13289-13297.
12. Schneider, D.J., Freed, J.H., in *Biological Magnetic Resonance*, Berliner, L.J., Reuben, J., Eds., Plenum, New York (1989), vol.8, p.1.
13. Eaton, G.R., Eaton, S.S.,*Coord.Chem. Rev.* (1978), 26, p.207-262.
14. Schreider, S., Polnaszek, C.F., Smith, I., C., P., *Biochim.Biophys.Acta,* (1978), 515, 375-436.
15. Du,J.L.,Eaton G.R.,Eaton S.S.,*J.Magn.Res.*(1995),series A,115,213-221.
16. Foster, J.R., in *Albumin structure, Function and Uses*, Rosenoer, V.M., Oratz, M., Rothschild, M.A., Eds., Pergamon, Oxford (1977), p.53-84.
17. Carter, D.C., Ho, J.X., *Adv. Protein. Chem.* (1994), 45, 153-203.
18. Carter, D.C., He, X.M., Munson, S.H., Twigg, P.D., Gernerd, K.M., Broom, M.B., Miller, T.Y., *Science* (1989), 244, 1195-1198.
19. Budker, V., Du, J-L., Seiter, M., Eaton G.R., Eaton, S.S., *Biophys. J.*, (1995), 68, 2531-2542.
20. Rakowsky, M.H., More, M.K., Kulikov, A.V., Eaton, G.R., Eaton, S.S., *J.Am.Chem.Soc.* (1995), 117, 2049-2057.
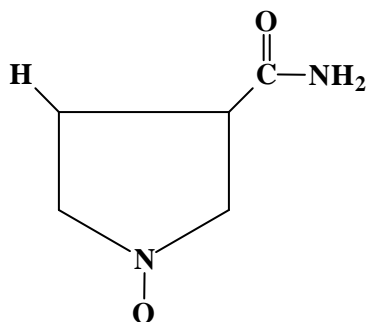
Fig.1*.* The structure of Tempyo label.
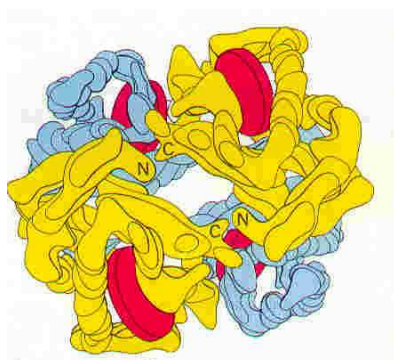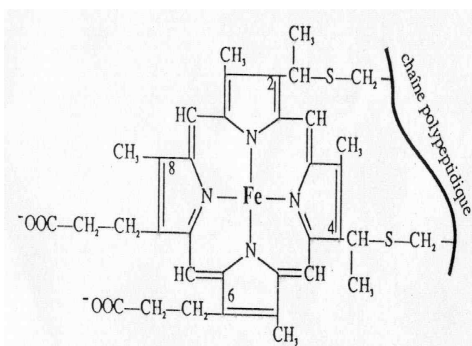
a **b**

Fig.2. Model for hemoglobin structure (a), and the local structure for the heme group of hemoglobin (b).
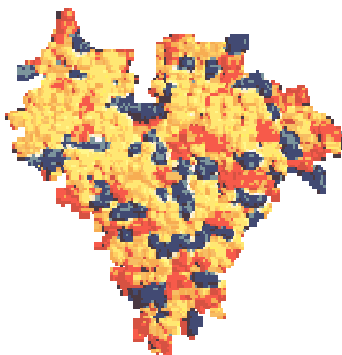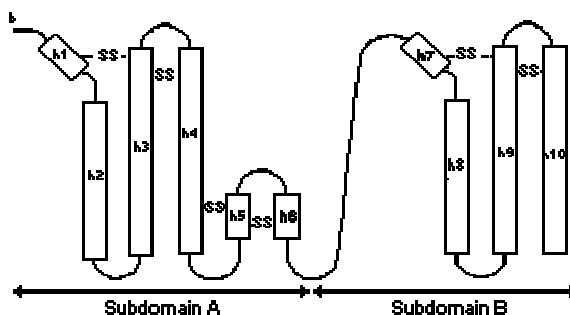
a **b**

Fig.3*.* Model for BSAstructure (a), and the localisation of disulfhidric bonds (b).

27
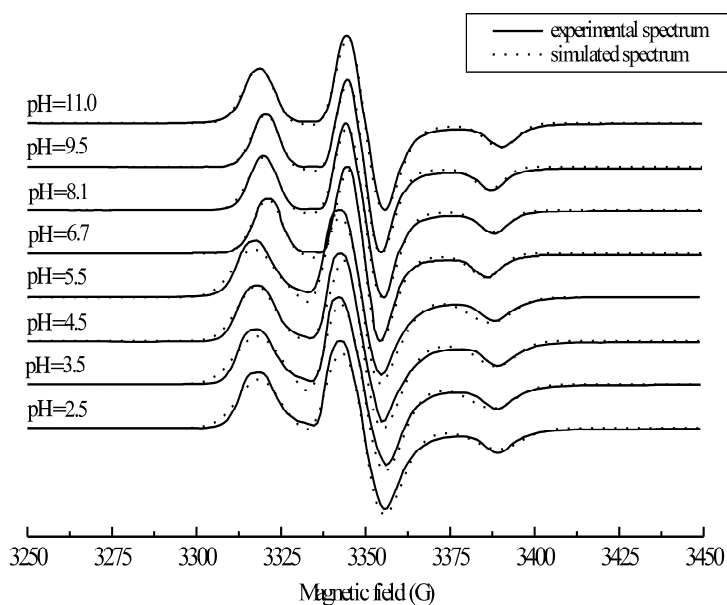
Fig.4. EPR spectra of noncovalent tempyo-labelled BSA at various pH values.
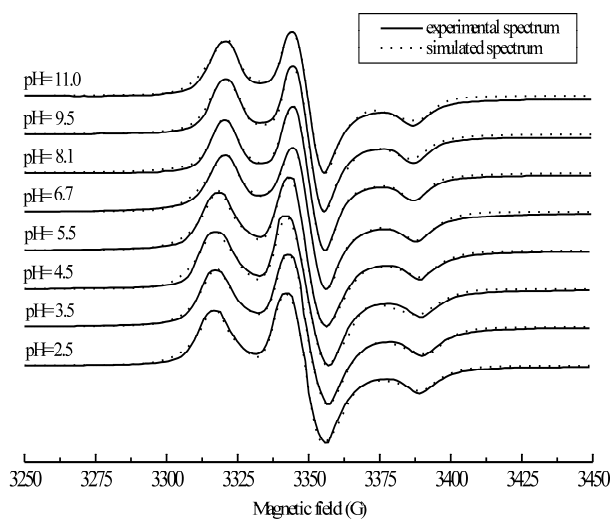
Fig. 5. EPR spectra of noncovalent tempyo-labelled hemoglobin at various pH values.
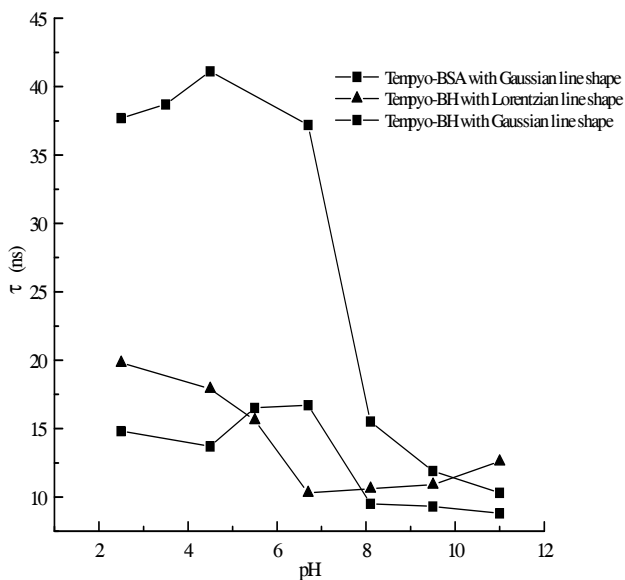
Fig.6. Correlation times (τ) as a function of pH for Tempyo labelled bovine serum albumin (BSA) and bovine hemoglobin (BH).
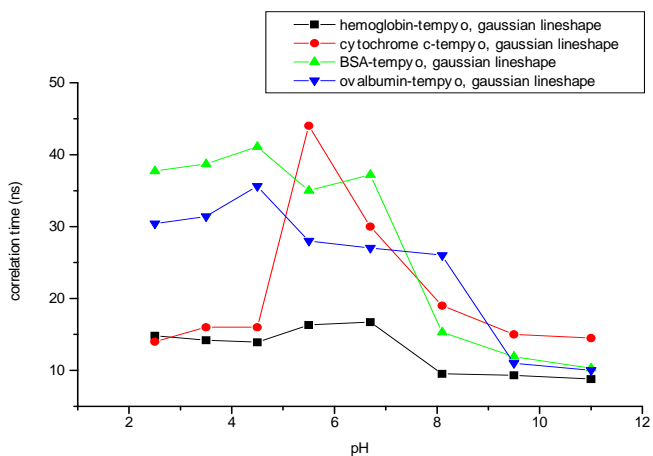
Fig.7. Correlation time versus pH for "gaussian" components in different tempyo labeled proteins.

VIBRATIONAL RAMAN STUDY OF FREE- AND ADSORBED TEMPYO LABELLED CYTOCHROME C ON SILVER COLLOIDAL SURFACE

S. CAVALU[1]*, S. CÎNTĂ-PÎNZARU[2], N. LEOPOLD[2], W. KIEFER[3]

[1]*University of Oradea, Biophysics Dept., 1 Dec. Square, No. 10,
RO-3700 Oradea, Romania*
[2]*Babes-Bolyai University, Physics Dept., Kogalniceanu 1,
RO-3400 Cluj-Napoca, Romania*
[3]*Institut für Physikalische-Chemie, Universität Würzburg,
Am Hubland, D 97074 Würzburg, Germany*

ABSTRACT. Resonance Raman spectra of cytochrome c were recorded and compared to those of the tempyo labelled cytochrome c in the pH range from 6.7 to 11. In this pH range the resonance Raman spectra indicate a stable conformation of the cytochrome c heme group. Surface enhanced resonance Raman spectra (SERRS) of pure or labelled cytochrome c were interpreted in terms of structural changes of the tempyo labelled protein adsorbed on the silver colloidal surface. The enhancement of the bands assigned to porphyrin macrocycle stretching mode allowed the supposition of N-adsorbtion from porphyrin ring on to the colloidal surface. Tempyo label was found to be inactive in the resonance Raman or SERRS spectra of cytochrome c and was supposed to be attached within a distance from the heme group.

Keywords: Cytochrome c, Raman, SERRS, tempyo label.

1.   Introduction

In spite of the existence of a large amount of data in the field of biological application of Raman spectroscopy, and, in particular, of resonance Raman applied to heme proteins, it is very difficult to outline a complete vibrational characterization of them [1]. The current traditional methods of analysis of proteins are time consuming and expensive, and therefore, more efficient techniques are desirable. Raman spectroscopy is an important tool for the determination of biomolecules structure and extensive research has been undertaken [2-4].

---

[1]* Corresponding author: Simona Cavalu, E-mail: meda@medanet.ro

The lower sensitivity and effects of fluorescence on the normal Raman spectra of these molecules have lead to the extension of research in the direction of surface enhanced Raman scattering (SERS) [5]. The latest consensus is that as a result of the electromagnetic enhancement, the SERS spectrum of molecules is virtually an enhanced version of the compounds of the normal Raman spectrum. However during charge transfer, some vibrations will be altered due to the interaction of molecule with the nanometric surface, resulting in the corresponding spectrum of the molecule-surface complex [6].

Cytochrome c is an essential component of mitochondrial respiratory electron transport chain [7]. The structure of cytochrome c is very similar to hemoglobin concerning the heme group, the active site of this protein (Fig. 1). This group is attached to the protein not only by one axial ligand (ε-imidazole nitrogen of histidine) of the iron atom, as in the case of hemoglobin. In both oxidation states, there is a second axial ligand, the sulfur atom of methionine 80, which is part of the protein. Additionally, the heme is linked to cysteine 14 and cysteine 17 by two thioether bonds [7, 8].
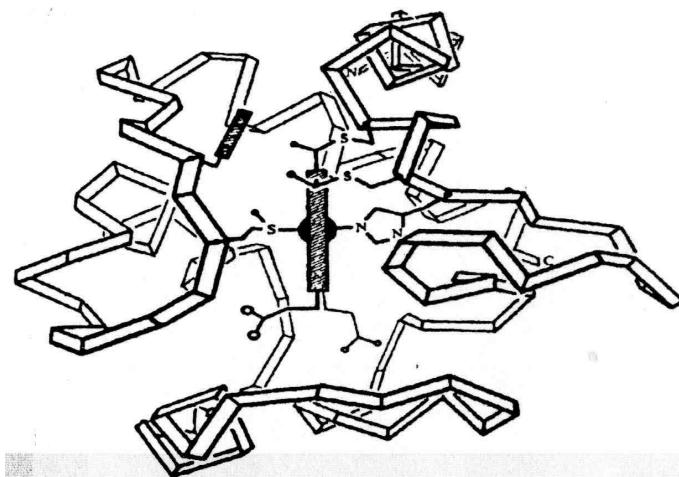
Fig. 1. Model for cytochrome c structure [8].

A typical stable nitroxyl free radical, widely used as ESR spin label, tempyo (2,2,5,5-tetramethyl-3 pyrrolin-1-yloxy-3 carboxamide)(Fig. 2) was applied for labelling the solutions of cytochrome c at various pH (6.7, 8.1, 9.5 and 11). In order to study the magnetic interaction between the spin label and the functional group of this protein (spin-spin and exchange phenomena) and also the motional effects in spin label spectra, samples for EPR spectroscopy were prepared and subject to a parallel investigation
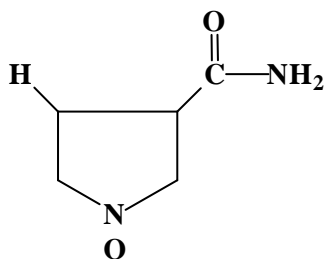
Fig. 2. *The structure of tempyo spin label.*

(data not shown here). The EPR investigations followed the pH influence in rotational correlation time of tempyo with respect to this protein in the framework of "moderate jump diffusion" model for rotational diffusion [9,10]. The localization of the label in the protein-label complex structure could influence the vibrational structure and, consequently, the adsorbtion behaviour of the protein. Therefore, in this paper we present vibrational Raman and SERS investigations on the tempyo labelled ferrocytochrome c in the pH range between 6.7 and 11, where the mobility of tempyo is assumed to be sensitive with respect to this protein. The extension of the study to the surface enhanced Raman spectroscopy was performed in order to check the influence of tempyo label to cytochrome c adsorbtion and to study the binding sites and binding mechanisms of tempyo in the tempyo-protein complex, if there exists any.

2. Experimental

2. 1.   *Chemicals*. Cytochrome c and tempyo spin label powder were purchased from Sigma and used without further purification. Figure 1 and figure 2 present a model for cytochrome and tempyo spin label structure, respectively. Cytochrome c was reduced with a small excess of sodium dithionite. Samples were prepared in phosphate buffer physiological saline at a final concentration of 10^{-3} mol/l. Non-covalent labelling of each cytochrome c sample was made in a protein/ tempyo spin label molar ratio 1:1. The pH range was adjusted between 6.7 to 11. A small amount of 5 ml from each sample was lyophilized for 30 hours at -50^0 C and than used as powder Raman sample.

Colloidal silver substrate was prepared according to the Lee-Meisel procedure [11]. The absorption maximum of the freshly prepared colloid was centered at 423 nm. Proteins were rehydratated in buffer solutions for each pH value. A small amount of about 10 μl 10^{-2} mol/l protein solution at each pH was added to 2 ml colloidal silver, resulting a final sample concentration of 5 x 10^{-5} mol/l.

2.2.   *Apparatus.*

A micro-Raman setup was employed in order to record the Raman spectra of lyophilized powder samples. The 514.5 nm line of an argon ion laser (Spectra Physics, Model 166) was applied for excitation. The scattered light was collected in back–scattering geometry by focusing a x50 objective (Olympus ULWD MSPlan50) on the entrance slit of a spectrometer LabRam, Dilor with 1800 grooves/mm diffractive grating. The detection system consisted of a charge–coupled multichannel detector (CCD, SDS 9000 Photometrics). The acquisition of a single spectrum typically takes about 100 s and 4 repeats on each sample were done. Each Raman spectrum is the result of 4 accumulations with 100sec. exposure time using a laser power of about 12 mW. The spectral resolution was 3cm^{-1}.

3. Results and Discussions

Excitation with the 514.5 nm line falls into one of the absorption bands (408, 520 and 544 nm) of cytochrome c, leading to the resonance Raman (RR) spectra of the sample. Fig. 3A presents the RR spectrum of pure cytochrome c in comparison with the spectra of cytochrome c at different bazic pH values (6.7, 8.1, 9.5 and 11). Very strong bands at 1580 ($\nu_{(C=N)}$) and 1308 cm^{-1} (porphyrin stretching), strong at 1530 ($\nu_{(C=C)}$), 1393, 1356 cm^{-1} ($\nu_{(=C-N)}$) and medium at 1225 ($\delta_{(C-H)}$), 1166, 1124 cm^{-1}($\nu_{(C-C)}$) are observed. These bands are in concordance with the previous reported results on cytochrome c [12-14]. The band at 1225 cm^{-1} is belived to arise from an in-plane bending vibration of the methine hydrogens . In our RR spectra this vibration seems not to be affected by the pH variation, even if H-NMR and visible absorbtion studies [15] have shown that pH, temperature or ionic strength perturbations readily displaced the methionine ligand. It has been proposed that the loss of the methionine ligand results in the loss of the electron transport capability of cytochrome c [15]. When comparing the resonance Raman of cytochrome c in both oxidation state, ferricytochrome c exhibited a very different Raman spectrum from ferrocytochrome c, the last one being much more sensitive to the resonance Raman [13].

For the ferricytochrome c (oxidized form, Fe^{3+}) three bands of medium intensity, at 1560, 1585 and 1638 cm^{-1} were reported and interpreted as mixed C=C and C=N stretching vibrations of the porphyrin macrocycle [13]. Other resonance Raman spectra [16] of oxidised and reduced cytochrome c in solution have correlated the spectral band at 1584 cm^{-1} with the existence of low spin iron in both oxidation states and the position of the spectral band at 1375 or 1360 cm^{-1} with oxidized or reduced cytochrome c, respectively. A general shift towards lower frequency was concluded upon reduction of to Fe^{3+} to Fe^{2+}. On the other hand, chemical

modification of heme protein resulted upon the conversion of iron from low to high spin state has been correlated with a 1584 to 1566 cm^{-1} shift which is ascribed to the movement of the iron atom out of the heme plane upon the increasing of its spin state [16-18]. Based on the previous observations, we conclude that the strong band located at 1580 cm^{-1} (Fig. 3A) indicate the presence of low spin Fe^{2+}.

Tempyo spin label was expected to reveal a scattering contribution in the cytochrome c–tempyo complex, based on its Raman spectrum (Fig. 3B, a). From the Figure 3B one can observe that the label does not bring
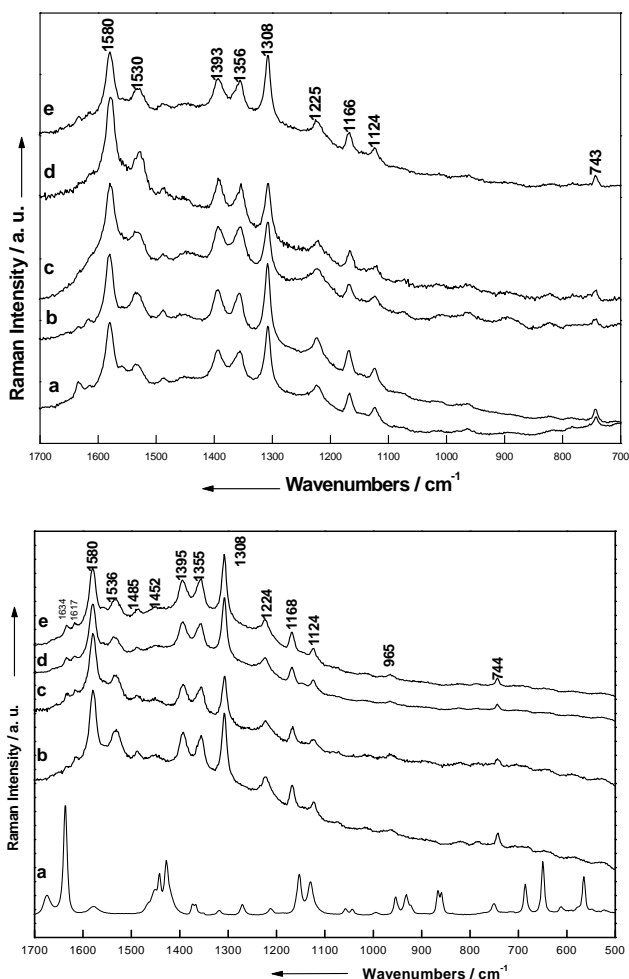
Fig. 3. A (top). Resonance Raman spectra of pure- a) and lyophilized cytochrome c, at various pH: b) 6.7; c) 8.3; d) 9.5; e) 11. **B** (bottom). Raman spectrum of tempyo a) and resonance Raman spectra of the lyophilized tempyo labeled cytochrom c, at various pH: b) 6.7; c) 8.3; d) 9.5; e) 11. Excitation:514.5 nm, 12 mW on the powder sample.

any contribution to the vibrational structure of the protein, in spite of its large Raman cross section. This is probable due to the folding complexity of the protein, which limits the scattering effect of the small tempyo label. We suposse that the label was attached within a distance from the heme group in the studied pH range. Comparison of the Fig. 3A and B reveals a very stable conformation of the cytochrome c heme group in the pH range from 6.7 to 11. Furthermore, RR spectra do not reflect changes in the protein content around the porphyrin ring, in spite of the fact that the amino acid residues are very sensitive to the pH variation. All these pH values are lower then the isoelectric point, excepting pH=11.

Fig. 4 A and B present the surface enhanced resonance Raman spectra (SERRS) of pure cytochrome c, at the corresponding pH values,
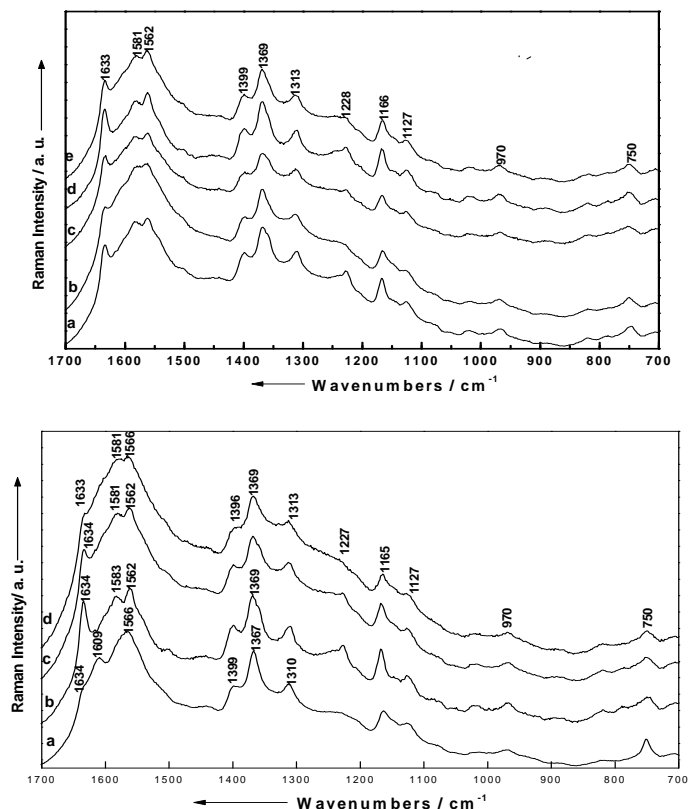
Fig. 4. A (top). SERRS spectra of pure a) and lyophilized cytochrom c at various pH: b) 6.7; c) 8.3; d) 9.5; e) 11; *B* (bottom). SERRS spectra of tempyo labeled cytochrom c, at different pH: a) 6.7; b) 8.3; c) 9.5; d) 11. Excitation: 514.5 nm, 12 mW on the sample.

cytochrome c [19] showed that this spectrum seems to be very similar to its solution resonance Raman spectrum. Other previous work, based upon the comparison between SERRS and RR spectrum of oxidased form concluded that the heme was detached from the protein at the silver surface and formed oxo-dimers [20].

In the present work, on passing from RR to SERRS , large differences can be observed both in band positions and relative intensities. The dominant SERRS bands are observed at 1633 ($\nu_{C=N}$) , 1581 ($\nu_{C=N}$), 1562($\nu_{C=C}$), 1399, 1369 ($\nu_{(=C-N)}$), 1166(ν_{C-C}) and 1127 cm^{-1}. In contrast with the coresponding RR spectra, the in-plane bending vibration of the methine hidrogens (1227 cm^{-1}) is poorly represented but it seems to depend on the pH.

The blue shift from 1356 cm^{-1} (RR) to 1369 cm^{-1} (SERRS) and the enhancement indicate an interaction of the N atoms from ($\nu_{(=C-N)}$) bonds of porphyrin ring, through the σ bonds with the metal surface [21]. From this analysis we conclude a chemisorption of the cytochrome c on the silver nanoparticles.

According to the literature [22], porphyrin macrocycles in cytochromes and other porphyrin compounds bind edge-on to silver surfaces via propionate functional groups. Other reports [1] showed that the protein envelope prevents the heme group from coming in direct contact with the silver electrode surface. If the heme group would be located far from the surface, the local electromagnetic enhancement of the heme modes would be less representative. Remaining only the resonance contribution in the signal intensity, this would be similar to the RR signal, which is not observed in our SERRS spectra.

The SERRS spectral features of cytochrome c are certainly due to the adsorbtion-induced structural changes in the heme pocket, resulting in the corresponding enhancement of the porphyrin – Ag complex modes, independent on the pH or the presence of tempyo label.

The pure tempyo was found to be SERS inactive, independent on the concentration in the colloidal final sample or laser power. A similar inert behaviour of tempyo label was found in the tempyo-labelled ovalbumin, where the resonance Raman contribution to the enhancement is absent [23].

Conclusions. In the studied pH range, the RR spectra of cytochrome c indicate a stable conformation of the heme group and the presence of low spin Fe $^{2+}$. The tempyo label was supposed to bind at a distance from the heme group in the bazic pH range from 6.7 to 11.The SERRS spectra of tempyo labelled cytochrome c at different pH values strongly differ from their corresponding RR spectra, both in band positions and relative intensities. From the SERRS study of cytochrome c, a chemical contribution to the total enhancement was concluded. The

enhancement of the bands assigned to the porphyrin macrocycle stretching modes allowed the supposition of nitrogen adsorbtion from the porphyrin ring on to the colloidal surface.The adsorbtion of the cytochrome c on the Ag surface under resonance condition is independent on the pH in the range from 6.7 to 11 or the presence of the tempyo spin label.

REFERENCES

1. 1.B. Schrader, Infrared and Raman Spectroscopy, Methods and Applications, Part I, VCH Publishers Inc., Winheim, New York, Basel, 1995, p. 362.
2. I. Nabiev, M. Manfait, Rev. Inst. Fr. Pet, 48, 1993, 261.
3. T.G. Spiro, Biological Application of Raman Spectroscopy, Vol. 1-3, Wiley & Sons, USA, 1987-1988.
4. M. Coletta, H. Costa, G. De Sanctis, F. Neri, G. Smulevich, D. L. Turner, H. Santos, J. Biol. Chem, 271, 40, 1997, 24800-24804.
5. J. A. Creighton, Anal. Proc. 30, 1993, 28.
6. S.Stewart, P. M. Fredericks, Spectrochim. Acta, Part A, 55, 1999, 1615-1640.
7. L. Stryer, Biochemistry, W. H. Freeman and co., San Francisco, 1981, p. 77-83.
8. E. Shechter,Biochimie et Biophysique des membranes-Aspects structuraux et fonctionnels, Masson, Paris, 1990, p. 223-238.
9. G. Damian, O. Cozar, V. Miclăuş, C. Paisz, V. Znamirovschi, V. Chis, L. David, Colloids.Surf.,137, 1998,1-6.
10. 10.K.A.Earle,D.E.Budil,J.H.Freed, J.Phys.Chem.97,1993,13289-13297.
11. P. C. Lee D. Meisel, J. Phys. Chem., 84, 1982, 3391.
12. T. C. Strekas, T. G. Spiro, Biochim.and Biophys.Acta, 351, 1974, 237-245.
13. H. Brunner, Biochem. and Biophys. Research Com.,vol.51,4, 1973, 888-894.
14. L. A. Nafie, M. Pezolet, W. L. Peticolas, Chem. Phys. Lett., 20, 1973, 563-568.
15. N.Ossheroff,D.Borden,W.H.Koppenol,E.Margoliash, J.Biol.Chem.225,1980,1689-1697
16. 16.T.Yamamoto,G.Palmer,D.Gill,I.T.Salmen,L.Rimai, J.Biol.Chem.,248,1973,5211.
17. T.C.Strekas,T.G.Spiro,Biochim.Biophys.Acta,263,1972,830
18. T. M. Loehr, J. S. Loehr, Biochim. and Biophys. Research Com., 55, 1, 1973, 218-223.
19. 19.T.M.Cotton,R.P.van Duyne, J.Am.Chem.Soc.,102,1980,7960.
20. 20.G.Smulevich,T.G.Spiro, J.Phys.Chem.89,1995,5168-5182.
21. 21.T. M. Herne, A. M. Ahern and R. L. Garell, J. Am. Chem. Soc. 113, 1991, 846-854.
22. J. deGroot, R.G. Hester, J. Phys. Chem., 91, 1987, 1693.
23. S. Cinta-Pinzaru, S. Cavalu, N. Leopold, R. Petry, W. Kiefer, J. Mol. Str., in press.

SEASON AND BUILDING MATERIAL INFLUENCE ON INDOOR RADON CONCENTARATION IN HOUSES FROM TRANSYLVANIA

C. COSMA[1], D. RISTOIU[1], C. CINDEA[2], STELA RÂMBOIU[3]

[1] *University "Babeş-Bolyai", Faculty of Physics, 3400 Cluj Napoca, Romania*
[2] *Health Public Division, 3400-Cluj-Napoca, Romania*
[3] *Centrul de Mediu şi Sănătate, 3400-Cluj-Napoca*

ABSTRACT. The purpose of this work is to see the influence of the heat preservation in the cold season and also to show the building material influence on the indoor radon concentration in dwellings. Three methods were used to measure the radon content in houses and buildings (workplaces). The results of measurements show that in the winter season the indoor radon concentration is about 2 times higher than in the summer season for these regions from Transylvania. This fact is due that in the cold season there is an evident tendency to preserve the heat, that is, the natural ventilation is very feebly. The influence of building materials on indoor radon concentration is clear shown in the fourth region namely Stei which is a region in the neighborhood of an uranium mine and in some of these houses uranium wastes were used as building materials.

INTRODUCTION

Radon sources are the main natural sources of population irradiation (about 50%). In some regions this percentage can increase even to 80-90% as in Cornwall (England) region [1]. Because, between the indoor radon exposure and the lung cancer risk seems to be a direct relation [2] the knowledge of the radon concentrations in buildings is a very important parameter characterizing the indoor air quality.

The assessment of lung cancer risk due to radon exposure for general public is based upon the research of epidemiological studies made on uranium miners [3,4]. The main difficulty in this estimation consists in the fact that uranium miners are exposed, besides to radon and radon progeny, also to the external doses and especially to the radioactive dust with uranium particles which can fasten on the bronchial tubes [5].

To find this parameter the epidemiological studies made on general public must be very carefully designed in order to obtain significant results since the effect is masked enough by other factors as smoking, chemical pollutants, stress, individual resistance and uncertainties in radon exposure assessment [6]. The last specified factor can be minimized by measuring of indoor radon concentrations for large time period (one year) and in the case when these measurements are shorter(3 months or 6 months) a correction or an adequate choice of time measurement interval is necessary. Sometimes these uncertainties can be found by retrospective radon measurements [7,8]. It is possible that incorrect estimation to the indoor radon exposure to be the reason for which the results of some performed epidemiological studies are inconclusive [9-11].

Romania is a country from Central Europe (237.000 km^2) having a continental climate, with +21°C in July and –6°C in January as average temperatures. Transylvania as northwestern part of Romania presents moreover a cold season prolonged. In the last years we made about 400 integrating measurements for indoor radon in houses in the frame of an epidemiological study in two districts of Transylvania [12] and with occasion was observed the influence of thermal comfort and building materials on the results of the indoor radon concentrations. Also, some measurements using Lucas cells method and especially the continuos monitoring with Radim device made in the last year confirm this influence.

EXPERIMENTAL METHOD

The integrating measurements were made using the Karlsruhe radon diffusion chamber with makrofol electrochemically etched track detectors. The makrofol detectors were exposed for three months period in the cold season (June-August) both for detached houses and flats in the blocks of flats. Also, some workplaces in public buildings were considered. The etching and reading of the detectors were made at the Nuclear Physics Laboratory of Gent.

The Lucas cells grab samples method utilizes the scintillation flasks of 500 ml and to standardize the measuring conditions all determinations were made after five hours of closing rooms. The calibration of Lucas cells was made using a radium chloride standard source.

Starting from this year we made continuos measurements of indoor radon by means of a Radim monitor (Czech Republic) which utilize a radon diffusion chamber where the alpha emission of RaA(^{218}Po) is measured with a Si detector. The minimum activity for an hour of sampling is 30 Bq/m^3 with statistical error of ±20%. The memory of this device allows the continuos monitoring of radon content for long time.

RESULTS AND DISSCUTION

In Figure 1 are shown the results for radon concentrations in the case of 18 dwellings and work places from Herculane city obtained by integrating measurements in the winter season (December-February) and in the summer season (June-August). The detectors were always settled in bedroom at the ground floor for exactly 3 months period in the case of the dwellings and in four offices of public buildings also at ground floor. One can see that with two exceptions the winter radon concentration is much greater as summer concentration. The first exception is remarked for No.1 sample, which is a hotel office where the same natural ventilation exists in the winter as in the summer. The sample No.11 is a bedroom with a poor ventilation also in the summer due to unutilization or a short time utilization in that year (1995).
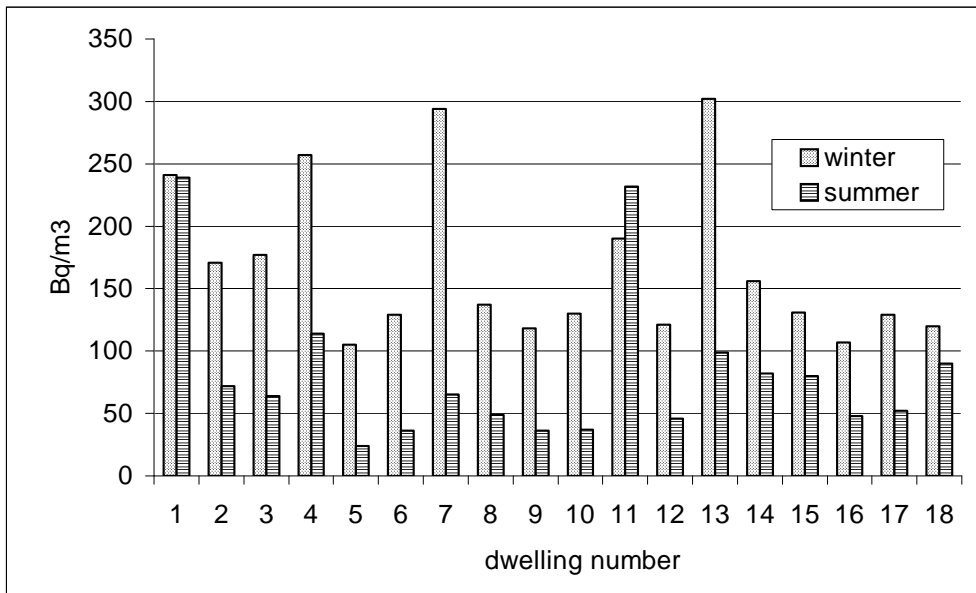
Figure 1. The radon concentration in winter and summer (14 bedrooms and 4 offices) from Herculane area

Seasonal variation of radon at ground floor (Bq/m³)
Herculane (H) and Cluj (C) cities.

Type of building	Number of samples	Radon average concentration Bq/m³		Ratio
		Winter	Summer	
Detached houses (H)	10	216	106	2:1
Flats block (H)	4	123	42.5	3:1
Offices (public) (H)	4	240	124	2:1
Cluj detached houses (C)	6	162	91	1.8:1
Cluj flats[*] (C)	4	115	55	2.2:1

[*]**upper level (>2)**

In the last two lines of Table 1 about the same ratio (1.8:1) was obtained for six bedrooms at ground floor from city Cluj in detached houses and (2.2:1) ratio for bedrooms in block of flats at upper level (>2).

In Figure 2 it is shown the daily variation of indoor radon in one house from Oradea city (bedroom in detached house) in January (1998) and in June (1998) registered with Radim device. The value of June is about 2.4 times smaller as January value. From this figure it is clear that an important variation of radon content exists during 24 hours due to accumulation of this gas in the night period. The computer program of this monitor directly indicates the mean value.
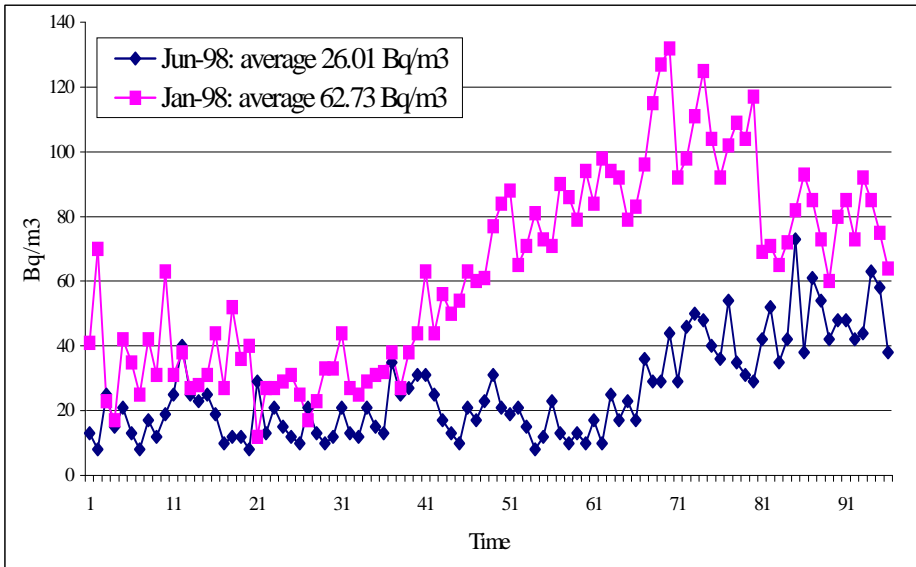
Figure 2. *Daily variation (Radim monitor) and averages of radon content in one house from Oradea city (24 hours of measurement).*

The grab samples method (Lucas cells) not confirm entirely these results being inadequately to establish this ratio because it apply the same protocol (0.5 h-strong ventilation following 5h-of room closing) to may standardize these determinations. Therefore, the adequately methods (integrating or continuos) for radon content determination in dwellings show that a ratio of 1.5 to 3 between winter/summer values exists for the all three regions investigated (Herculane, Cluj, Oradea). It is clear that tendency to preserve the heat during winter season can explain these ratios. Generally the cost for monthly heating in the cold season for a normal detached house is about 10-15% from the monthly amount gained by a standard family.

In addition, further two mechanisms can contribute of this growth of indoor radon during cold time. These are: (a) the chimney effect which contributes to the radon extraction from sublab of dwelling; (b) the soil frost during winter which can conduct the diffusive or connective soil flux towards house sublab.

The influence of building material was considered in this work by including in our study an uranium region. This is Stei city and its neighborhood. Stei city is placed at 15 km from an uranium mine (Baita) intensively worked in the 1950-1960 period. The results obtained by integrating radon measurement of three months for 80 dwellings of Stei area are shown in lognormal distribution in Figure 3. In this figure can be seen that this curve with two maxim presents high (234 Bq/m^3 and 269 Bq/m^3) and very high(1070 Bq/m^3 and 1231 Bq/m^3) values both for geometric mean (GM) and arithmetic mean (AM).

These results can be compared with the results obtained for 105 dwellings in different places from Cluj and Bihor districts (Transylvania) shown in Figure 4. representing about the first quarter of the results which will be gathered in the frame of an epidemiological study regarding the lung cancer risk. The geometric mean of 132.14 Bq/m^3 for these measurements is very closed to median value of 134 Bq/m^3, therefore, a classical lognormal distribution was found. The difference between the dwelling radon from Stei area and the other regions from Transylvania is rather high (234 Bq/m^3 for GM in Stei area comparatively with 132 Bq/m^3 as GM for the other regions) and can be attributed to building materials with a higher radioactivity of uranium in Stei region.
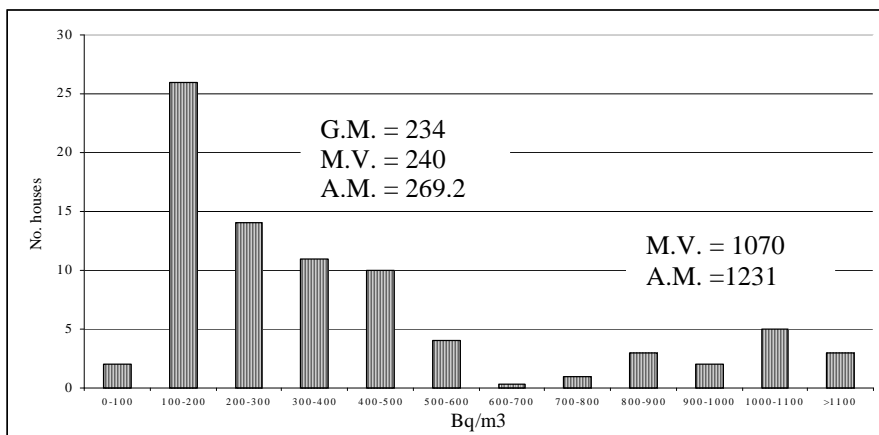
Fig.3. Distribution with two maxima for radon concentration in Stei area.
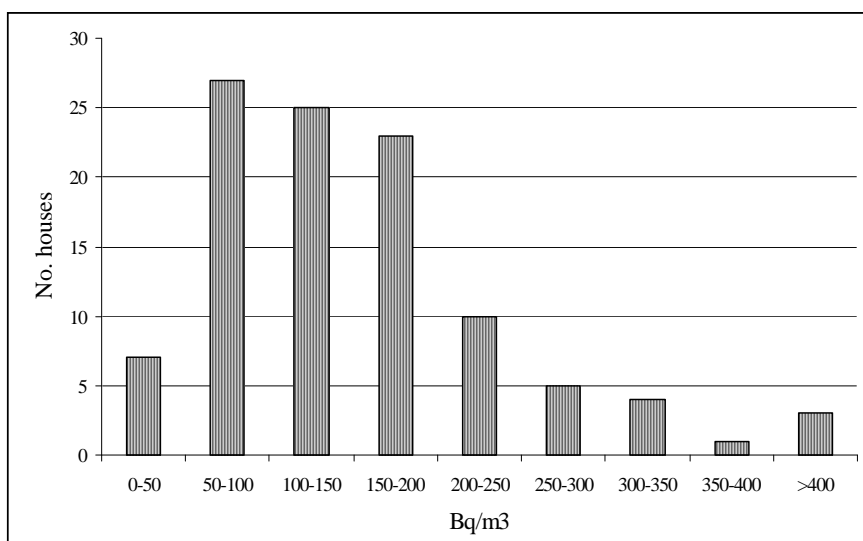
Fig.4. Lognormal distribution for radon in 105 dwellings from Transylvania region.

Moreover the second very high maximum of 1231 Bq/m^3 from Figure 3 shows clearly that in some cases the men were utilized as building materials (probably as ground walls or as filling) the uranium waste arising from Baita uranium mine. All 15 dwellings forming this group are built after 1950.Many measurements are still necessary for a good characterization of this area.

CONCLUSION

Rather high indoor radon concentration in Transylvania region comparing with other European countries [13] and according with Scandinavian [14] and Ukrainian [15] values were found. Generally the values for indoor radon are two times higher in the cold season as in the warm season in direct connection with the tendency to preserve the heat. This ratio was found for all three areas investigated.

The using of some materials with grown uranium content even of uranium waste as building material is evidently for Stei area where high and very high average indoor radon concentrations were measured.

REFERENCES

1. T. K.Ball, J. K. H. Miles, *Environ. Geochem. Health*, **15**, 1993, 27-36.
2. D. Bodansky, M.A. Robkin, D. Stadler, *Indoor Radon and its Hazards,* University Washington Press, Seatle and London, 1990.
3. J. M. Samet, D. R. Pathak, M. V. Morgan,. *Health Phys*, **61**, 1991, 745-752.
4. I. Sevec, E. Kunz, L.Tomasek, V. Placek, I. Horacek, *Health Phys*. **54, 1988,** 27-46.
5. M. Tirmarche,. *Radiation and Society*, *International Atomic Energy Agency. Vienna.* Vol.2, 397-398, 1996
6. O. Axelson, K Anderson,. *Scan. J. Work Environ. Health***, 14** , 1988, 286-292,
7. G. Messen, A.Poffijn, I.Uyttenhove,. *Radiation. Measurements*, **25**, 1995, 591-594.
8. C. Samuelsson,. *Nature,* **334**, 1988, 338-340.
9. C. Svensson, G. Pershagen, I. Klaminek, I. *Cancer Res*., **49**, 1989, 1861-1865.
10. A. Auvinen, I. Makelainen, *Cancer Inst*. **88**, 1996, 966-972.
11. I. M. Samet. *I. Natl. Cancer Institute*, **81**, 1989, 745-757.
12. C. Cosma, A. Poffijn, T. Jurcut, D. Ristoiu, Doina Coroian, Roxana Buda, *Balkan Phys. Lett*.,**5**, 1997, 1693-1697.
13. NRPB *Natural Radiation Maps of Western Europe*, National Radiological Protection Board, Chilton, Didcot, Oxon, 1993.
14. G. Perhagen, Z. Liang, Z. Hrubek, C. Sevensson, J. Boice, *Health Phys*., **63**, 1996, 179-186.
15. T. A. Paveklo, I. P. Los, *Radiation Measurements*, **25**, 1995, 595-600.

THE INFLUENCE OF THE RELATIVE HUMIDITY ON THE DETECTION EFFIENCY OF RADIM 2P RADON MONITORING DEVICES

F. DANCEA[1], A. POFFIJN[2], C. COSMA[1]

[1]*Babeş-Bolyai University, Faculty of Physics, 3400 Cluj-Napoca, Romania*
[2]*University of Gent, Nuclear Physics Institute, 9000 Gent, Belgium*

ABSTRACT. The aim of the present study is to determine the humidity corrections, which has to be taken into account for Radim 2P radon monitor devices when accurate measurements in humid conditions are desired. We experienced the response of a Radim 2P device at different radon concentration levels (0.5 - 10kBq/m^3) when relative humidity varies in a large interval (20-90 %). Our results show a sharper decrease of device efficiency with humidity than the producer's prediction.

Keywords: Radon, Radim 2P, Relative humidity

Introduction

The Radim 2P device is a "grab sampling" radon monitor, which has been initially developed for continuous monitoring of indoor radon concentrations. The basic principle of this instrument is the measurement of the alpha activity of the radon decay product Po^{218} using a semiconductor detector. The measurement takes place in a diffusion chamber where only the radon entrance is allowed (without its air-borne decay products). Because most of the Po^{218} formed ions are positively charged the chamber wall is connected to the positive pole of a high voltage source and the surface of the semiconductor electrode is connected to the negative pole. The ion collection efficiency on the detector is also increased by the optimization of chamber design that leads to a specific electric field distribution in the detector vicinity. If in this chamber are vapors of water they will neutralize a part of the Po^{218} ions and affect the instrument sensitivity. The producer has studied this effect and describes in Operational Manual the dependence of the device efficiency on the relative humidity [1]. Also in the work [2] has studied the effect of humidity testing

four monitors and the results show that the corrections proposed by the constructor in the manual shows a systematical underestimation.

In the case of the precise measurements, e.g. intercomparison exercises [3] or special experimental setups [4], when accurate results are desirable, the results should be corrected for the humidity effect.

Many laboratories in Europe use such devices and a systematic study regarding especially high humidity influence is not reported. The aim of this work is to estimate the précis correction, which can be made in the case of the continuous monitoring of indoor radon using these devices.

Methods and materials

The Radim 2P device determine the radon concentration using the following equation:

$$C_{Rn} = \frac{N \cdot Cal}{t \cdot V_{eff}}$$

(1)

where:
- N is the measured number of impulses
- Cal is a calibration constant, only dependent by the instrument
- t is the sampling interval
- V_{eff} effective volume, include the collection and detection efficiencies and the forming probability of Po^{218} as a positive charged ion. This parameter is affected by the relative humidity and the device producer proposed the following linear dependence:

$$V_{eff} = A \cdot (1 - B \cdot RH_{22})$$

(2)

where A and B are two experimental constants and RH_{22} are the relative humidity at 22℃.

The slope of this linear dependence (B value) is the measure of the humidity effect degree: a larger value means a sharper decrease of effective volume with humidity. Producer's constants are A= 0.209 respectively B= 0.0021 and Van Deynse's constants are A= 0.197 respectively B= 0.0043. In the second case the B value is about two times larger than the first and 'official' one, meaning a twice-stronger effect of the humidity on the device efficiency than the producer prediction.

The relative humidity (RH_T) is the ratio between the amount of the water vapor present in the air and the maximum amount that the air could contain at the same temperature, in this case atmosphere being fully saturated with water. Because is strongly temperature-dependent the relative humidity must be recalculated for a fixed temperature. The

standard temperature was chosen to be 22℃ and the relative humidity at 22℃ (RH_{22}) can be calculated using the formula:

$$RH_{22} = RH_T \cdot (0.0013 \cdot T^2 + 0.006 \cdot T + 0.3516) \tag{3}$$

where T units are ℃

The Radim 2P instrument is calibrated for RH_{22} of 60%, meaning an effective volume of 0.182 l, i.e. a ratio between the measured (displayed) concentration and the real concentration level of about:

$$\frac{C_{measured}}{C_{real}} = \frac{V_{eff}}{0.182} = A^* \cdot (1 - B^* \cdot RH_{22}) \Rightarrow V_{eff} =$$

$$= 0.182 * \frac{C_m}{C_r} = A \cdot (1 - B \cdot RH_{22}) \tag{4}$$

If we introduce Radim 2P into an enclosure in which radon concentration and relative humidity can be strictly controlled, using a linear regression algorithm we can determine the above dependence.

The experiments were carried out by placing Radim 2P detector in bulb (a closed glass vessel of 231 l) of the Laboratory of Nuclear Physics in Gent, Belgium. The radon concentration in the bulb was increased at a certain level using a dry airflow flushed to a radon source with a known released activity (31 Bq/min). After the needed radon concentration level in the bulb was achieved the flow rate was stopped and the radon level was verified performing Lucas cell measurements. Considering only the radon decay (no leakage) the concentration level in the bulb is well known in every moment. Fig. 1 presents schematically the experimental set-up.
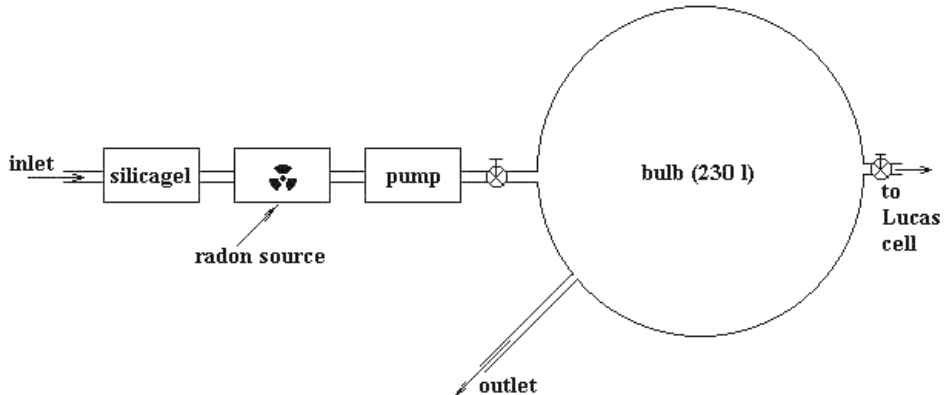
Figure 1. *The experimental setup.*

The relative humidity was increased by pumping the water vapors in the enclosure and measured using a Weather Monitor. In this way we achieved intervals of constant humidity, which were maintained for about

10 h each of them. Using Eq. (4) we have calculated the effective volume and for the each of these intervals of constant relative humidity an average value of V_{eff} has been considered. In this way the dependence of effective volume on relative humidity was determined.

Results and discussions

Three experiments were carried out on the three different radon concentration intervals: (8-1.3), (2.5-5) and (5-10) kBq/m^3. Fig. 2 plots the real radon concentration (in the case of 2.5-5 kBq/m^3), the measured radon concentration using the Radim 2P device and the relative humidity during the experiments. The obtained dependency of the effective volume versus relative humidity is presented in the Fig. 3. The large values of Pearson's correlation coefficient R>0.95, show a strong linear correlation between the experimental points.
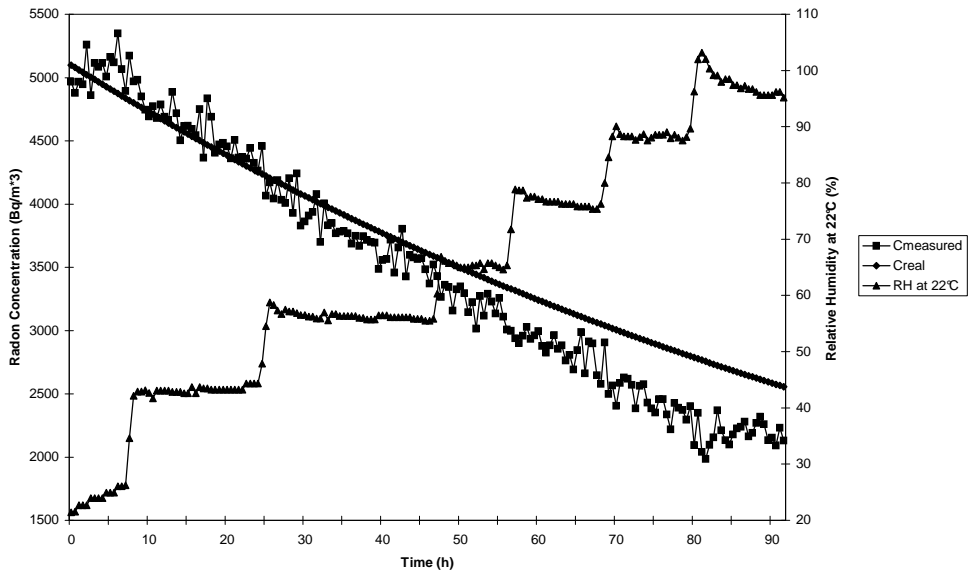
Figure 2. The real radon concentration, the Radim 2P measured radon Concentration and the relative humidity variation during the experiments.

Table 1 presents the dependencies of the effective volume on the relative humidity obtained for the each radon concentration interval. The good agreement between the humidity response functions of the Radim 2P device obtained in each of these three trials shows that the measured radon concentration level doesn't have any effect as regards our investigation.
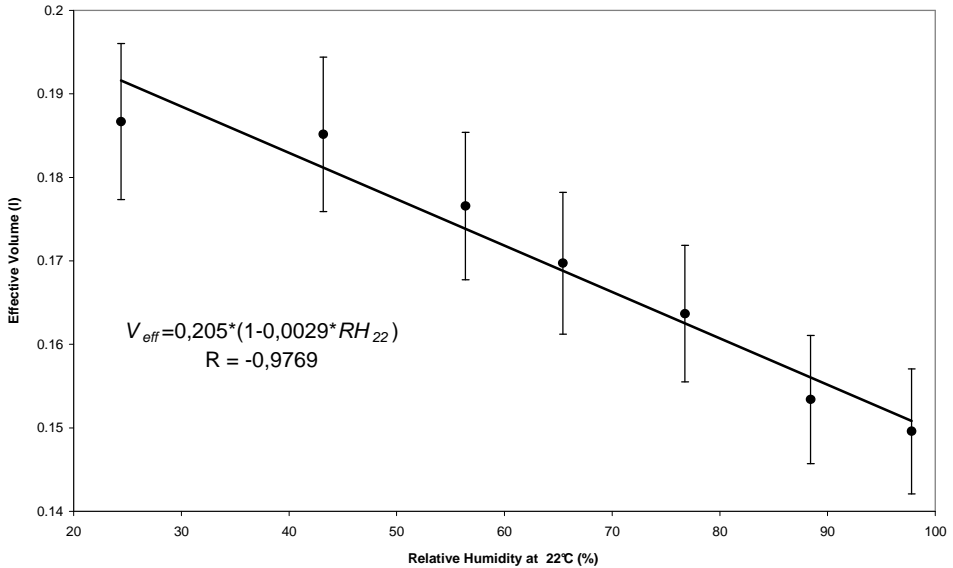
Fig. 3. *The results for the humidity correction of the effective volume obtained for the three different radon concentration intervals.*

Table 1

The results for the humidity correction of the effective volume obtained for the three different radon concentration intervals.

^{222}Rn Conc. Interval kBq/m^3	Effective Volume versus Relative Humidity at 22°C
0.8-1.3	$V_{eff}=0.210*(1-0.0028*RH_{22})$
2.5-5	$V_{eff}=0.205*(1-0.0029*RH_{22})$
5-10	$V_{eff}=0.206*(1-0.0029*RH_{22})$

In all of these cases the measurement error increase with humidity, meaning that a growing up in the relative humidity leads to a drop of the device accuracy. For large levels of humidity (RH_{22}>80 %) the device measurements are seriously underestimated. The explanation is that water vapors can neutralize the ions of Po^{218} and in this way decrease the efficiency of the collection of this radioisotope on the device detector. Our results show that the slope of the linear dependence is larger than the producer's predict, i.e. a sharper decrease of device efficiency with humidity.

51

For the tested device (Serial Number R/98/70) we propose the following correction for humidity:

$$C_{real} = \frac{C_{measured}}{1.137 * (1 - 0.0029 * RH_{22})} \qquad (5)$$

Conclusions

The response of the tested Radim 2P device is strongly affected by an extreme variation of the relative humidity, but using the determined humidity correction the result can be safely reconstructed.

Measurements in high humidity conditions using such devices need a special correction for humidity, the producer's correction being underestimated. The measured concentration level doesn't require a supplementary correction. The above described procedure could be routinely performed in the radon laboratories because for accurate measurements each Radim 2P device should be separately calibrated versus humidity level.

REFERENCES

1. J. Plch, Radon Monitor Radim 2P. Instruction Manual. Ing. Jiri Plch - SMM, Prague, 1998, pp.25.
2. Annick Van Deynse, *Study of the effect of extreme variation in relative humidity on the response of the Radim 2P radon monitoring devices.* Intern technical note, Laboratory of Nuclear Physics, Gent University.
3. N. P. Petropoulos, M. J. Anagnostakis, S. E. Simopoulos, *Radon in the living environment.* Book of Abstracts, National Technical University of Athens, 19-22 April, 1999, pp.130-132.
4. C. Cosma, F. Dancea, T. Jurcut, D. Ristoiu, Appl. Rad. Isot. 54, 2001, 467-473.

RAMAN SPECTROSCOPIC INVESTIGATION OF THE $3B_2O_3$-K_2O-V_2O_5-CUO GLASSES

[1]D. MANIU*, [1]I. ARDELEAN, [1]S. CÎNTĂ, [1]T. ILIESCU AND [2]W. KIEFER

[1]*Faculty of Physics, Babes-Bolyai University, Kogalniceanu 1,
3400 Cluj-Napoca, Romania*
[2]*Institut für Physikalische Chemie, Universität Würzburg,
Am Hubland, D-97074 Würzburg, Germany*

ABSTRACT. The influence of $V_2O_5 \cdot CuO$ content on the structure of $3B_2O_3 \cdot K_2O$ glass was investigated by Raman spectroscopy. With increasing vanadium and copper content the number of non-bridging oxygen increases and the glass structure becomes more randomised. For the $V_2O_5 \cdot CuO$ concentration higher than x = 0.03, borate and boroxol rings are broken and the orthoborate groups are formed. Further addition of $V_2O_5 \cdot CuO$ determines the appearance of "loose" BO_4^- tetrahedra and for x > 0.1 the decrease of orthoborate groups number. A small number of chain-type metaborate and pyroborate groups are also present in this glass. Therefore, we conclude that the vanadium and copper ions act as network modifier in these glasses.

INTRODUCTION

Raman spectroscopy becomes an effective tool for resolving the structure of local arrangements in glasses. Raman spectra and identification of glass forming structural units in alkali borate glasses were also analysed by other authors [1-9]. The introduction of the transition metal in the glasses leads to the change of the glass structure, metal oxide acting as modifier [10-14]. In this paper Raman spectra of $x(V_2O_5 \cdot CuO) \cdot (1-x)[3B_2O_3 \cdot K_2O]$ glasses with $0 \leq x \leq 0.5$ have been analysed.

EXPERIMENTAL

The glasses were obtained by mixing H_3BO_3, K_2CO_3, V_2O_5 and CuO in suitable proportions and melting this admixture in sintered corundum crucibles at T=1150 °C for 30 min. The parallelepiped shaped samples

---

* Corresponding author

were obtained by pouring the melts in stainless steel forms. These glasses are fairly hygroscope and thus special care has to be taken to protect them from hydrolysis. The Raman spectra have been excited using the 514.5 nm line of an Ar ion laser Spectra-Physics Model 165. The laser beam was carried through a filter prism (Anaspec) to avoid the plasma lines and then was focused with an Olympus microscope objective on the sample. The 180^0 back-scattered light was collected by the same objective. After reflection on a beam-splitter the light was focused with a Fuji camera objective on the entrance slit of a Double Monochromator Spex Model 1404, equipped with 1800 gr/mm holographical gratings. A Photometrics Spectra 9000 CCD camera detection system working at liquid nitrogen temperature was used. The back scattering configuration of the micro Raman set-up allows the observation of the sample surface before exposure. The laser power was 500 mW. The measurements were carried out at room temperature.

RESULTS

Raman spectra of x(V$_2$O$_5$·CuO)·(1-x)[3B$_2$O$_3$·K$_2$O] glasses with various content of vanadium and copper oxides (0 ≤ x ≤ 0.5) are presented in Fig. 1. For the acquisition data an analysing software package (MAPS VO.98.5) was employed. The spectra were taken with a resolution of 2 cm^{-1} and were analysed with Spectra-calc software.
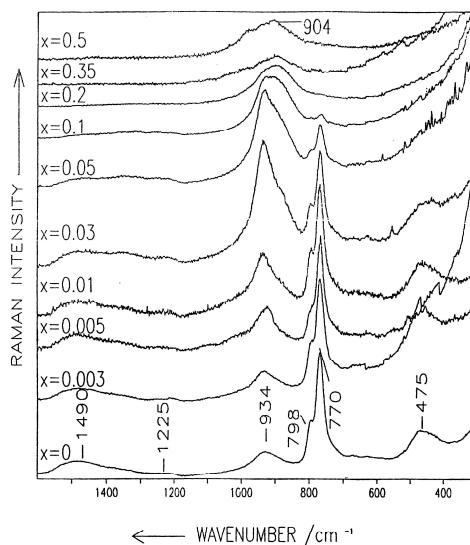
Fig. 1. *Raman spectra of x(V$_2$O$_5$.CuO)·(1-x)[3B$_2$O$_3$.K$_2$O] glasses with x as indicated in the range 0 ≤ x ≤ 0.5.*

In obtained spectra the following bands can be observed: ~475 cm^{-1}, ~770 cm^{-1}, ~798 cm^{-1}, ~904 cm^{-1}, ~ 934 cm^{-1}, ~1225 cm^{-1} and ~1490 cm^{-1}.

For the glasses with $0 \leq x \leq 0.1$ the intensity of the ~770 cm^{-1} band is higher than that of the ~798 cm^{-1} band. These two bands are dominant for the glasses with $0 \leq x \leq 0.01$. Introduction of copper and vanadium oxides determines an intensity increase of the band from ~934 cm^{-1}. This band is dominant for the glasses with $0.03 \leq x < 0.1$. For $x = 0.03$ appears a shoulder at ~904 cm^{-1} which increases in intensity with concentration. For $x > 0.1$ the band centered at ~904 cm^{-1} becomes higher than that from ~934 cm^{-1}. For the spectra with $0 \leq x \leq 0.05$ the bands centered at ~475 cm^{-1} and ~1400 cm^{-1} also appear.

DISCUSSION

The Raman spectrum of the vitreous B_2O_3 is dominated by an intense and narrow band centered at ~806 cm^{-1}, assigned to the boroxol ring oxygen breathing, involving a very little boron motion (boron atom is three-coordinate) [3]. With the addition of alkali oxide, a strong band centered at ~770 cm^{-1} appears and the band from ~806 cm^{-1} is shifted to the lower wavenumber at ~798 cm^{-1} [1]. The Raman band centered at ~770 cm^{-1} was assigned by Bril [5] to the symmetric breathing vibration of six-membered rings with one BO_4 tetrahedron (i.e., triborate, tetraborate or pentaborate) and the band from a lower wavenumber (~755 cm^{-1}) was
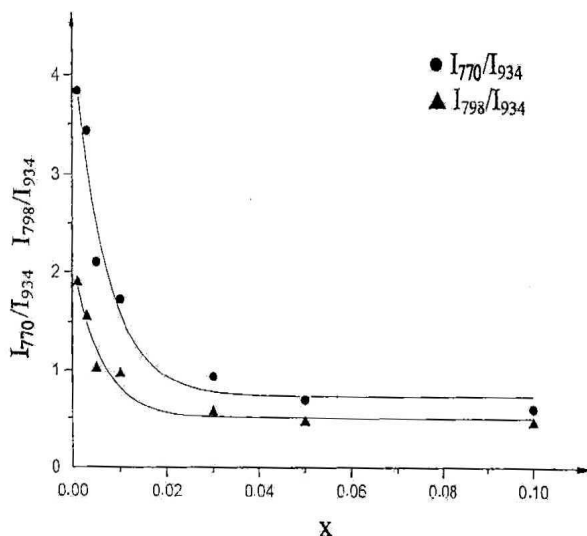
Fig. 2. *I_{770}/I_{934} and I_{798}/I_{934} intensity ratios as a function of $V_2O_5 \cdot CuO$ concentration. The lines only serve to guide the eye.*

55

assigned to the symmetric breathing vibration of six-membered rings with two BO_4 tetrahedra (i.e., diborate, ditriborate, or dipentaborate) [5]. Addition of K_2O at vitreous B_2O_3 determines a change of the boron coordination number from 3 to 4. (In a previous paper [15] we presented a list of borate groups found in borate glasses.)

For the spectra without V_2O_5·CuO (x = 0) the number of borate rings is larger than the number of boroxol rings because the intensity of the ~770 cm^{-1} band is higher than that from ~798 cm^{-1}. Since the position of the ~770 cm^{-1} band is constant within the limits of experimental error, we conclude that in the studied glasses the six-membered borate rings contain only one BO_4 tetrahedron. Crystalline α and β K_2O-$5B_2O_3$, which contain only pentaborate units give Raman bands at ~765 and ~885 cm^{-1}, and at ~785 and ~930 cm^{-1}, respectively [2]. Crystalline Na_2O-$4B_2O_3$ (consisting of tetraborate groups) and crystalline Cs_2O-$3B_2O_3$ (consisting of triborate groups) have only a very weak response in the ~930 cm^{-1} region [2]. Thus, the presence of the band centered at ~770 cm^{-1} and the band centered at ~934 cm^{-1} region can be taken to be indicative of the presence of pentaborate groups in the studied glasses.

The increase of vanadium and copper concentration determines the rise of the ~934 cm^{-1} intensity band compared with those of the ~770 cm^{-1} and ~798 cm^{-1} bands. Figure 2 shows the ratio of the 770 cm^{-1} and 934 cm^{-1} bands as well as that of the 798 cm^{-1} and 934 cm^{-1} bands as a function of the V_2O_5·CuO concentration.

With increasing V_2O_5·CuO concentration the I_{770}/I_{934} and I_{798}/I_{934} ratios decrease, and for x ≥ 0.03 the band centered at ~934 cm^{-1} becomes dominant (I_{770}/I_{934} and I_{798}/I_{934} ratios become smaller than one). Crystalline lithium and magnesium orthoborates exhibit a strong peak in ~ 930 cm^{-1} region [1,9]. The band centered at ~934 cm^{-1} can be assigned to orthoborate groups because in the observed spectra a band at ~1050 cm^{-1} does not develop simultaneously [1]. (In borate glasses the bands centered at ~1050 cm^{-1} and at 934 cm^{-1} have been attributed to the presence of diborate groups [1]). The increase of the 934 cm^{-1} intensity band indicates the break of the regular structure and the formation of orthoborate groups. Thus, growth of V_2O_5·CuO concentration up to 0.03 determines the formation of orthoborate groups and the disruption of boroxol rings. Therefore, the number of non-bridging oxygen ions increases while vanadium and copper concentration rises, and the glass structure becomes more randomised.
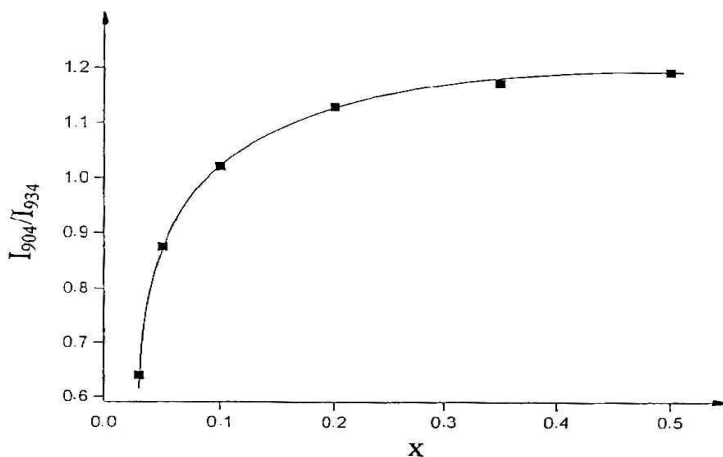
Fig. 3. I_{904}/I_{934} intensity ratio as a function of $V_2O_5 \cdot CuO$ concentration. The lines only serves guide the eye.

For the glasses with $x \geq 0.03$ appears a shoulder at ~904 cm^{-1}. For $x > 0.1$ the band centered at ~904 cm^{-1} becomes more intense than the one centered at ~934 cm^{-1}. The band centered at ~904 cm^{-1} is assigned to the anti-symmetric vibration of "loose" BO_4^- tetrahedra (i.e., tetrahedra connecting various segments without participating in specific borate arrangements) [8,9].

Figure 3 shows the ratio of I_{904}/I_{934} determined at band position as a function of $V_2O_5 \cdot CuO$ concentration. With increasing $V_2O_5 \cdot CuO$ concentration, this ratio also increases. Therefore, the addition of vanadium and copper ions determines the appearance of "loose" BO_4^- tetrahedra and the decrease of the number of orthoborate groups (BO_3^{3-}).

For the glasses with $0 \leq x \leq 0.05$ the bands centered at ~475 cm^{-1} and ~1490 cm^{-1} also appear. The 475 cm^{-1} band is assigned to a ring angle bending (B-O-B) of borate units [6], which is observed at 470 cm^{-1} for pure B_2O_3 [7]. The presence of a very large band at 1490 cm^{-1} in the Raman spectra is an indication that the chain-type metaborate groups are present [9]. One observes an anti-symmetric band at ~1225 cm^{-1}, which indicates the formation of pyroborate groups $\left(B_2O_5^{4-}\right)$ [2].

CONCLUSIONS

There are two effects caused by addition of ($V_2O_5 \cdot CuO$) in $3B_2O_3 \cdot K_2O$ glass: (i) the breaking of the regular structure of the rings (borate and boroxol) and the appearance of orthoborate groups for $x \geq$

0.03, and (ii) the decrease of the number of orthoborate groups and the appearance of "loose" BO_4^- tetrahedra for x > 0.1. In these glasses a small number of chain-type metaborate and pyroborate groups are also present. Therefore, we conclude that the vanadium and copper ions act as a network modifier in the studied glasses.

REFERENCES

1. B. N. Meera, A. K. Sood, N. Chandrabhas and J. Ramakrishna, *J. Non-Cryst. Solids* **126**, (1990), 224.
2. W. L. Konijnendijk, Philips Res. Rep. Suppl. **1**, (1975), 224.
3. B. P. Dwivedi, M. H. Rahman, Y. Kumar and B. N. Knanna, *J. Phys. Chem. Solids* **54**, (1993), 621.
4. F. L. Galneer, Solid St. Commun. **44**, (1982), 1037.
5. T. W. Bril, *Philips Res. Rep. Suppl.* **2**, (196), 117.
6. W. L. Konijnendijk and J. M. Stevels, *Mater. Sci. Res.* **12**, (1977), 259.
7. J. Krong-Moe, Phys. Chem. Glasses **61**, (1965), 46.
8. E. I. Kamitsos and G. D. Chyssikos, J*. Mol. Struct.* **247**, (1991), 1.
9. E. I. Kamitsos, M. A. Karakassides and G. D. Chyssikos, *Phys. Chem. Glasses* **30**, (1989), 229.
10. T. Iliescu, S. Simon and D. Calugar, J. Mol. Struct. **267**, (1992), 231.
11. T. Iliescu, S. Simon, D. Maniu and I. Ardelean, J. Mol. Struct. **294**, (1992), 201.
12. T. Iliescu, I. Ardelean, and S. Simon, *Solid St. Commun.* **90**, (1994), 507.
13. D. Maniu, I. Ardelean and T. Iliescu, *Mat. Lett.* **25**, (1995), 147.
14. D. Maniu, I. Ardelean and T. Iliescu, *J. Mat. Sci. Lett.* **16**, (1997), 19.
15. D. Maniu, I. Ardelean and T. Iliescu, *Studia Univ Babes-Bolyai, Physica,* **2**, (1994), 13.

OPTICAL AND E.S.R. STUDY ON V_2O_5-MoO_3 SOLID SOLUTION

GH. CRISTEA[*] L. STĂNESCU[*] AND I. ARDELEAN[*]

*) Physics Department of "Babes- Bolyai" University, str. Kogalniceanu, 3400, Cluj-Napoca.

ABSTRACT. Our study on paramagnetic defects associated with the V^{4+} ions in the lattice of V_2O_5-5 mol% MoO_3 solid solution is reported. The diffuse reflectance and ESR spectra on powder sample have been recorded at room temperature. It has been established that optical absorption beginning at 2.36 eV is due to charge transfer and not to band-band transition. Tetragonal (C_{4v}) point symmetry of local crystal field at V^{4+} ion sites explains the experimental data. From optical transition energies of 16666 cm^{-1} and 15043.5 cm^{-1} the crystal field parameters have been determined. Taking the spin-orbit coupling constant of V^{4+} ion in the lattice λ = 150 cm^{-1} the values of $g_{\chi\chi\Lambda}$ and $g_{\perp}$ components has been evaluated and compared with those experimentally determine from ESR spectrum.

1. INTRODUCTION

The pure V_2O_5 and its solid solutions were intensely studied by optical and ESR methods due to their physical and chemical properties, especially for catalytic activity. It has been established that because pure V_2O_5 crystallize with considerable oxygen deficiency a complex defect is responsible for ESR spectra, such $V_{6-3x}^{5*} V_{2x}^{4*} V_x^{3*} O_{15-2x}^{2-}$, instead V^{4+} alone [1,2]. In solid solutions of the type V_2O_5-MoO_3, where M is a transition metal, unpaired electron localizes at V^{4+} ions sites [3]. Several remission bands appear between 400 nm and 700 nm that may be assigned to band-to-band, charge transfer or colour spectra. Many authors have been used diffuse reflectance spectra for determining optical energy gap, in both pure

and doped V_2O_5 [4,5] supposing always that they have to do with band-to-band spectra.

In this paper, we present the results of our diffuse reflectance and ESR study on a 95mol%V_2O_5-5mol%MoO_3 powder sample and show that in V_2O_3-MoO_3 solid solutions with more than 0.1mol%.MoO_3 the diffuse reflectance beginning at 2.36 eV is not of band-to-band type but of charge transfer type. Therefore, in such cases the measured energy gap is just the energy of electron charge transfer from ligand (oxygen) to transition metal ion. Also, using crystal field model we were able to get an insight into the problem of the local electric crystalline field symmetry in the neighborhood of the V^{4+} ions, to determine the crystal field parameters and calculate theoretical values of g factor components. The agreement between theoretical calculated and experimentally measured values of g factor components is satisfactory.

2 EXPERIMENTAL

The solid solutions have been prepared by melting together the components in a platinum crucible. We stated from a zonal purified V_2O_5 (ten passages) and reagent grade MoO_3. After a first grinding in an agate mortar the mixture has been subjected to a thermal treatment between 620 and 640^0C for a week. A separation by settling in CCl_4 has been carried out, after a new grinding. The V_2O_5-MoO_3 solid solutions preserve the V_2O_5 crystal structure up to about 15mol%.MoO_3 [6]. By increasing the MoO_3 concentration the V^{4+} ions concentration electrical conductivity as well as the intensity of the ESR line increase, the sample colour gets darken, while the asymmetry of the line becomes more marked. Grain size less than 20 μm has been selected for the diffuse reflectance measurements.

The optical spectra have been recorded by a Zeiss-VSU spectrophotometer equipped with accessories for diffuse reflectance within the range of 400 - 1000 nm. Magnesium oxide has been used as reference for reflectance and "pure" V_2O_5 for colour spectra. The Kubelka-Munk [7] remission function $F = (1-R)^2/2R$ has been used for evaluation of the optical absorption coefficient, where R is the sample reflection coefficient. The ESR spectra have been recorded as first derivative of absorption curve, at room temperature, with a TE102-X band cavity, using an improved JES-3B Jeol spectrometer at 100kc/s modulation frequency.

3 RESULTS

A. Diffuse reflectance and colour spectra. It is well known that in V_2O_5 occur optical transition associated with the electron transition from the valence band to the conduction band at E_g between 2.15 eV and 2.50 eV [8,9,10]. Fig. 1 displays the remission intensity versus the wavelength, for 95%mol. V_2O_5-5%mol. MoO_3 sample, against magnesium oxide as a reference. [11]. In order to determine E_g we made use of the Tandem and Guppy [12] method. The MoO_3 concentration modifies significantly the charge transfer and ESR spectra but has very small effect on the energy gap value [3,11]. For the 5 moll MoO_3 sample an $E_g = (2.36 \pm 0.02)$ eV has been found. We believe that the absorption band that begins 2.36 eV is of charge transfer type due to electron transfer from ligand to transition metal ion.
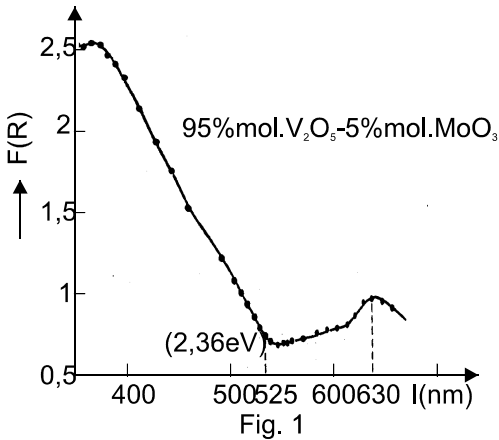
Fig. 1
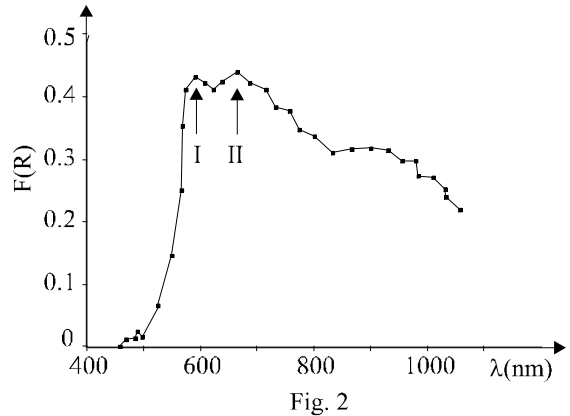
Fig. 2

In order to obtain only the colour spectra of the V_2O_5-5mol% MoO_3 (Fig.2),"pure" V_2O_5 has been used as reference. In this manner we have avoided the appearance in the spectrum of the band – band transition as well as the overlapping of the host lattice absorption bands with the colour centers absorption bands. Two bands were observed in the colour remission spectrum instead of a single band: the band I positioned at 600 nm (16666 cm^{-1}) and the band II positioned at 660 nm (15084 cm^{-1}). As these absorption bands correspond respectively to the red and orange-red regions of the spectrum it follows that the center responsible for the absorption should endow a blue colour to the sample. It is known [13] that V^{4+} ion causes the blue colour to some compounds, as ZrO_2 for instance. The brownish – green colour of the V_2O_5-5mol% MoO_3 is a mixture of brown and blue colours, due to the lattice and the V^{4+} centers respectively. The fact that destruction, by doping, of the narrow 3d conduction band and appearance of localized states does not change significantly the E_g value

61

suggests that optical transition beginning at 2.36 eV is not of band-to-band type but of charge transfer type. The charge transfer is from ligand (oxygen) to the transition ion (vanadium). A shoulder is also noticeable between 800 nm and 860 nm in the spectrum. It could be due to a forbidden transition that becomes allowed in an oscillating lattice.

B. ESR spectrum. The electronic structure of V^{4+} ion is [Ar] $3d^1$, so it has S = 1/2 and ground state ^2D. As the nuclear spin of ^{51}V (99.75% isotopic abundance) is I=7/2, the ESR spectrum should consist of a single fine structure line with eight hyperfine components. Gillis and Boesman [2], have shown that ESR spectra of pure V_2O_5 single crystal is much complicated consisting generally of 15 hyperfine components dependent on magnetic field orientation relative to the crystallographic axis of the crystal. These authors also have shown that by doping V_2O_5 with MoO_3 the system establishes and the V^{4+} ions appear as singular entities, giving an ESR spectrum with only of eight well-resolved hyperfine lines. As the molybdenum concentration is increased, enriching thus the V^{4+} ion concentration, the dipolar-dipolar interaction should causes the broadening of ESR lines and disappearance of the hyperfine structure of the spectrum. Fig. 3 shows our ESR spectrum recorded on powder V_2O_5-5mol% MoO_3 solid solution. The ESR spectrum consists of a single broad and asymmetric line characterized by an asymmetry parameter $\rho \cong 3$ [14]. Such a spectrum is due to a localized electron near the V^{4+} ion or defect associated to it.
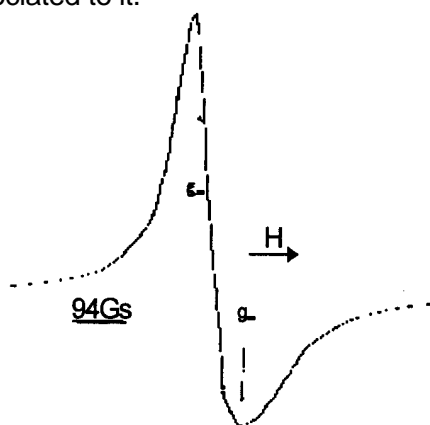
Fig. 3.

4. CRYSTAL STRUCTURE

V_2O_5 crystallizes in an orthorhombic lattice with space group Pmmn (D_{2h}^{13}) and lattice constants: a = 11.512Å, b = 3.564 Å and c = 4.368 Å [15]. Primitive cell comprises two formula units. The crystal structure is displayed

in Fig. 4a where we also indicate the three different types of oxygen. They are designated as vanadyl (O_v), chain (O_c) and bridge (O_b) oxygen. It can be seen that, the crystal structure consists of alternating, horizontal, layers which contain either vanadium, chain and bridge oxygen atoms or, alternatively, only vanadyl oxygen atoms. Within the first mentioned layer, vanadium and chain oxygen atoms form double zigzag chains along the *b* (010) direction, which within the planes are connected via the bridge oxygen atoms. The vanadyl oxygen atoms are located just below and above the vanadium atoms: so, the vanadium atoms reside near the centers of VO_6 octahedra, formed by one bridge, two vanadyl and three chain oxygen atoms. However, the vanadium atom experiences displacements away from the centers of the octahedra. First, the vanadium and vanadyl oxygen atoms move vertically towards each other. One short (1.577Å) and one long (2.791Å) $V-O_v$ distance evolves, and the chemical bond between the latter reduces to rather weak van der Waals forces. This fact explains the observed easy cleavage of V_2O_5 crystals parallel to the (*ab*) layers. Second, the vanadium and chain oxygen experience shifts parallel to *a* (100) axis towards the bridge oxygen atoms. This leads to the zigzag shape of the (010) double chains. The resulting in-plane distances within the octahedra amounts to: 1.779 Å for the $V-O_b$ bond atom and 1.878 Å and 3.017 Å bonds parallel to the (010) and (100) axis respectively. Due to this displacements the remaining basic units finally became approximately squared VO_5 pyramids rather than regular octahedra, as shown Fig. 4b.

a) b)
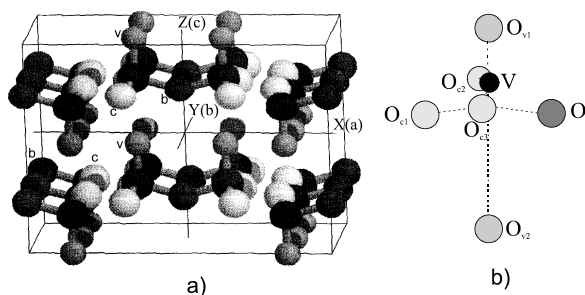
Fig. 4

5.THEORY

The ^2D free ion ground state of V^{4+} has five folds orbital degeneracy. Under the supposition that the local symmetry of the electric crystalline field, at V^{4+} sits in V_2O_5-MoO_3 is octahedral, in the first approximation, the orbital degeneracy of ground state should be partially lifted, arising a lower

triplet T_2 and a upper doublet E states. In this case a single absorption line should have been appeared in the colour optical spectrum which corresponds to the $T_2 \leftrightarrow E$ transition, while the ESR spectrum should have been symmetric. As it has been pointed out into previous section, the colour diffuse reflectance spectrum consists of (at least) two remission bands and the ESR spectrum is asymmetric. Therefore we must admit that there is lower local symmetry at the V^{4+} ion sits. On the other hand, ESR spectra of V^{4+} ions in orthorhombic single crystals of V_2O_5-MoO_3 [2] and V_2O_5-WO_3 [4] have clearly established that $g_a = g_b = g_\perp$ and $g_c = g_{ll}$, This means that the local symmetry at V^{4+} ion sit is axial, namely C_{4v} with C_4 axis parallel to (001) direction. So much the more is true for powder samples, due to the average taken over a great number of crystallites. Moreover, in order to compensate for electrical charge the Mo^{6+} ions occupy V sites close to V^{4+} forming, in this way, paramagnetic defects of the type Mo^{6+}-O- V^{4+}. In tetragonal crystalline field the T_2 and E representations of octahedral point group decomposes in irreducible representation of tetragonal point group as follows: $T_2 = B_2 + E$ ant $E = A_1 + B_1$.From the group theory approach of the problem does not result the order of the levels on energy scale. A quantitative treatment, in the single-ion model of crystal field theory frame, assumes the solution of Schrödinger equation for determining the eigenvalues and eigenfunctions of the crystal field Hamiltonian. In this case of tetragonal crystal field symmetry the Hamiltonian has the expression [16]:

$$\hat{H}_c = B_2^0 O_2^0 + B_4^0 O_4^0 + B_4^4 O_4^4 \qquad (1)$$

Here $B_4^0 = B_4^4/5$ and B_2^0 are, respectively, cubic and tetragonal crystal field parameters. The O_n^m are equivalent operators and have the expressions:

$$O_2^0 = 3L_z^2 - L(L+1)$$
$$O_4^0 = 35L_z^4 - 30L(L+1)L_z^2 - 25L_z^2 - 6L(L+1) + 3L^2(L+1)^2 \qquad (2)$$
$$O_4^4 = (1/2)(L_+^4 + L_-^4)$$

By calculating the matrix elements of $\hat{H}_c$ operator between the states $\tilde{\omega}LM_L>$ for $L = 2$ and $M_L = \pm2, \pm1, 0$ and solving the corresponding secular equation we obtain the following values for the energy levels of the V^{4+} ion in tetragonal crystal field.

$$W(A_1) = 72B_4^0 + 6 \mid B_2^0 \mid \qquad \mid 0 > \sim 3z_2 - r^2$$

$$W(B_1) = 72B_4^0 - 6 \mid B_2^0 \mid \qquad \mid 2^s > \sim x^2 - y^2 \qquad (3)$$

$$W(E) = -48B_4^0 + 3 \mid B_2^0 \mid \qquad \mid \pm \tilde{1} > \sim xz, yz$$

$$W(B_2) = -48B_4^0 - 6 \mid B_2^0 \mid \qquad \mid 2^a > \sim xy$$
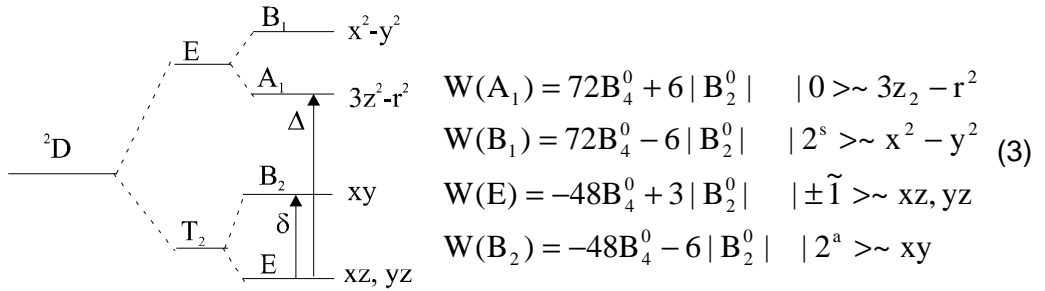
Fig. 5

At the right we have given the corresponding wave functions, which diagonalises the secular equation. Now we are able to present, in Fig. 5, the diagram of V^{4+} orbital energy levels in tetragonal crystal field. At room temperature the unpaired electron lies in the lower singlet orbital $3d_{xy}$. The electric-dipole transitions between these energy levels, stimulated by unpolarized light, and allowed by group theoretical selection rules, are the following: $E \leftrightarrow B_1$, $E \leftrightarrow B_2$, $E \leftrightarrow A_1$. However, forbidden transitions may also appear due to the fact that lattice oscillations lower the crystal field symmetry.

We assign the two observed remission bands to the electric - dipole transitions between orbital energy levels of V^{4+} in the crystalline field as follows:

$$W(E) - W(B_2) = \delta = 9 \mid B_2^0 \mid = 15083.5 \text{ cm}^{-1}$$

$$W(B_1) - W(E) = \Delta = 120B_4^0 - 3 \mid B_2^0 \mid = 16666 \text{ cm}^{-1}$$

where from we have: $\left| B_2^0 \right| = 1675,9 \text{ cm}^{-1}$, $B_4^0 = 180,8 \text{ cm}^{-1}$ and $B_4^4 = 903,9 \text{ cm}^{-1}$.

In order to verify the assignment correctness of the absorption bands to transitions we have used $g_{\parallel}$ and $g_{\perp}$ values of spectroscopic factor components of V^{4+} ion, as determined experimentally by ESR measurements. The theoretical values of these components are [5]:

$$g_{\parallel} = g_e - \frac{8\lambda}{\Delta}$$

$$g_{\perp} = g_e - \frac{2\lambda}{\delta} \qquad (4)$$

Table 1. Measured and calculated values $g_\parallel$ and $g_\perp$

	Measured by ESR	Computed with (4)
$g_\parallel$	1.931±0.002	1.9303
$g_\perp$	1.995±0.002	1.9825

In agreement with [2] we have chosen for λ - the spin-orbit coupling constant- a value of 150 cm^{-1}. The table 1 allows us to compare the experimentally measured with the calculated ones: The medium deviation from the $g_\perp$ average value, calculated from optical data and measured by ESR is less than 0.0032. Taking into account that the error of experimental positioning of $g_\perp$ on ESR spectrum is principially larger than 0.0032 we concluded that the agreement between measured and calculated values of g factor components is quite good. Therefor, we think that the proposed model concerning the local crystal field symmetry in the proximity of V^{4+} ion, as well as the crystal field splitting of orbital energy ground level, are valid.

REFERENCES

1. V. A. Ioffe, and I. B. Patrina, *Fiz Tverd. Tela*, 6, 3045 and 3227, (1964).
2. E. Gillis, and E. Boesman, *Phys. Stat. Sol. 14*, 337 and 349, (1966).
3. J. Livege, C. R'kha, D. Ballutaud, and J. C. Grenet, *J. Solid State Chem.*, 33, 335, (1980).
4. N. Kenny et all. *J. Phys. Chem. Solids*, 27, (1237)
5. Bodó and I. Hevesi, *Phys.Stat. Sol.* (a), 20, K45, (1967)
6. L. Stanescu, I. Ardelean, Studia Univ. "B-B", Cluj, Ser. Math-Phys, (1) 101, (1969)
7. P. Kubelka and F. Munk, *Zh.Tekh.Fiz. 12*, 592, (1931)
8. F. Vratny and F. Micale, *Trans. Farad. Soc. 59*, 2739, (1966).
9. J Boros, Z. Physik 126, 721, (1949).
10. N. Kenny, C. R. Kannewurf and D. F. Whitmore, *J. Phys. Chem. Solids*, 27, 1237, (1966).
11. L. Stănescu, Gh. Cristea, I. Ardelean, M. Bassanyi, Studia Univ. "B-B", Physica, 6, (1976).
12. S. P. Tandom and J. P. Gupta, *Phys. Stat. Sol. 38*, 363, (1970)
13. K. Hauffe, *Reaccyi v tverdyh telakh i na ikh poverkhnosti*, Izd.Inostr. Lit. Moscova, (1962)
14. M. Che, J. Vedrine and Cl. Naccache, *J. Chim. Phys. 66*, 579, (1969)
15. V.Eyert, K. H. Höck, *Phys. Rev.* (B), 57 (20), 12727 (1998)
16. S. A. Altshuler, B. M. Kozirev, *Electron Paramagnetic Resonance*, Nauka, Moscow (1972).

RAMAN AND SERS STUDIES ON COBALT(II) CUPFERRONATO COMPLEXES

M. BOLBOACA[a], S. CÎNTĂ-PÎNZARU*[a], O. COZAR[a], T. ILIESCU[a], P. RÖSCH[b], AND W. KIEFER[b,*]

[a]Babes – Bolyai University, Physics Department, 3400, Cluj – Napoca, Romania
[b]Institut für Physikalische Chemie, Universität Würzburg, Am Hubland, D – 97074 Würzburg, Germany

ABSTRACT. Raman and surface-enhanced Raman scattering (SERS) spectra of cupferron, $[PhN_2O_2]NH_4$ and the new corresponding cobalt(II) cupferronato complexes, CoL_2A_2, L = $PhN_2O_2^-$, A = MeOH, o-$C_6H_4(NH_2)_2$, p-$C_6H_4(NH_2)_2$ were recorded and discussed. All the complexes show a Raman band at about 1302 cm^{-1} and the characteristic ν(N-N) and δ(ONNO) modes of the anionic ligand. The vibrational analysis of the title compounds reveals the electron delocalisation over the N-nitroso-N-hydroxylaminato (ONNO) unit as well as the bidentate coordination of the cupferronato ligand to the metal center through the oxygen atoms. These complexes were found to adsorb on different Ag SERS substrates. SERS spectra of the title compounds bring additional arguments for the bidentate coordination of the ONNO group.

Keywords: Raman spectroscopy, SERS, cupferron, Co(II) cupferronato complexes.

1. Introduction

The salt of N–nitroso–N–phenylhydroxylamine $[PhN_2O_2]NH_4$ (cupferron) is a well known analytical reagent (Fig. 1, a). Additionally, the cupferron is a biologically active compound, known to display carcinogenic, genotoxic, mutagenic and DNA–damaging effects [1]. The N-nitroso-N-phenylhydroxylaminato (cupferronato) anion ($PhN_2O_2^-$) has been extensively used as ligand in coordination chemistry, acting mostly as bidentate chelating or bridging ligand [1].

---

*Corresponding author.
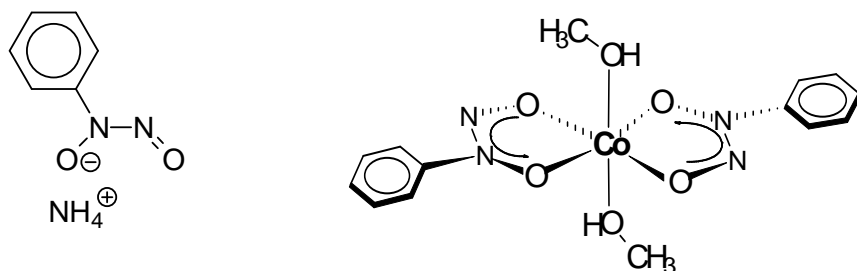
Fig. 1. Schematic drawing of cupferron ($NH_4PhN_2O_2$) (a) and the corresponding $Co(PhN_2O_2)MeOH_2$ complex (b).

We become interested in cobalt (II) cupferronato complexes with different neutral donor molecules (e.g. methanol, *o*-diaminobenzen, *p*-diaminobenzen) since only one related compound, $Co(PhN_2O_2)_2(MeOH)_2$ was structurally investigated so far (Fig. 1, b) [2]. The cupferron and the corresponding main group metal complexes were investigated by Raman spectroscopy, and the selected vibrational data were reported [1, 3, 4]. A detailed Raman analysis could provide important and rich information about the coordination pattern and the structure of the cupferronato ligand bind to cobalt.

Here we report the first Raman studies on N-nitroso-N-phenylhydroxylaminato (cupferronato) cobalt(II) complexes: dimethanol-bis-cupferronato-cobalt(II), $CoL_2(MeOH)_2$ (**1**), di-*o*-diaminobenzene-bis-cupferronato-cobalt(II), $CoL_2(o\text{-}NH_2C_6H_4NH_2)_2$ (**2**), di-*p*-diaminobenzene-bis-cupferronato-cobalt(II), $CoL_2(p\text{-}NH_2C_6H_4NH_2)_2$ (**3**), where $L = PhN_2O_2^-$. Moreover, these compounds are easily adsorbed to metals, like silver, on which the effect known as surface-enhanced Raman scattering (SERS) takes place. SERS, as a very sensitive technique, is now an established method used in fields as analytical, biological and surface science [5].

Experimental

The starting materials were obtained from commercial sources (Aldrich) as analytical pure reagents. The complex $CoL_2(H_2O)_2$ was prepared by the reaction of cupferron with $CoCl_2 \bullet 6H_2O$ in water, at room temperature. The reaction of this complex with different neutral donors (methanol, *o*-diaminobenzene and *p*-diaminobenzene) in ethanol, at room temperature, yielded the complexes **1-3** in microcrystallin state. The spectral purity of **1-3** is supported by elemental analysis.

For recording the absorption spectra we prepared 10^{-3} mol l^{-1} ethanol solution of each complex. The absorption spectra of cupferron and complexes *1-3* were recorded with a Perkin Elmer Lambda 19 UV-VIS-NIR spectrometer with a scan speed of 240 nm/min.

The FT-Raman spectrum of cupferron has been recorded using a Bruker IFS 120 HR spectrometer with an integrated FRA 106 Raman module. Radiation of 1064 nm from a Nd-YAG laser was employed for excitation with an output of 95 mW. A Ge detector operating at liquid nitrogen temperature was used. The spectral resolution was 3 cm^{-1}.

Only poor FT-Raman spectra of *1-3* were obtained. Therefore a higher energy excitation line was required. A Kr or a Ar ion laser Spectra-Physics model 2020 was used for excitation of the micro-Raman and SERS spectra of complexes using the 647.09 and 514.5 nm lines with an output power of 300 mW. The laser beam was carried through a filter prism (Anaspek) in order to avoid the plasma lines and then was focused with an Olympus ULWD MSPLAN 80 microscope objective on the powder sample. The back scattered light was collected by the same objective and after reflection by a beam-splitter, focused with a lens (f=150 mm) on the entrance slit of a Spex Model 1404 double monochromator equipped with 1800 grooves/mm holographic gratings. 90° and back-scattering geometry were adopted for collecting the SERS spectra. A Photometrics Model 9000 CCD camera detection system and analyzing software package (MAPS V1.0) were employed for acquisition of data. The spectra were taken with a resolution of 2 cm^{-1} for this case.

A sodium citrate-reduced Ag colloid, roughened Ag electrode and thermally evaporated Ag films, respectively, were employed as SERS substrates. Ag colloid was prepared according to the literature [6]. Small amounts of cobalt(II) cupferronato complexes 10^{-3} moll^{-1} ethanol solution were added to 3 ml of colloid. 10^{-2} moll^{-1}. NaCl solution was also added (10:1) for producing a stabilization of the colloidal dispersion and a considerable enhancement of the SERS spectrum [7]. Final concentration of sample was 1.52 10^{-4} moll^{-1}. Thermally evaporated Ag films with particles roughness of 6.5 Å, were prepared [8]. The surface of the working electrode was roughened through the electrochemical treatment prior to the recording of the SERS spectrum.

3. Results and discussion

The absorption spectra of the complexes *1-3* were very similar. Figure 2 presents the absorption spectra of the cupferronato complexes. The electronic absorption peaks of the samples under study are located at 908 and 1014 nm, respectively. Therefore, we assume that a resonance or pre-resonance contribution to the Raman intensity is not significant, either in further investigation using the green laser line [9].
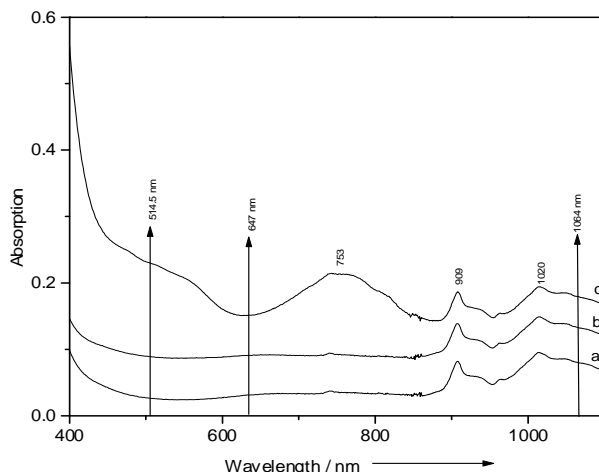
Fig. 2. Absorption spectra of CoL_2A_2, L = $PhN_2O_2^{-1}$, A=MeOH (a), o-$C_6H_4(NH_2)_2$ (b) and p-$C_6H_4(NH_2)_2$ (c), 10^{-3}mol l^{-1} ethanol solution.

The Raman spectra of cupferron and the new cobalt(II) cupferronato complexes (**1-3**), recorded in the spectral range 1650-850 cm^{-1}, are presented in Fig. 3. The observed bands in the region of 850–1650 cm^{-1} with the tentative assignment [10] are summarized in Table 1.
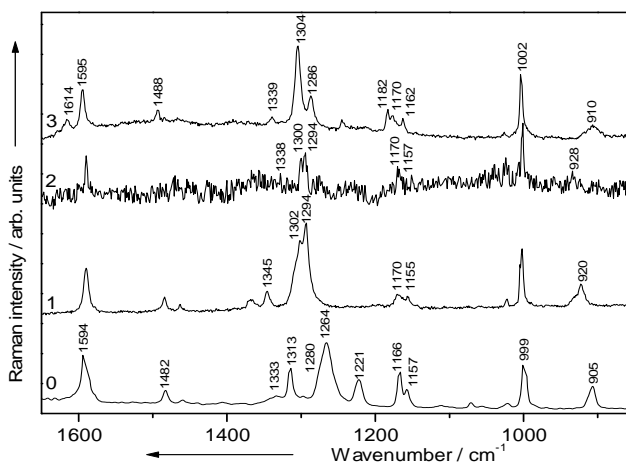
Fig. 3. FT-Raman spectrum of $Ph[N_2O_2]NH_4$ (**0**) and micro-Raman spectra of (**1**) $CoL_2(MeOH)_2$, (**1**) $CoL_2(o\text{-}NH_2C_6H_4NH_2)_2$, (**2**) $CoL_2(p\text{-}NH_2C_6H_4NH_2)_2$, (**3**), L = $PhN_2O_2^-$. Laser line 1064 nm, P = 96.4 mW, (**0**), 647 nm, P = 300 mW (**1-5**)

Table 1.

Vibrational Raman data (cm^{-1}) of cupferron (NH$_4$L, L = PhN$_2$O$_2^-$) and corresponding Co(II) complexes: CoL$_2$A$_2$, A = MeOH (**1**), o-C$_6$H$_4$(NH$_2$)$_2$ (**2**) and p-C$_6$H$_4$(NH$_2$)$_2$ (**3**).

Raman				SERS			Vibrational Assignment
NH$_4$L	**1**	**2**	**3**	**1'**	**2'**	**3'**	
			1614w			1614sh	δ(NH$_2$)
1594s	1592s	1591s	1591s	1573m	1593vs	1602s	quadrant ring stretch
						1523vs	δ(C$_6$H$_4$) para substituted
1482w	1484w	1486w	1488w	1500m	1402s	1517sh 1455s	semicircle ring stretch
				1396vs			δ(C-OH)
1333w	1345m	1338m	1339m	1372s		1366m	ν(N-N)
1313 s							ν(ONNO)
	1302s	1301s	1304vs		1305s	1311sh	ν$_{symm}$(ONNO)
1284sh	1294vs	1294s	1286s		1298sh		ν(C-N)
1264vs 1221m							ν(N=O)
1166s	1170m	1170m	1170m			1171m	δ(C-H) ofC$_6$H$_4$
1157m	1156w	1157w	1162m	1157m	1156m	1146m	δ(C-H)
996s	1001s	1001vs	1002s		1003m		ring breathing
905m	923m	928m	910m				δ(ONNO)
					238sh		ν (Ag-N)

^{a}Abbreviations:

vs- very strong, s-strong, m-medium, w-weak, sh-shoulder, ν-stretching, δ-bending.

The following discussion is based on the comparison of the spectra of complexes *1-3* to that of cupferron, many similarities as well as some specific differences being observed.
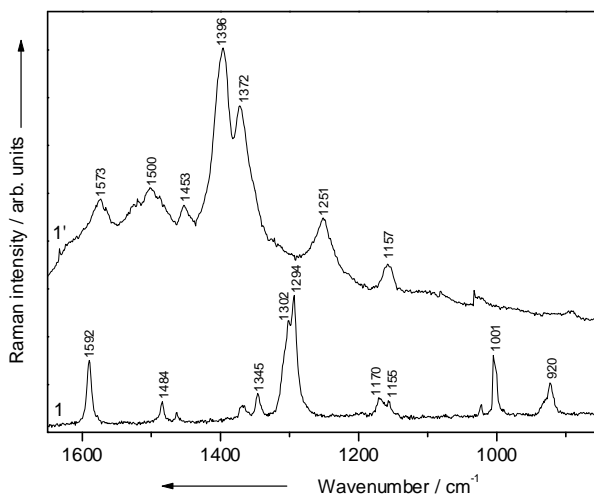
Fig. 4. Micro-Raman (**1**) and SERS (**1'**) spectra of CoL$_2$(MeOH)$_2$ complex on thermally evaporated Ag films. Laser line:647 nm (**1**)and 514.5 nm (**1'**), P=300 mW

The assignment of the ν(N-N) and δ(N$_2$O$_2$) vibrational modes, specific for the cupferron at 1336 and 905 cm^{-1} respectively, is in good agreement with the correspondingIR data [1, 4, 11, 12]. In addition, the ν(N=O) mode provides two bands at 1270 and 1220 cm^{-1}, respectively, due to the *cis-trans* configuration of the N-nitroso-N-hydroxylaminato group (ONNO) in cupferron [13]. After coordination, the *cis*-configuration of the ligand is expected to be present in the title complexes [2]. Comparing the Raman spectra of *1-3* to that of the ligand, significant changes in the position and relative intensities of the mentioned bands can be observed. Thus, the ν(N-N) and δ(ONNO) modes are shifted to higher wavenumbers up to 1346 and 928 cm^{-1}, respectively. Analogue to the tin(IV) and nickel(II) cupferronato complexes, where the ν(N=O) modes are located at around 1215 cm^{-1} as weak or very weak bands [1, 14], similar corresponding signal is observed in the Raman spectra of the Co(II) cupferronato complexes. Two strong bands are located in the spectrum of cupferron at 1313 and 1284 cm^{-1}. The first one is observed in the spectra of all complexes, shifted to lower wavenumbers by 11-12 cm^{-1}. This band, considered as a fingerprint, was also noticed in a previous Raman report on main group metal cupferronates [3], being tentatively assigned to the new symmetric mode of the coordinated ONNO unit. The second band was assigned in the spectrum of the ligand to the ν(C-N) mode [13, 14]. In the spectra of

complexes *1-3* this band is constantly shifted to higher wavenumbers by 10 cm^{-1} due to the involvement of the C-N bond in the electron delocalisation.

The characteristic vibrational modes of aromatic groups were observed in the expected spectral regions [10, 14] (Fig. 3), the most representative being assigned to the ring stretching (1592-1591, 1486-1484 cm^{-1}) and ring breathing (1001 cm^{-1}) modes.

The SERS spectra (*1'*), (*2'*), (*3'*) of CoL$_2$A$_2$ with L=PhN$_2$O$_2^-$, A=MeOH, o-C$_6$H$_4$(NH$_2$)$_2$ and p-C$_6$H$_4$(NH$_2$)$_2$ complexes on thermally evaporated Ag films, Ag sol and roughened Ag electrodes are presented in Fig. 4, 5 and 6 respectively, in comparison to their corresponding Raman spectra. SERS spectra of the cobalt(II) cupferronato complexes are different from those of the corresponding Raman spectra, which indicates a strong interaction of these compounds with the silver surface. The expected Ag-N stretching band characteristic for the N-adsorbed species in the SERS spectra under 250 cm^{-1} was observed only in spectrum (*2'*) at 238 cm^{-1}.
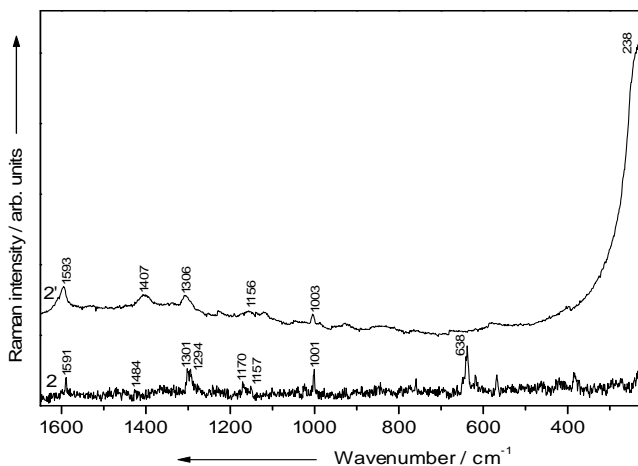
Fig. 5. Micro-Raman (**2**) and SERS (**2'**) spectra of CoL$_2$(o-NH$_2$C$_6$H$_4$NH$_2$)$_2$ complex on roughened Ag electrode. Laser line: 647 nm (**2**) and 514.5 nm (**2'**), P=300 mW

The SERS spectrum of complex *1* present enhanced and shifted bands characteristic for the ring stretching (1573 and 1500 cm^{-1}), υ(N-N) (1372 cm^{-1}) and δ(C-H) of C$_6$H$_4$ (1157 cm^{-1}) vibrational modes. The more enhanced band at 1396 cm^{-1} was assigned to δ(C-OH) mode [10]. Therefore, it can be concluded that the complex *1* is adsorbed to the Ag surface through the MeOH molecule being more probably perpendicular to the surface.
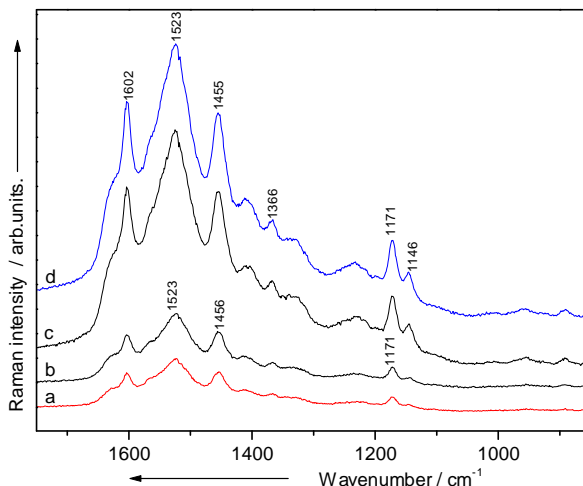
Fig. 6. Micro-Raman (**3**) and SERS (**3'**) spectra of $CoL_2(p\text{-}NH_2C_6H_4NH_2)_2$ complex on Ag sol. Laser line: 647 nm (**3**) and 514.5 nm (**3'**)

The SERS spectrum **2'** shows the Ag-N stretching band at 238 cm^{-1} and the shifted band at 1305 cm^{-1}, assigned to the new symmetric mode, characteristic for the bidentate coordination of the ONNO unit in interaction to the metal surface [15]. The bands characteristic for phenyl vibrational modes are enhanced but not significantly shifted to higher wavenumbers, therefore we suppose that this molecule is laying near the surface.

The SERS spectrum **3'** was recorded on the nanometer Ag colloid particles. The bands characteristic for the donor molecule, ring stretching (1602, 1517 and 1455 cm^{-1}), $\delta(C_6H_4)$ para substituted (1523 cm^{-1}) and δ(C-H) of C_6H_4 (1171 and 1146 cm^{-1}) are very enhanced but not significantly shifted. Therefore, we assume that this molecule is adsorbed to the surface through the donor molecule and is laying near the surface.

The above results obtained from silver colloidal dispersion are confirmed by SERS experiments on cobalt(II) cupferronato complex (10^{-3} moll^{-1}) adsorbed on roughened Ag electrod. A similar interaction between the molecule and each Ag substrate was concluded based on the near coincidence in wavenumbers of the observed bands. The cobalt(II) cupferronato complexes were found to adsorb on different Ag substrates.
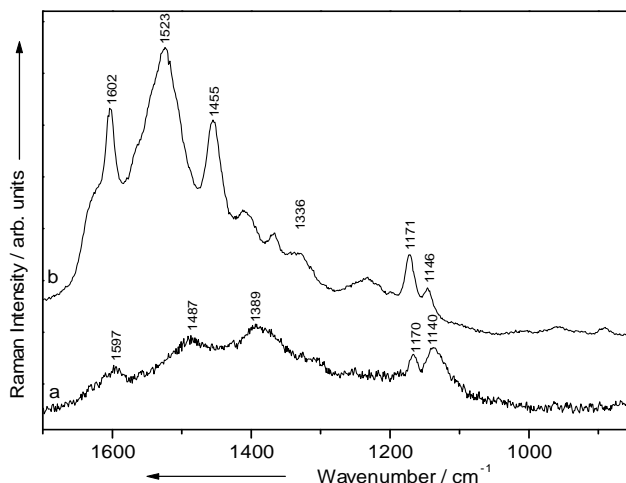
Fig. 7. SERS spectra of $CoL_2(p\text{-}NH_2C_6H_4NH_2)_2$ complex on different substrates: roughened Ag electrode (a) and Ag sol (b). Laser line: 647 nm (a) and 514.5 nm (b), P=300 mW

The SERS spectra of **3** on Ag colloid at different concentration are presented in Fig. 7. It can be observed that increasing the concentration of the sample in the silver sol the intensity of the signal increase. The optimal concentration for getting the best SERS spectrum was $1.52 \cdot 10^{-4}$ moll^{-1}.
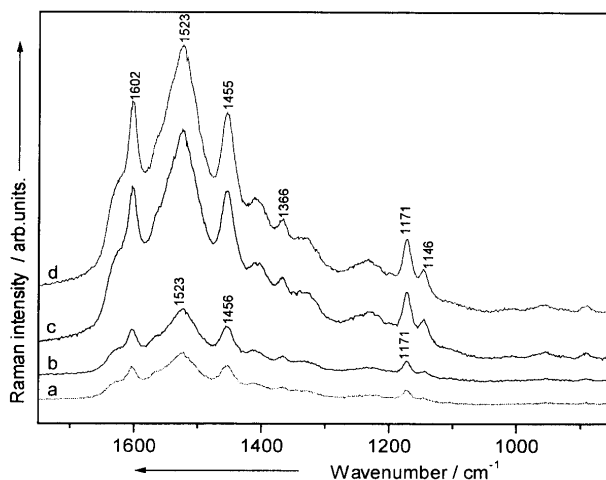
Fig. 8. SERS spectra of $CoL_2(p\text{-}NH_2C_6H_4NH_2)_2$ complex on Ag sol at different concentrations: $6.6 \cdot 10^{-6}$ moll^{-1} (a), $9.9 \cdot 10^{-6}$ moll^{-1} (b), $2.2 \cdot 10^{-5}$ moll^{-1} (c), $1.52 \cdot 10^{-4}$ moll^{-1} (d). Laser line: 514.5 nm.

Two main mechanisms can explain the enhancement of the Raman signal, the electromagnetic and the chemical one, respectively [16]. The chemical mechanism assumes the forming of metal-molecule complex, when a charge transfer (CT) between the metal and molecule can occur. This can explain the shift of peaks position and change of relative intensity in SERS compared to ordinary Raman spectrum of molecule. In our case both the electromagnetic and CT mechanisms were supposed to be involved in the Raman enhancement [16].

For the complexes *2* and *3* there was a decomposition to graphitic carbon under the laser excitation. The video camera coupled to the micro-Raman set-up allowed the visualization of the resulted photodecomposition "craters" localized under the laser spot after exposure.

Conclusions. FT-Raman spectra of the cupferron exhibit the typical ν(N-N), ν(N=O) and δ(ONNO) modes. The vibrational behavior of the cupferronato anion bound to the metal center confirms the electron delocalisation over the ONNO unit as well as the bidentate coordination pattern. Furthermore, the band at about 1302 cm^{-1}, assigned to a new symmetric vibrational mode of the ligand, is representative for all the cupferronato cobalt(II) complexes. SERS spectra of cobalt(II) cupferronato complexes bring additional arguments for the assignment of the ONNO unit in the Raman spectra.

REFERENCES

1. L. Parkanyi, A. Kalman, A. Deak, M. Venter and I. Haiduc, Inorg. Chem. Commun. 2 (1999) 265.
2. A. Deak, L. Parkanyi, A. Kalman, M. Venter, I. Haiduc, Acta Cryst. C C54 (1998) CIF access.
3. S. Cîntă, M. Venter, and I. Haiduc, *Spectroscopy of Biological Molecules: New Directions*, Ed. by J. Greve, G. J. Puppels, C. Otto, Kluwer Academic Publ., 1999, p. 559, Dordrecht, Boston, London.
4. A. Deak, I. Haiduc, L. Parkanyi, M. Venter and A. Kalman, Eur. J. Inorg. Chem. (2000).

5. G.D.Sockaligum, Y. Chourpa, J.M. Millot, Y. Nabiev, S. Sharanov and M. Manfait, *Biomedical Applications of Spectroscopy*, R. J. Clark and R. E. Hester (eds.), Wiley, Chichester, (1996), 49.

6. P. Lee and D. Meisel, J. Phys. Chem., 86 (1986), 3391.

7. E. Steven Brandt and T. M. Cotton, *Physical Methods of Chem. Series*, 2nd ed., J. Wiley and Sons, Inc., (1993), vol. IXB, 670.

8. E. V. Albano, S. Daiser, R. Miranda and K. Wandelt, Surf. Sci. 150 (1985), 367.

9. I. Pavel, S. Cinta, M. Venter, A. Deak, I. Haiduc, O. Cozar, T. Iliescu, P. Rösch and W. Kiefer, Vibr. Spectrosc., 23 (2000) 71-76.

10. F. R. Dollish, W. G. Feteley, F. F. Bentley (Eds.), *Characteristic Raman Frequency of Organic Compounds*, J. Wiley and Sons, New York, (1974), 162.

11. S. T. Srivastava, J. Inorg. Nucl. Chem. 37 (1975) 1546.

12. R. Kellner and P. Prokopowski, Anal. Chim. Acta 86 (1976) 175.

13. N. B. Colthup, L. H. Daly, and S. E. Wiberley, *Introduction to Infrared and Raman Spectroscopy*, 2nd edn., Academic Press, New York, (1964), 360.

14. S. Cîntă, M. Venter, C. Fickert, I. Haiduc, P. Scholz and W. Kiefer, J. Mol. Struct. 446 (1998) 209.

15. S. Cinta, M. Venter, W. Kiefer, P. Scholz, T. Iliescu, O. Cozar, Balk. Phys. Lett. 5 (1997), 317.

16. M. Moskovits, Rev. Mod. Phys. 57 (1985), 783.

VIBRATIONAL STUDY OF THIAMINE

N. LEOPOLD[*1,2], S. CÎNTĂ-PÎNZARU[1], M. BOLBOACĂ[2], O. COZAR[1], W. KIEFER[2], J. POPP[2]

[1]*Babeş-Bolyai University, Physics Dept., M. Kogalniceanu 1, 3400 Cluj-Napoca, Romania*
[2]*Institut für Physikalische Chemie, Universität Würzburg, Am Hubland, 97074 Würzburg, Germany*

ABSTRACT. FT-Raman, FT-IR, Raman and surface-enhanced Raman scattering (SERS) spectra of thiamine hydrochloride at various pH values have been obtained. Raman spectra of thiamine hydrochloride at pH values between 2 and 10 reveal different thiamine species. SERS spectra at different pH values allowed to evidence different chemisorbed geometry species of thiamine molecules.

Keywords: Thiamine, FT-Raman, FT-IR, SERS

1. Introduction

Thiamine (Fig.1) which is also known as vitamin B_1, was first isolated by Jansen and Donath in 1926 from rice bran[1]. Thiamine is a water-soluble substance, consisting of thiazole and pyrimidine substituted rings joined by a methylene bridge. It is needed to process carbohydrates, fat and protein. Nerve cells require thiamine in order to function normally.
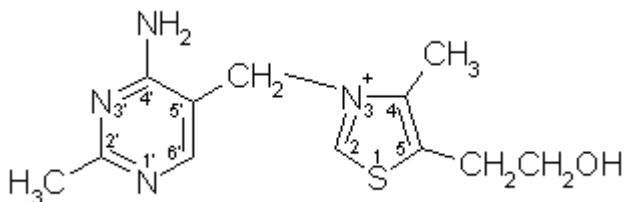
Fig.1. *Chemical structure of thiamine.*

---

[*] Corresponding author. E-mail: mleopold@phys.ubbcluj.ro

Thiamine diphosphate is the active form of thiamine, which serves as a cofactor for several enzymes. For the mechanism of action of thiamine enzymes, the mechanism proposed by Breslow[2] is now widely accepted. Questions on this mechanism are still unanswered today: (i) the role of bivalent metal ions Mg^{2+}, Ca^{2+} for the action of thiamine enzymes; (ii) the conformation that the whole molecule may take during the enzymatic action[1].

In this work, Raman, IR and SERS spectroscopies are applied to study the vibrational structure and the adsorption of this biomolecule on metal surfaces at acidic and basic pH values. SERS technique is based in the employing of roughened metal surfaces, mainly of silver, gold and copper, to enhance the Raman scattering radiation coming from adsorbed molecules[3]. This effect is useful for studying small amounts of sample and to quench fluorescence which the studied molecule could emit[4]. SERS spectroscopy provides a versatile and elucidating approach in studying the interaction and conformational behavior of biomolecules and allows for the in situ characterization of the chemical identity, structure, and orientation of surface species in the adsorbed state[5]. Additionally, this method can be successfully employed in the study of the interaction between drugs and biomolecules[3].

2. Experimental

2. 1. Chemicals

Thiamine hydrochloride was purchased from Aldrich. All the reagents were of analytical grade and distilled water was employed to prepare the aqueous solutions.

Colloidal gold substrates were prepared according to the Lee-Meisel procedure[6] and were found to be stable over several weeks at room temperature. Moreover the sol does not display any significant further aggregation or coagulation pattern on varying the pH within the range 1-12. This feature was also reported by G. Levi et al[7]. Dilute HCl and NaOH solutions were used to adjust the pH of the gold sol. The addition of thiamine hydrochloride caused an immediate colloid aggregation, which was necessary for the SERS spectrum to be observed. The SERS final concentration of thiamine was 10^{-5} mol/l.

2.2 Instrumentation

FT-Raman spectra were obtained by using an IFS 120 HR Bruker spectrometer with an integrated FRA 106 Raman module. The 1064 nm line, provided by a Nd:YAG laser, was used for the excitation. Resolution was set to 2 cm^{-1}, and a 180^0 geometry was employed. The output laser power was 200 mW.

For Raman and SERS spectra at different pH values a micro-Raman setup was employed. The 632.81 nm line from a He-Ne laser was applied for excitation. The scattered light was collected in back-scattering geometry by focusing a x10 objective (Olympus ULWD MSPlan10) on the entrance slit of a Dilor LabRam spectrometer with 900 grooves/mm diffractive grating. The laser power was kept below ca. 100 mW and the spectral resolution was 4 cm^{-1}. The detection system consisted of a charge-coupled device detector (CCD). Each Raman spectrum is the result of 2 accumulations with 100 s exposure time. For each SERS spectrum one accumulation with 40 s exposure time was needed.

The infrared spectrum was obtained with a Perkin–Elmer FT-IR spectrophotometer. Pellets for IR measurements were prepared by dispersing thiamine hydrochloride in KBr.

3. Results and discussions

Figure 2 shows the FT-Raman spectrum of thiamine hydrochloride in solid state (Fig. 2a) and in aqueous saturated solution (Fig. 2b).

In the spectra of Fig. 2 the protonated form of thiamine, due to the presence of hydrochloride, have a main contribution.

Theoretical calculations[8] show that the protonation of the N_1' atom is energetically favoured; the N_1'-H isomer is more stable than the N_3'-H isomer. Strekal et al[9] also consider center of the protonation the N_1' atom.
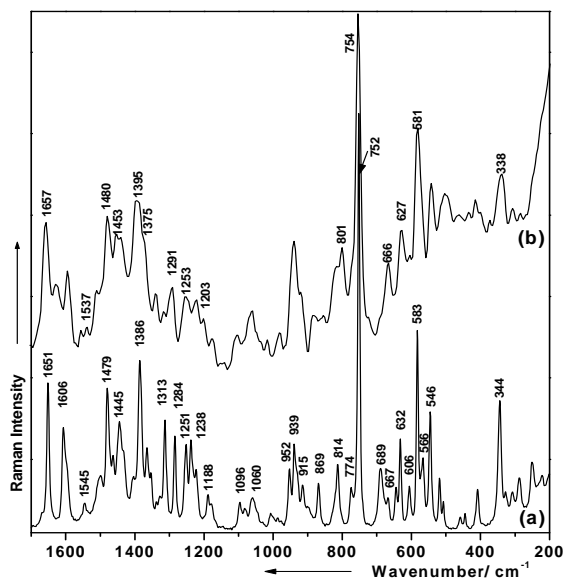
Fig. 2. *FT-Raman spectra of powder thiamine hydrochloride (a) and of its aqueous saturated solution (b). Laser 1064 nm, power 200 mW on the sample*

According to the literature[10] the thiazole ring breathing mode is present at 939 cm^{-1} and the ring stretching modes at 1479, 1431, 1284, 869 cm^{-1} respectively. The ring breathing of the pyrimidine moiety of thiamine is present at 752 cm^{-1}. Pyrimidine ring stretching vibrations are observed at 1651 (protonated form), 1606 (normal form), 1545, 1365 cm^{-1}. In particular the bands at 1096, 1222, 1251 cm^{-1}, are attributed to C-H deformation vibrations. The FT-Raman spectrum of thiamine saturated solution reproduces the main peaks of the title compound with the broadening of the bands due to solvent.

The FT-IR spectrum (Fig. 3) shows strong bands at 1614, 1656, 1480,1381, 1234, 1225,1047, and 776 cm^{-1} in agreement with the previous published data[11].
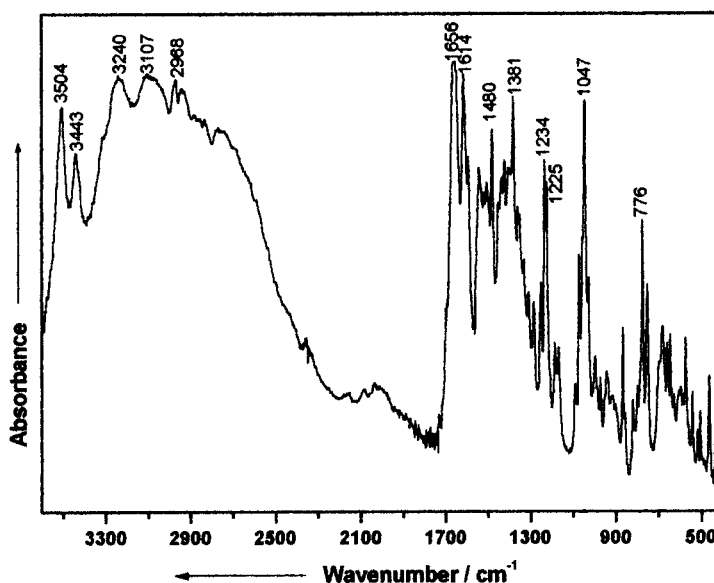
Fig. 3. FT-IR spectrum of thiamine hydrochloride.

The chemical reactions involved in biological processes are often very sensitive to the concentration of the hydrogen ions of the medium. In Fig. 4. Raman spectra of thiamine aqueous solution at pH values between 2 and 10 are presented. The reported[9] pK value for this molecule is 4.9.

On passing from neutral to acidic pH values, differences in the Raman spectra could be observed. The process of protonation leads to low wavenumber shifts of some bands (e. g. 760 to 755 cm^{-1}, 592 to 583 cm^{-1}, 1603 to 1599 cm^{-1}). Based on the assignments, the drastic increase of the band at 1657 and 1514 cm^{-1} and the modification of the band positions and intensities assigned to pyrimidine modes from thiamine suggest a protonation of the pyrimidine ring at pH values under 7.
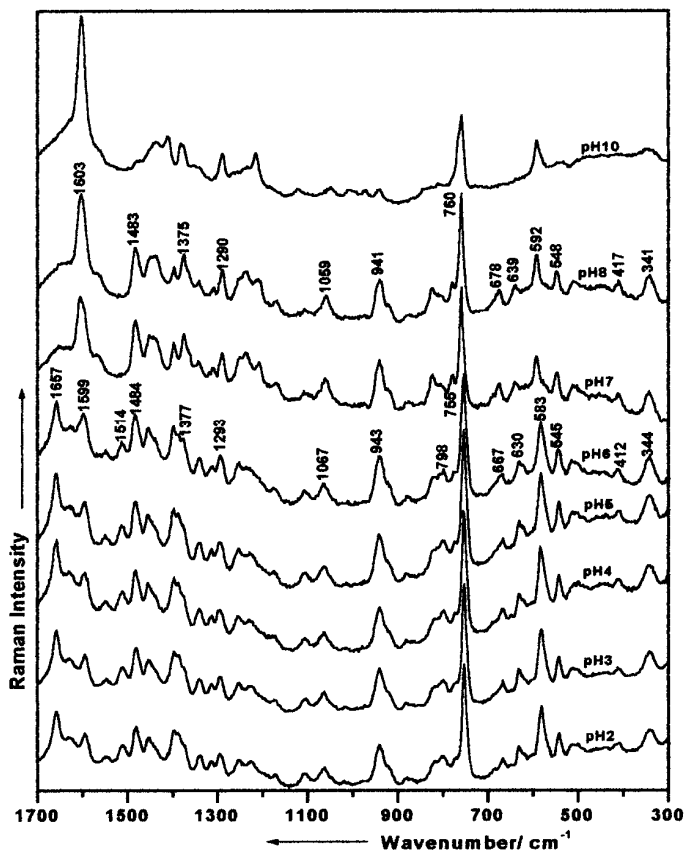
Fig. 4. *Raman spectra of thiamine hydrochloride (10^{-1} mol/l) in water solution at different pH values. Excitation: laser 632.81 nm, power 100 mW on the sample.*

In this region the pyrimidine ring breathing mode at 755 cm^{-1} dominates the Raman spectra.

At basic pH values above 9 the Raman spectra revealed the denaturation of thiamine structure.

According to literature[12], in alkaline medium thiamine transforms into disulphidic form (oxidated) (Fig. 5) which reduces to a thiol form (reduced), forming a redox system.

SERS spectra of thiamine on gold sol at different pH values are presented in Fig. 6.

On passing from Raman to SERS spectra, the modes corresponding to the pyrimidine part of molecule are gently shifted and enhanced. In particular, we have observed shifts of the 1657 and 755 cm^{-1} bands to 1650

and 747 cm^{-1}, respectively. This fact suggests that the interaction with the metal is established through a σ bond with gold. The changes observed in the SERS spectra in relation to the corresponding Raman spectra can be attributed to the interaction of thiamine with the Au-surface through the N atoms from the pyrimidine moiety. This is confirmed by the great contribution to the most intense SERS bands from normal modes in which the pyrimidine ring is involved.
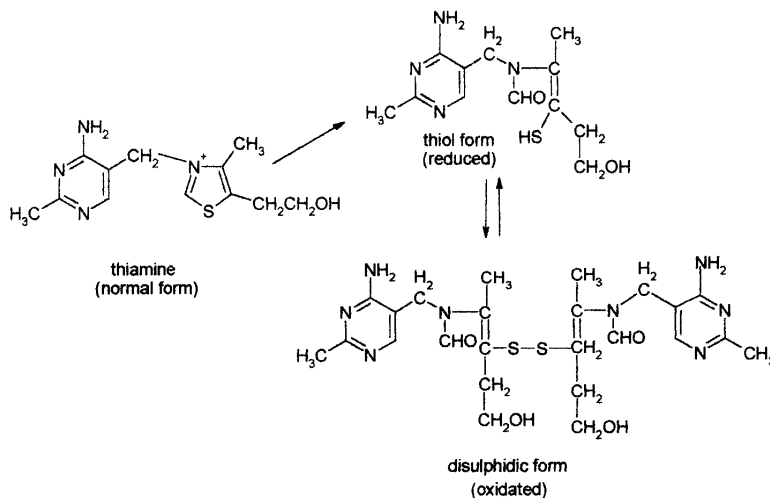
Fig. 5. Oxido-reduced forms of thiamine at basic pH.

Three distinct behaviors in the SERS spectra could be observed. Firstly, in the pH range between 2 and 4 where the protonated species are dominant, the most enhanced bands correspond to the pyrimidine ring streching modes of thiamine at 1655, 1544, 1495 cm^{-1}. In this case, the most favorable adsorption site would be through the N_3' atom. Further comparison between Raman and SERS spectra (Figs. 4 and 6) for this corresponding pH range displays a drastic change in the relative intensities and positions of the pyrimidine bands, supporting the arguments for N_3' adsorption.

Secondly, for pH 5 and 6 an increase in the relative intensity of the SERS band at 1590 cm^{-1} is observed, whereas the ring breathing mode of pyrimidine is dominant. For this pH values a number of unprotonated species could coexist together with the protonated ones. The adsorption possibilities are therefore expanded to the N_1', N_3' or both atoms. As a consequence, three different orientation geometries could be possible: two of them when the pyrimidine ring "stands up" to the surface being adsorbed through N_1'or N_3', or the third possibility, with adsorption through both the N' atoms which leads to a flat orientation of the pyrimidine moiety to the surface.
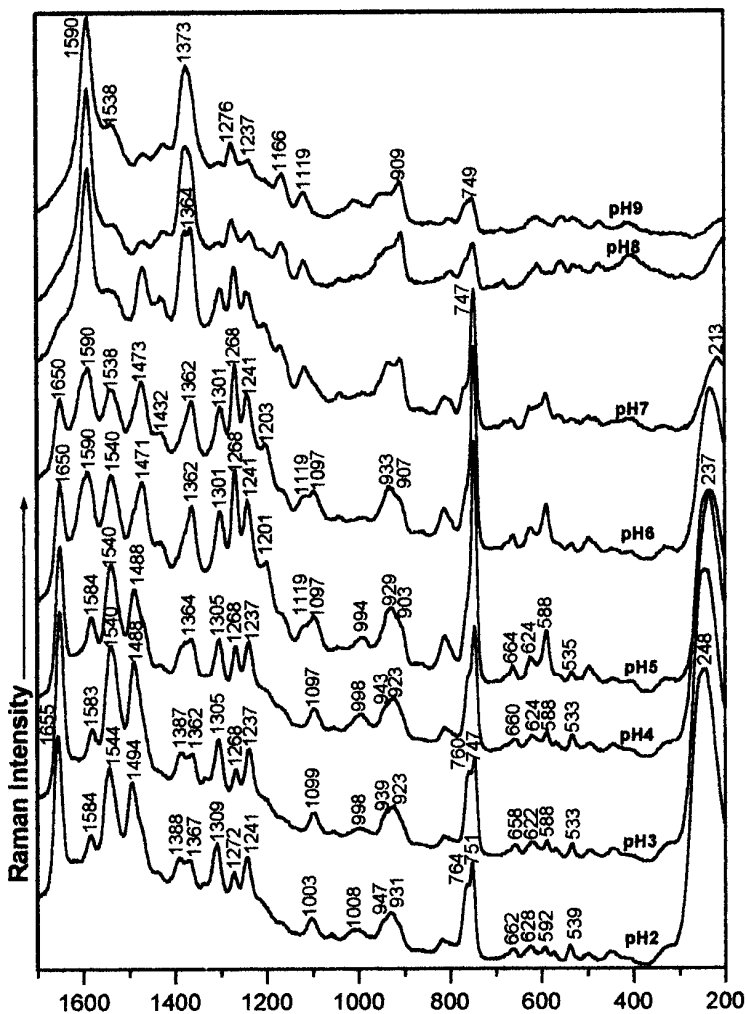
Fig. 6. *SERS spectra of thiamine hydrochloride (10^{-5}mol/l) in Au sol at different pH values. Laser 632.81 nm, power 10 mW on the sample*

According to the surface selection rules[13] the modes with a favorable perpendicular orientation of the polarizability component with respect to the surface are enhanced. The enhancement of the pyrimidine breathing mode is therefore obtained for a perpendicular orientation of the pyrimidine ring. When the orientation is more parallel with the surface (adsorption through both N_1' and N_3'), this mode is less enhanced. This last geometry is mainly suggested by the SERS spectra at pH values over 7. For these spectra dominantly enhanced bands are 1590, 1373, 1364 cm^{-1},

corresponding to the pyrimidine stretching modes favourable oriented in a flat adsorption from thiamine.

The modes assigned to the thiazole ring were observed to be unaffected in positions and relative intensities with pH variations (up to pH 9, when the denaturation previously discussed takes place). This fact supports our suppositions that the interaction of thiamine with the metal surface takes place through the pyrimidine ring.

The low wavenumber region is dominated by a broad band at 248-230 cm^{-1} in the SERS spectra of protonated species (pH up to 6) which indicates a multiple contribution: Au-Cl, Au-N, binding modes for these species. In the basic pH range, this band is shifted to lower wavenumbers (up to 213 cm^{-1}).

4. Conclusions

The pH dependent Raman spectra of thiamine reveal two different molecular species in aqueous solution: normal and protonated form.

The changes observed in the SERS spectra in relation to the Raman spectra of solutions can be attributed to the chemical interaction of thiamine with the surface through the N atoms of the pyrimidine part of thiamine. Although the SERS enhancement of thiamine is due to both an electromagnetic and a chemical mechanism, the importance of the latter mechanism is clearly demonstrated by the shifts and changes in relative intensities observed in the SERS in relation to the solid and aqueous solutions sample spectra.

Three different orientation geometries were concluded to be possible for these thiamine species, for neutral form through one or both N atoms of pyrimidine part and for the protonated species through the unprotonated N atom of pyrimidine ring of thiamine.

REFERENCES

1. G. Malandrinos, K. Dodi, M. Louloudi, N. Hadjiliadis, *J. Inorg. Chem.,* **79**, 21, (2000).
2. R. Breslow, *J. Am. Chem. Soc.*, **80**, 3719, (1958).

3. L. Rivas, S. Sanchez-Cortes, J. Stanicova, J.V. Garcia-Ramos, P. Miskovsky, *Vibr. Spectrosc.*, **20**, 179, (1999).
4. T. M. Cotton, "The application of surface-enhanced Raman scattering to biochemical systems", in *Spectroscopy of Surfaces*, ed. by R. J. H. Clarck, R. E. Hester, John Wiley & Sons, New York, 1988.
5. J. A. Creighton, in *Spectroscopy of Surfaces*, ed. by R. J. H. Clarck, R. E. Hester, John Wiley & Sons, New York, 1988, vol.16, p 37.
6. P. C. Lee, D. J. Meisel, *J. Phys. Chem*, **86**, 3391, (1982).
7. G. Levi, J. Pantigny, J. P. Marsault, J. Aubard, *J. Raman Spectrosc.*, **24**, 745, (1993).
8. R. Friedmann, H. Neef, *Biochim Biophys. Acta,* **1385**, 245, (1998).
9. N. D. Strekal, G. A. Gachko, L. N. Kivach, S. A. Maskevich, *J. Mol. Structure*, **267**, 287, (1992).
10. F.R. Dollish, W.F. Fateley, F.F. Bentley, Eds. *Characteristic Raman Frequencies of Organic Compounds*, J. Wiley & Sons, New York 1974.
11. B. Schrader, Ed. *Infrared and Raman Spectroscopy, Methods and Applications*, VCH Weinheim, 1995, p. 219.
12. H. T. Clarcke, S. Gurin, in *Biochimie Medicala & Farmaceutica*, ed. by D. D. Bedeleanu, I. Manta Editura Dacia, Cluj-Napoca, 1985.
13. J. A. Creighton, in *Spectroscopy of Surfaces*, ed. by R. J. H. Clarck, R. E. Hester, John Wiley & Sons, New York, 1988, p. 83.

MASS SPECTRAL ANALYSIS OF SOME p-ARYL SUBSTITUTED THIPHOSPHORORGANIC COMPOUNDS

*SIMONA NICOARÃ[1], MONICA CULEA[2], Z. MOLDOVAN[2], I. FENESAN[3] AND O. COZAR[4]

[1]Technical University of Cluj-Napoca, Physics Department, C. Daicoviciu str, nr. 15, Cluj-Napoca, Romania, <simona.nicoara@personal.ro>
[2]Institute of Isotopic and Molecular Technology, Cluj-Napoca, Romania
[3]Institute of Chemistry "Raluca Ripan", Cluj-Napoca, Romania
[4]Faculty of Physics, "Babes-Bolyai" University, Cluj-Napoca, Romania
*Author to whom correspondence should be addressed

ABSTRACT. This paper presents a comparative analysis between the mass spectra of two series of compounds: S*eries I*, the S-methyl derivatives of the compounds of *Series II*: the p-methyl-(**4**), p-fluorine-(**5**) and p-bromide-(**6**) arylsulfonamides of the dimethylamidocyclohexyl-thiophosphonic acid.

The normal mass spectra recorded on a MAT-311 mass spectrometer, the HR mass measurements and the metastable ions cleavage detection were analized to elucidate the fragmentation processes and the elemental composition of the ion fragments.

Keywords: electron impact mass spectra, metastable ions analysis, fragmentation patterns, organophosphorus compounds.

INTRODUCTION

It is wellknown that aromatic organic compounds with heteroatoms like N, S, P and O have biological potential [1-9], being used as antibacterial and antimicrobial agents [3,4], as medicine drugs [5,6] or as pesticides [7,8]. Many newly synthesized compounds of this type are studied by physico-chemical methods, among wich, the mass spectrometry plays an dominant role, since it provides important structural information on the molecules studied [2,10-14].

Both *Series I* and *Series II* of compounds were synthesized at the Chemistry Institute "Raluca Ripan" from Cluj-Napoca, and have the following molecular structure (here cC_6H_{11} = the cyclohexyl radical):

Series I: the S-methyl derivatives **1-3**:

$$cC_6H_{11} \underset{\underset{N(CH_3)_2}{|}}{\overset{\overset{S - CH_3}{|}}{P}} = N \underline{\qquad} SO_2 \underline{\qquad} C_6H_4 \underline{\qquad} R$$
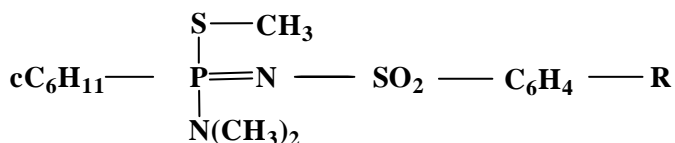
R=CH$_3$ (1)   **R=F (2)**   **R=Br (3)**

Series II: the p-arylsulfonamides of the dimethylamido-cyclohexilthiophosphoric acid (the chemical precursors of the compounds in *Series I*):

$$cC_6H_{11} \underset{\underset{N(CH_3)_2}{|}}{\overset{\overset{S}{||}}{P}} = NH \underline{\qquad} SO_2 \underline{\qquad} C_6H_4 \underline{\qquad} R$$
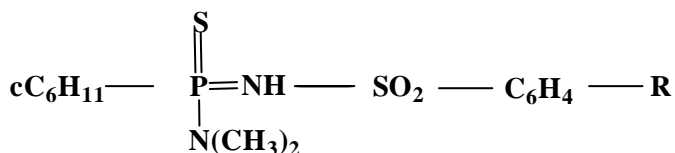
R=CH$_3$ (4)   **R=F (5)**   **R=Br (6)**

The compounds *1-3* were synthesized for their expected biological activity, owing to their molecular composition and structure [9]. The purpose of this study is to analyze, compare and interpret the main features in the mass spectra of compounds *1-3* and of their chemical precursors *4-6*, respectively, and to elucidate the electron impact induced molecular fragmentation processes, by discussing the similarities and differences observed in the behavior of the two series of thiophosphororganics.

EXPERIMENTAL. The spectra were registered using a MAT-311 double focusing mass spectrometer. The 70 eV electron impact mass spectra of compounds *1-6*, combined with the HV and DADI recording of metastable ions [15] for the p-methylbenzene sulfonamide of the N,N-dimethylamidocyclohexyl thiphosphonic acid (*1*), were used to elucidate the fragmentation pathways. The accurate mass measurements for the ion fragments was performed by means of the peak-matching unit of the mass spectrometer and by using the PFK ions as mass reference, to confirm the elemental composition of certain ionic fragments in the spectrum of compound (*1*).

The direct inlet for solid samples was used and the samples were maintained at the optimum evaporation temperatures for each compound: 110 ^{o}C (*1*), 120 ^{o}C (*2*), 125 ^{o}C (*3*), 120 ^{o}C (*4*), 110 ^{o}C (*5*) and 165 ^{o}C (*6*).

The standard operating conditions were: 150 ^{o}C ion source temperature, 70 eV electron energy, and 60 µA electron emission current. The HR mass measurements were done at a resolution R=4000 and the mass spectra were recorded at R=600 resolution.

RESULTS AND DISCUSSION. The electron impact mass spectra of compounds *1-3* are presented in figure 1 a-c, and those of compounds *4-6* in figure 3 a-c. In all the six spectra, the molecular ion peak is very low (< 5 %), a feature that indicates a high molecular lability, due to the high degree of molecule ramification.

Figure 2 shows the fragmentation pattern proposed for the *Series I* of compounds *1-3* and the metastable ion cleavages detected in compound *1* are marked with an asterix. The molecules of *Series I* initiate their cleavage reactions by the elimination of the methyl group bonded to the sulfur atom from the molecular ion, ***M***$^{+.}$, m/z (359+R), resulting the ion *a*, m/z (344+R). The latter subsequently produces the ion *b*, m/z (301+R), by losing a neutral NC_2H_5 molecule, through a transition state involving the rearrangement of a H atom on the phosphorus, a process described in similar cases [11]. The ion *b* then loses a neutral SO molecule, as remarked in other similar compounds [11,15], to generate the ion *c*, m/z (253+R), of a low abundance (<6 %) in spectra *1-3*.

The molecular ion ***M***$^{+.}$ in *Series I* may alternatively lose the neutral molecule NC_2H_5 through a four membered transition state(Fig. 4), involving the rearrangement of a hidrogen atom from nitrogen to phosphorus, yielding the ion *d*, m/z (316+R).

The metastable ions detection confirmed that the molecular ion ***M***$^{+.}$ generates the fragment ion structure *d* and that this subsequently eliminates the methyl radical and the neutral molecule of sulfur dioxide (fig. 2), to result in the ion *e*, m/z (237+R) whose elemental composition was confirmed via HR mass measurements.
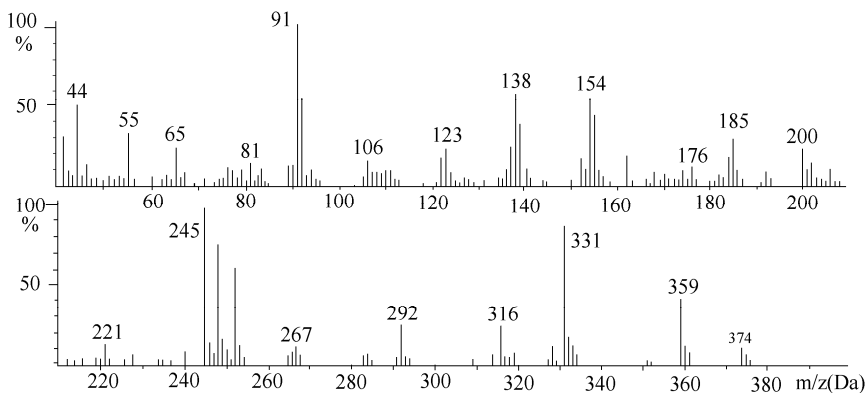
Fig. 1-a) *70 eV EI mass spectrum of the p-methylbenzenesulfonimide of the N,N-dimethylamidocyclohexyl S-methylthiophosphonic acid (1).*
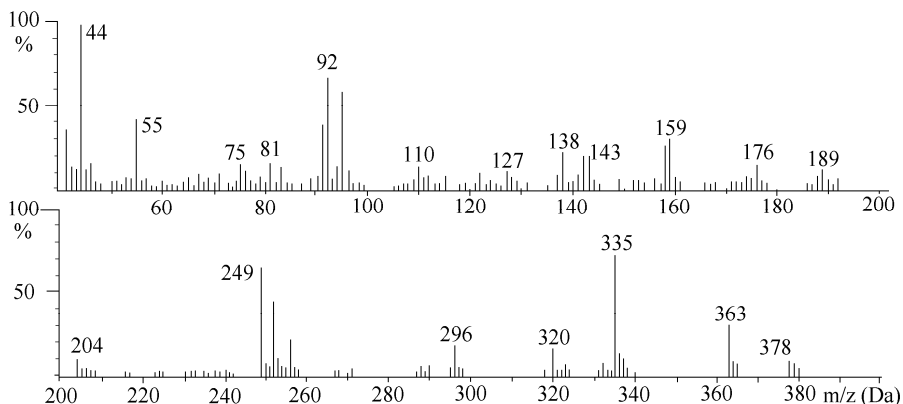
Fig. 1-b) *70 eV EI mass spectrum of the p-fluorinebenzenesulfonimide of the N,N-dimethylamidocyclohexyl S-methylthiophosphonic acid (2).*

The molecular ion **M⁺·** may initiate another cleavage pathway and generate the ion *f,* m/z (277+R), by the elimination of a cyclohexene neutral molecule, involving a five membered transition state (Fig. 5) with the transfer of a H atom from the cyclohexyl group to P, a process specific to molecules with a phosphorus atom bonded to the cC_6H_{11} group [11,13,16,17]. The fragment ion *g*, m/z (233+R) with 33 % abundance in spectrum (**1**), probably results from the ion *f*, by the loss of the neutral $N(CH_3)_2$ radical, subsequent to the simple fission of the P-N bond. The cleavage of the N-S simple bond in structure *f* produces the ion *h*, m/z (140+R), fairly abundant (> 23 %) in all spectra of *Series I,* the transition *f → h* being confirmed through metastable ions detection.
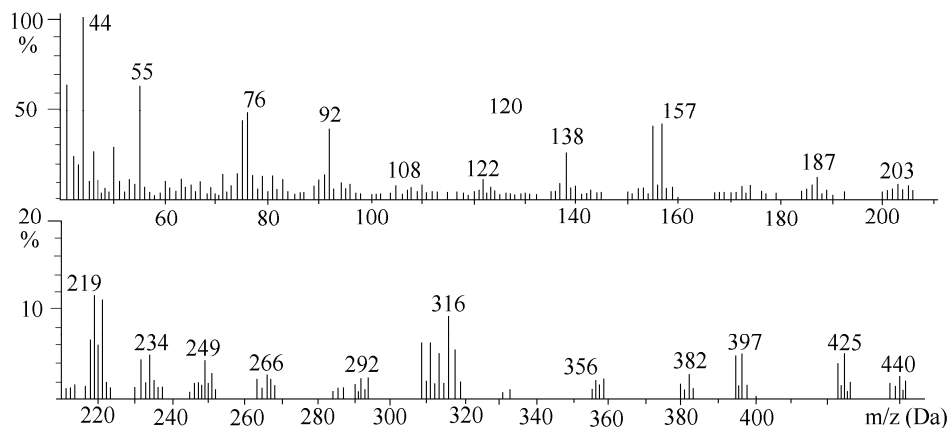
Fig. 1-c) *70 eV mass spectrum of the p-bromidebenzenesulfonimide of the N,N-dimethylamidocyclohexyl S-methylthiophosphonic acid.* (***3***).

In spectrum (***1***) there was exclusively observed the elimination of a H atom from the ion *h*, to form the *tropyl* structure (C_7H_6, m/z 90 Da) in the fragment ion *i*, m/z 154. The DADI analysis of the metastable ions confirmed the formation of the ion *i* as well as its subsequent transition to the ion *j*, m/z 138, by the elimination of an oxigen atom, a process encountered in other compounds with substituted phenyl [17,18].

Following another cleavage pathway, the ionic structure *h* loses a neutral O atom, as confirmed by metastable ions analysis in (***1***), to form the ion *k*, m/z (124+R), that further possibly eliminates another O atom to rersult in the ion *l*, m/z (108+R).

The fragment ion *f* may also undergo the simple fission of its P-S bond, to form the ion *m*, m/z (230+R), a process detected as a metastable ion cleavage. The ion *m* undergoes the rearrangement of a H atom from the amidic methyl onto the P atom, subsequently losing a neutral NC_2H_5 molecule, through a metastable ions transition, to generate the ion *n*, m/z (187+R). The latter then probably eliminates the neutral SO_2 molecule to form the abundant (> 37 %) ion *o*, m/z (123+R). Even though this process was not recorded as a metastable ion transition, it is very typical and often encountered in similar compounds containing the SO_2 group in their molecule [12,17,19,20].
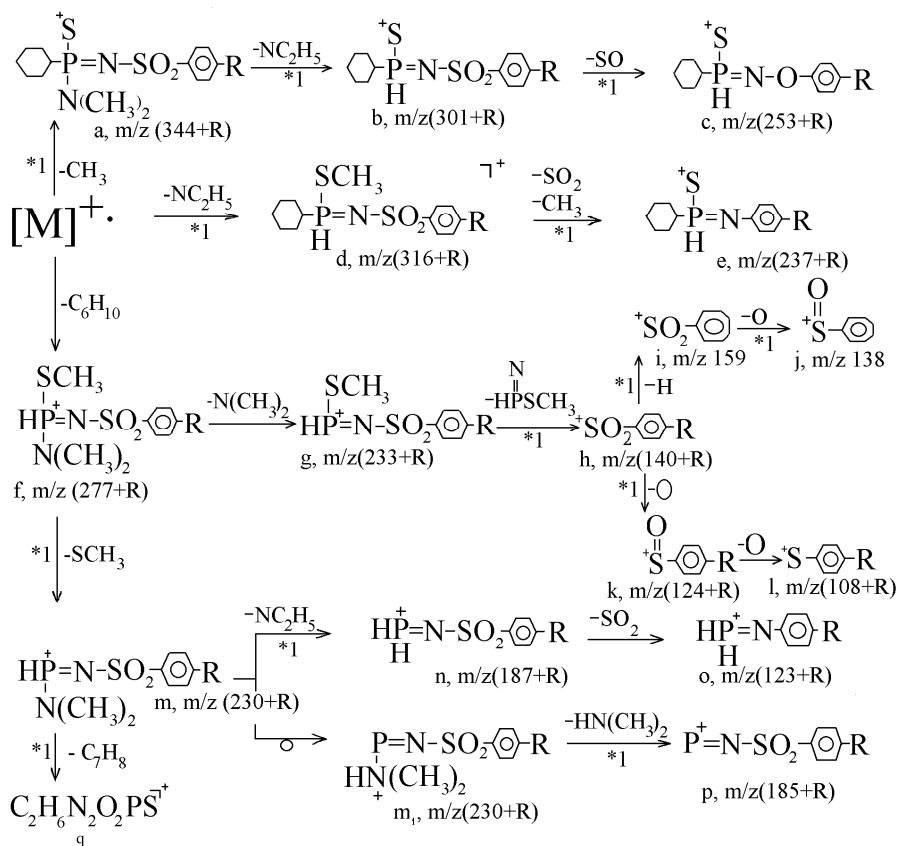
Fig. 2. *Scheme of the fragmentation pattern proposed for the analytes of Series I. (*metastable ion cleavage detected in HV or DADI mode).*

In the fragmentation pathways proposed for these compounds (*1-3*) in the Scheme of fig. 2, the ion *m* may also undergo the isomerisation to the structure m_1, further eliminating the $HN(CH_3)_2$ neutral molecule and yielding the ion *p*, m/z (185+R), a transition recorded in the DADI spectra. Metastable ions analysis also confirmed the cleavage of the neutral C_7H_8 group from the ion *m*, to produce the ion *q,* m/z 153 in Fig. 2.

In the first (*1-3*) spectra, the abundant ion *r*, m/z (76+R) was remarked, being the base peak in spectrum (*1*), at m/z 91. The elemental composition of this ionic structure was confirmed through accurate mass measurements to be $[C_6H_4R]^+$ (*1*). Another set of abundant ions were those recorded at m/z 92, in the first three spectra, with the elemental composition $[(CH_3)_2NSO]^+$ confirmed by HR mass measurements. The formation of this

fragment ion involves the rearrangement and migration of the heteroatoms, as remarked in other thiophosphororganic molecules [18,21].

Two abundant peaks were recorded in the first three compounds spectra, at m/z 45 and m/z 44, the latter being the base peak in spectra (*2*) and (*3*). The HR mass measurements confirmed their elemental compositions to be $[N(CH_3)_2]^+$ at m/z 44 and $[HN(CH_3)_2]^+$ at m/z 45, respectively and the fragment ions were also reported for other similar compounds [12].

All the six spectra of *Series I* and *Series II*, show the sets of low mass peaks recorded at m/z 76, 51, 50, and at m/z 83, 55, 43, 41, that are typical for the cleavage of the C_6H_4 [14,18] and cC_6H_{11} [13,18] groups, respectively.

The figure 3 (a-c) shows the normal mass spectra of compounds (*4-6*), the chemical precursors of compounds in *Series I.* A common feature with spectra of compounds (*1-3*) is the low abundance or even missing peak for the molecular ion, **M$^{+\cdot}$**, with a high degree of ramification.

In spectra (*4*) (Fig. 3-a) and (*5*) (Fig. 3-b), the molecular ion loses the neutral SO_2 molecule to produce the ions with peaks registered at m/z (M - 64 Da), the typical loss for organic molecules containing the SO_2 group [12,17].
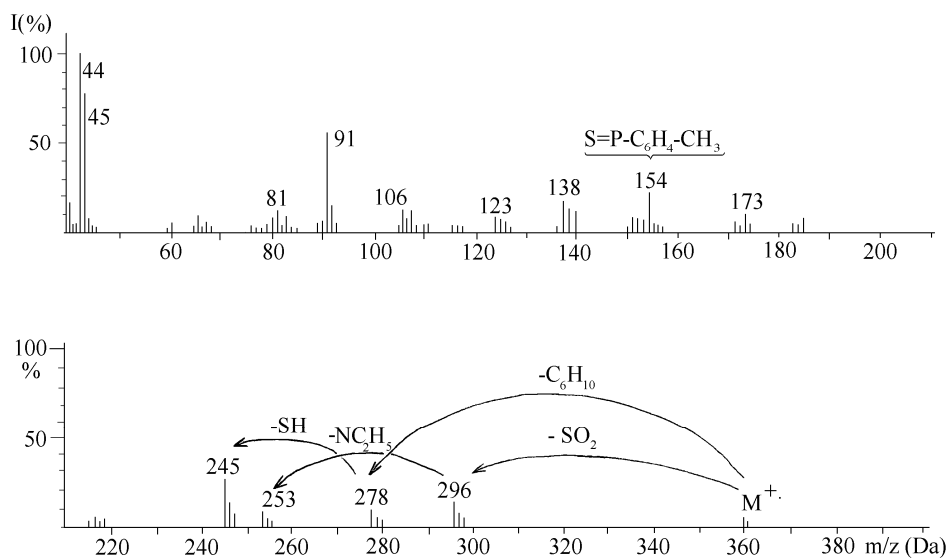
Fig. 3-a) *70 eV EI mass spectrum of the p-methylbenzenesulfonamide of the N,N-dimethylamidocyclohexyl thiophosphonic acid (4).*

In spectrum (*4*), the peaks have all rather low abundances. The molecular ion *M*$^{+\cdot}$, m/z 360 probably eliminates the typical fragment SO_2 to generate the ion recorded at m/z 296, which subsequently undergoes the rearrangement of a H atom from the amidic methyl to the P atom, eliminating the neutral NC_2H_5 molecule and generating the ion at m/z 253, through a fragmentation process similar to the EI behaviour of other analogous molecules [11,12].

The abundant peak recorded at m/z 154 with the elemental composition $S=PC_6H_4-CH_3$ is also observed in spectra (*5*) (Fig. 3-b) and (*6*) (Fig. 3-c) at m/z (139+R).

In spectrum (*4*), another remarkable peak was registered at m/z 91 corresponding to the composition $[C_6H_4 + R]^+$, as in compound (*1*), and was also reported in the spectra of similar molecules [11]. The base peak in spectrum (*4*) is at m/z 44, with its neighbour at m/z 45, both weighted in HR and confirmed as the $[N(CH_3)_2]^+$ and $[HN(CH_3)_2]^+$ fragment ions, respectively. They were previously reported for other molecules containing the $N(CH_3)_2$ group [11-13].
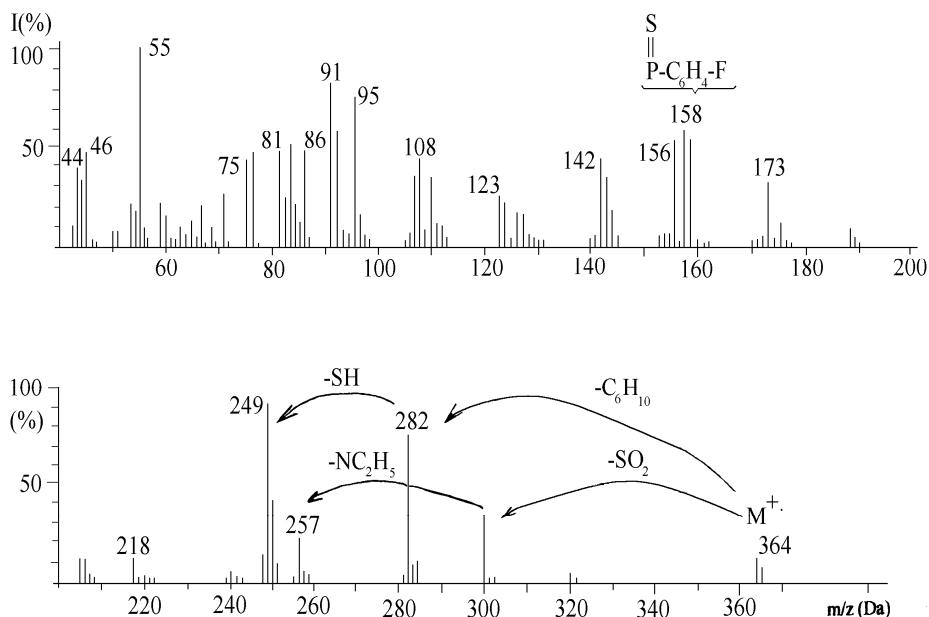
Fig. 3-b) 70 eV mass spectrum of the p-fluorinebenzenesulfonamide of the N,N-dimethylamidocyclohexylthiophosphonic acid (*5*).

In spectrum (*5*), the ion resulted from *M*$^{+\cdot}$ by the typical SO_2 elimination, may undergo the rearrangement of a H atom, through a four

membered transition state and may lose the neutral NC_2H_5 group as described in (*1*), to produce the fairly abundant ion recorded at m/z 257 (25 %).

As found in compounds (*1-3*), the intense peak at m/z 282 in spectrum (*5*), most probably indicates the rearrangement of a H atom from cyclohexyl to P, followed by the loss of a neutral cyclohexene molecule (- 83 Da).

The ion at m/z 282 probably undergoes the rearrangement of a H atom from P onto S, subsequently eliminating a neutral SH radical, resulting in the abundant ion (88 %) recorded at m/z 249 in spectrum (*5*). The next relatively abundant ion in this spectrum, at m/z 173, could be formed either by the fission of the molecular ion $M^{+\cdot}$, m/z 364, or by the cleavage of the ion at m/z 249, that could both undergo the rearrangement of a hydrogen atom onto P, followed by the loss of the neutral $HP-N(CH_3)_2$ group. The next fairly abundant ion (70 %) at m/z 158 is most probably given by the fragment ion $[SPC_6H_4F]^+$.
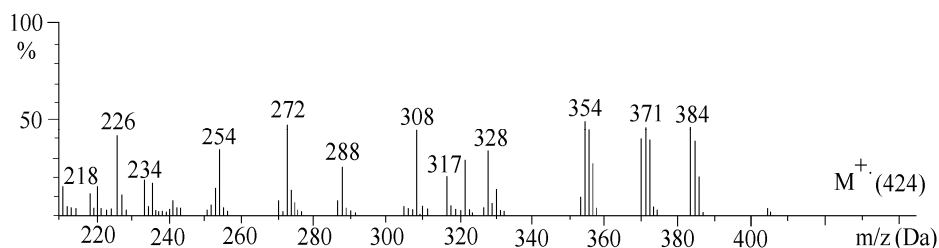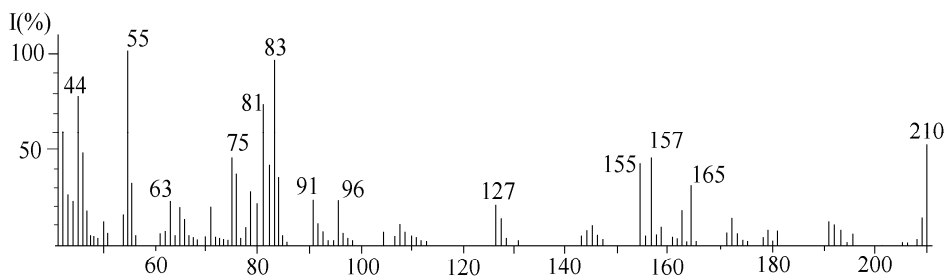
Fig. 3-c) 70 eV mass spectrum of the p-bromidebnzenesulfonamide of the N,N-dimethylamidocyclohexylthiophosphonic acid (*6*).

In the 70 eV mas spectrum of compound (*6*) (fig. 3-c), the paired peaks corresponding to the Br isotopes (79 amu and 81 amu) can be remarked, at: m/z 234 -- 236 ($[HN-SO_2-C_6H_4Br]^+$); m/z 218 -- 220 ($[SPC_6H_4Br]^+$) and at m/z 155 -- 157 ($[C_6H_4Br]^+$), respectively.
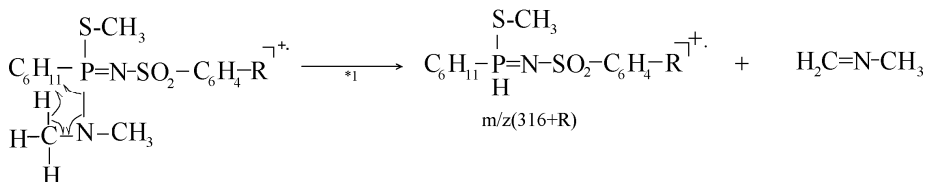
Fig. 4. *The cleavage of the molecular ion $M^{+\cdot}$, by the elimination of the NC_2H_5 neutral molecule through a four membered (P,N,C,H) transition state.*

Fig. 5. *The cleavge of the molecular ion $M^{+\cdot}$, through a five membered (P,N,H,C,H) transition state and the formation of the ion f, m/z (277+R).*

In all the spectra of *Series II* (*4-6*), the presence of the relatively strong P=S double bond could explain the abundant (>15 %) ions at m/z 107 and m/z 108, with the elemental compositions: $[S=PN(CH_3)_2]^+$ and $[S=PH-N(CH_3)_2]^+$, respectively.

By comparing the main features in the spectra of compounds in S*eries I* (*1-3*) and of those in *Series II* (*4-6*), a common characteristic is that they all have low abundance or even missing peaks for the molecular ions $M^{+\cdot}$, this reflecting the high degree of the molecules ramification.

In all the spectra of both series of compounds, many of the ions resulted from the electron impact were produced through the elimination of a neutral cyclohexene molecule, or a neutral NC_2H_5 molecule, processes that were subsequent to the rearrangement of a H atom either from N or from C onto the P atom.

Unlike their chemical precursors (*4-6*), and unlike other similar compounds described in the literature, the analytes of *Series I* (*1-3*) did not undergo in the early stages of their cleavage pathways the typical loss of the neutral sulfur dioxide molecule (SO_2). This could probably be due to the relatively stronger P=N double bond in *series II* (*4-6*), compared to the simple N-P bond in *series I* (*1-3*), where other bonds were more readily subjected to cleavage than those allowing the SO_2 elimination, and requiring two S-C bonds to be simultaneously broken.

The base peaks are: at m/z 91 ($[C_6H_4-CH_3]^+$) (*1*); at m/z 44 ($[N(CH_3)_2]^+$) (*2-4*); and at m/z 55 ($[C_4H_7]^+$) (*5,6*). In the region of low mass peaks in spectra (*4-6*), the set of ions at m/z 83 (90 %), 55, 43 and 41 from the cyclohexyl cleavage and the set of ions at m/z 76, 51 and 50, from the fragmentation of the aryl group were observed, as described in compounds (*1-3*) and in other molecules containing the cC_6H_{11} and C_6H_4 groups, respectively [13,14,18].

CONCLUSIONS. In all the spectra discussed here, the molecular ion peaks show low abundance, due to the ramification of the molecules. The electron impact molecular fragmentations involved the migration of the hydrogen atoms from carbon, sulfur or nitrogen, onto the P atom, subsequently favouring the elimination of neutral molecules like: C_6H_{10}, NC_2H_5, SO, neutral radicals: SH, $HN(CH_3)_2$, $N(CH_3)_2$, SCH_3, C_7H_8, or atoms: H, O.

The loss of a neutral SO_2 molecule was the initiating process of fragmentation in compounds (*4-6*), but it was not among the main clavages of the molecules (*1-3*), probably due to their molecular bonds. The spectra of compounds (*3*) and (*6*) respectively, contain the paired peaks of comparable intensities, separated by 2 Da, very specific to organic molecules with Br among the heteroatoms, due to its isotopes of 79 and 81 amu, respectively, with about 50 % natural abundance each. Certain similarities were observed between the fragmentation patterns of the two series of compounds, as well as some evidence of the dependence of the fragmentation pathways on the nature of the radicals bonded to the aryl and to the molecular structure, composition and bonds.

REFERENCES

1. C. Fest and K. J. Schmidt: "The Chemistry of Organophosphorus Pesticides", Springer Verlag, Berlin (1985).
2. S. Safe and O. Hutzinger: "Mass Spectrometry of Pesticides and Pollutants", CRC Press Cleveland, Ohio (1976).
3. I. Fenesan, I. Chioreanu, A. Hantz, Al. Alexandru and Rodica Popescu, *FARMACIA* Vol. **XXXI** Nr. **3**, (1988) 143.
4. J. Ollig, M. Morbach, G. Hagele and E. Brauer, *Phosphorus, Sulfur and Silicon*, Vol. **111** (1996) 55.
5. L. Almasi: "Les composees thiophosphororganiques", Ed. Masson, Paris (1976).
6. K. Imai, S. Uzu, K. Nakashima and S. Akiyama, *Biomed. Chromatogr.*, **7** (1993) 56.
7. S. Hemmamda, M. Calmon and J. P. Calmon, *Pestic. Sci.*, **40** (1994) 9.

8. P. Wieczoreck and D. Milliszkiewicz, *Pestic. Sci*., **40** (1994) 57.
9. C. T. Supuran, Viorica Muresan, Rodica Popescu and I. Fenesan*, Main Group Metal Chemistry*, **18**, 11 (1995) 629.
10. Rodica Popescu, I. Opreanu, N. Palibroda and Z. Moldovan, *Studia Univ. Babes-Bolyai, Seria Chemia*, **XXXIV** (1989) 23.
11. Z. Moldovan, Simona Nicoarã, Monica Culea, O. Cozar, I. Fenesan, P. Vegh and J. J. Rios, *J. Molec. Structure*, **348** (1995) 393
12. Simona Nicoarã, Monica Culea, N. Palibroda, O. Cozar, I. Fenesan and A. Hantz, *Rapid Commun. Mass Spectrom*., **9** (1995) 61.
13. Z. Moldovan, N. Palibroda, Monica Culea, I. Fenesan and A. Hantz, *Org. Mass Spectrom*., **24** (1989) 81.
14. Z. Moldovan, Monica Culea, N. Palibroda and Olga Musat, *The Sci. Total Environ*., **132** (1993) 147
15. Z. Moldovan, N. Palibroda, V. Mercea and G. Mihãilescu, *Org. Mass Spectrom*., **20**, 2 (1985) 77.
16. J. Seibl: "MassenSpektrometrie", Akademische VerlagsGesellschaft, Frankfurt am Main (1970).
17. I. Opreanu: "Spectrometria de masã a compusilor organici", Ed. Dacia Cluj-Napoca (1974).
18. Q. N. Porter and J. Baldes: "Mass Spectrometry of Heterocyclic Compounds", Wiley Interscience, New-York (1971).
19. Rodica Popescu, I. Opreanu, N. Palibroda and Z. Moldovan, *Studia Univ. Babes-Bolyai, Chemia* **XXXIII** (1988) 1.
20. Rodica Popescu , I. Opreanu, N. Palibroda and Z. Moldovan, *Studia Univ. Babes-Bolyai, Chemia* **XXXIV** (1989) 1.
21. G. Giordano, *Biol. Mass Spectrom*., **20** (1991) 63.